NANYANG TECHNOLOGICAL UNIVERSITY

STUDY OF Pt-M (M=Au and Co) NANO-CATALYSTS WITH LOW Pt LOADING FOR PEMFC APPLICATIONS

STUDY OF Pt-M (M=Au and Co) NANO-CATALYSTS WITH LOW Pt LOADING FOR PEMFC APPLICATIONS

NOEL KRISTIAN

NOEL KRISTIAN

SCHOOL OF CHEMICAL AND BIOMEDICAL ENGINEERING

2010

2010

STUDY OF Pt-M (M=Au and Co) NANO-CATALYSTS WITH LOW Pt LOADING FOR PEMFC APPLICATIONS

NOEL KRISTIAN

School of Chemical and Biomedical Engineering

A thesis submitted to the Nanyang Technological University
in partial fulfillment of the requirement for the degree of
Doctor of Philosophy

2010

ACKNOWLEDGEMENT

I want to express my gratitude to Asst/P. Wang Xin for his patience, supervision and kind advice for the completion of this thesis, where his encouraging words always keep me enthusiastic throughout the duration of this PhD course.

I would like to thank Mr. Poernomo Gunawan for helping me with many things in my research including characterization and experimental techniques and Mr. Yu Yaolun for being such a great mentor in the field of electrochemistry.

I would like to thank all my co-workers in the fuel cell lab: Mr. Nguyen Truong Son, Mr. Wang Shuangyin and Mr. Nguyen Tien Hoa for sharing all the joy and frustration in the lab, also to undergraduate students, Mr. Guo Kanghui and Ms. Xiong Beili for being such a hardworking students for their final year project.

I would like to appreciate the help of the Technical Executives whom have been helping me in many aspects especially Ms. Mah Sook Yee and Ms. Ervinna for helping me with all the hustle and bustle of doing purchasing work. I am also indebt with the help of Dr. Ong Teng Teng and Dr. Wang Xiujuan in running the characterization instruments.

I finally thank my parents and my relatives in Indonesia for their precious love and support through all the years. Thank you, Mom and Dad, for raising me up and always be there whenever I need you. The last but the most important, I want to thank Lord, Jesus Christ for all His grace and blessing that bestowed on me.

Table of Contents

List of Figures

List of Schemes

List of Tables

SUMMARY

The research work presented in this thesis is focused on the synthesis of electrocatalysts that contain less amount of platinum but with very high activity for fuel cell reactions to address the scarcity of Pt and its high overpotential during fuel cell operation. Firstly, Pt_{shell}-Au_{core} electrocatalysts with a controlled shell thickness have been successfully prepared using the successive reduction method. The physicochemical properties have been characterized and their activities have been tested for methanol oxidation reaction. It is found that due to the increase Pt utilization; this structure shows a 3-fold improvement higher than the conventional Pt/C for methanol electrooxidation.

Secondly, a novel structure of electrocatalysts, submonolayer Pt-decorated Au nanoparticles with a controlled surface coverage has been successfully prepared and it was found that this novel structure exhibits a remarkably high activity towards formic acid electrooxidation. The origin of the enhancement has been elucidated using electrochemical techniques and it is proposed that this novel structure shows high activity due to the "ensemble" effect and "electronic" effect where the decreasing availability of adjacent Pt atoms this structure posses is responsible for the first effect and the increase in the Pt-d band centre due to adding Au is responsible for the second effect. Moreover, a new reaction mechanism is proposed and the activity-stability-size relation has been studied to optimize the structure and size of this novel structure.

Finally, a facile preparation of Co_{core}-Pt_{shell} has been developed and it was found that pH has critical effect to obtain a well controlled composition of core-shell structure. This novel structure shows an increase in the activity of 4 times higher than that of Pt/C towards oxygen reduction reaction. It is hypothesized that the origin of the enhancement is due to the less defect and also due to the favorable Pt-Pt intermetallic distance that this structure possesses.

Keywords: electrocatalyst, core-shell, Pt-decorated Au, oxygen reduction reaction, formic acid, methanol oxidation reaction.

Chapter 1

Introduction and scope of the thesis

1.1. Introduction

As the number of cars, trucks and buses on the road increases, the need for alternative technologies to the internal combustion engine becomes ever more apparent. The largest of the world's oil reserves are in the politically unstable Middle East and in any event cannot last indefinitely. On the other hand, it is well known that the vehicle exhausts can cause health hazards, and concerns about emissions of the greenhouse gas carbon dioxide are also growing. Although vehicles are made more efficient and cleaner, the gains are being offset by the rapid growth in the total number of vehicles, particularly in Asian markets. According to the International Energy Agency,[1, 2] in 1996 around 634 million vehicles were on the road worldwide, an increase of almost 30 percent from a decade earlier; and totally 3.7 billion tons of carbon dioxide were emitted by them.

Automakers are investigating a variety of ways to reduce emissions drastically. Electrochemical fuel cells producing power for electric drive motors are now widely seen as a promising possibility. Unlike familiar dry cell batteries, which store a fixed amount of energy in their electrodes, fuel cells can run as long as fuel and oxidant are supplied-or at least until components in the cells degrade. One type of fuel cell that may potentially replace internal combustion engines in automobiles is Proton Exchange Membrane Fuel Cells (PEMFCs).

PEMFCs are typically classified based on the fuel which is being used like methanol, ethanol, formic acid or hydrogen. The usage of lower aliphatic alcohol and formic acid

are considerably safer and easier to store compared to hydrogen, but the applications still face several challenges due to the poor anode kinetics. A great deal of research has been focused on improving the poor anode kinetics mainly on improving the catalyst activity and durability.[2-4]

While many significant improvements have been made to enhance the catalyst activity, challenges still remain toward commercialization of PEMFCs. A key factor impeding the commercialization is its cost competitiveness where the predominant cost driver is the amount of precious metal being used. In order to reduce the usage of Pt and without lowering its activity, in this research we synthesize two kinds of structures which are core-shell and decorated structures with low platinum loading that can significantly reduce the amount of Pt usage while maintaining its high activity for fuel cell reactions such as methanol oxidation reaction, formic acid oxidation reaction and oxygen reduction reaction (ORR).

1.2. Scope of the thesis

As described in the previous section, the research work here is focused on the development of Pt based electrocatalyst with two types of nanostructures namely core-shell structure and decorated structure with low Pt loading. This study is directed on the development of different wet chemistry methodologies, which are successive reduction method and replacement reaction method. For the methanol oxidation reaction and formic acid oxidation reaction, Au metal was chosen as the core for the Pt deposition while for the ORR Co was chosen as the core for the Pt deposition.

Following the above explanations, the main work in this research is summarized as follows:

1) Synthesis and characterization of carbon supported Pt_{shell}-Au_{core} electrocatalysts for methanol oxidation reaction.
2) Synthesis and characterization of submonolayer Pt-decorated Au nanocatalysts for formic acid electrooxidation.
3) Study of the effect of Au particle size on the activity of Pt-decorated Au towards formic acid electrooxidation.
4) Study of the effect of reducing Au precursor onto the as-prepared Pt-decorated Au on the activity and stability of decorated structure during formic acid oxidation.
5) Synthesis and characterization of Co_{core}-Pt_{shell} electrocatalysts prepared by replacement reaction for oxygen reduction reaction.

Following the above summary, Chapter 2 provides the overview of PEMFCs and the state of the art catalysts used in methanol oxidation reaction, formic acid oxidation reaction and oxygen reduction reaction together with the fundamental mechanism involving these reactions on the surface of Pt electrocatalysts during fuel cell operations.

Chapter 3 presents the work on the preparation of Pt_{shell}-Au_{core} electrocatalysts and their activity for methanol oxidation reaction. It has been found that such a core-shell structure exhibits improved catalytic activity due to the high Pt utilization this structure possesses. The effect of different shell thickness was studied. It is found that core-shell catalysts with a complete and thin shell obtained at Pt/Au mole ratio of 1:1 shows an enhanced activity up to 3 times higher compared to that of Pt/C.

Chapter 4 presents the systematic study of Pt-decorated Au electrocatalyts and their activity for formic acid electrooxidation. The effect of different Pt/Au mole ratio

was studied ranging from Pt/Au 1:10 to 1:2. It is found that the specific activity of this structure increases with the decrease of Pt/Au mole ratio. This enhancement is attributed to the ensemble and electronic effect as revealed by the electrochemistry experiments. Moreover, a new formic acid eletrooxidation mechanism is proposed.

The size of the catalysts when reduced to nanoscale could affect their characteristic and activity.[5, 6] Hence, the effect of nanoparticle size together with the effect of adding more Au onto the Pt-decorated Au electrocatalysts is discussed in Chapter 5 in order to optimize the structure of the decorated structure. It is found that the durability of the catalysts increases with the decrease of size albeit with a lower initial activity. Also the effect of adding Au onto the Pt-decorated Au has been found to enhance the specific activity and increase the durability of the catalysts.

Chapter 6 presents the preparation of Co_{core}-Pt_{shell} electrocatalysts for ORR. It has been demonstrated that pH has critical effect for the optimum formation of this core shell structure, where a neutral pH is beneficial to prevent the extensive dissolution of Co nanoparticles without any subsequent deposition of the Co ions in the form of Co-oxide. It is found that the optimized structure of Co_{core}-Pt_{shell} exhibits an ORR specific activity of 4 times higher than that of Pt/C, which could originate from the favorable Pt-Pt interatomic distance that this catalyst possess.

Finally, Chapter 7 summarizes the findings and provides the directions and recommendations for future work.

Chapter 2

Literature review

2.1. Basics of fuel cell

Fuel cell is electrochemical device that directly convert chemical energy to electrical energy without taking the loop of heat production. It is similar to a conventional battery, but unlike the battery, the fuel for fuel cell must be fed continuously thus no time-consuming charging circuits are required as in a battery. It is the most attractive technology that can replace the common combustion engine because it is not limited to Carnot efficiency. However there are still a lot of obstacles that have to be overcome in order to commercialize the fuel cell technology.

Anode, electrolyte and cathode represent the main components of a single fuel cell. The output voltage of a single cell is limited by the Nernst potential of the two half-cell reactions on the two opposite electrodes. Electrochemical oxidation of the fuel occurs on the anode and the electrochemical reduction of the oxidant on the cathode. Ions generated from the electrochemical reduction or oxidation processes are transported through the electrolyte which is ionically conductive but electronically insulating. During the reaction, the electrons generated will flow through the external circuit thus producing electrical energy, while the ions generated will flow through the electrolyte from one side to the other side of the electrode thus completing the overall fuel cell reactions.[2-4, 7-9]

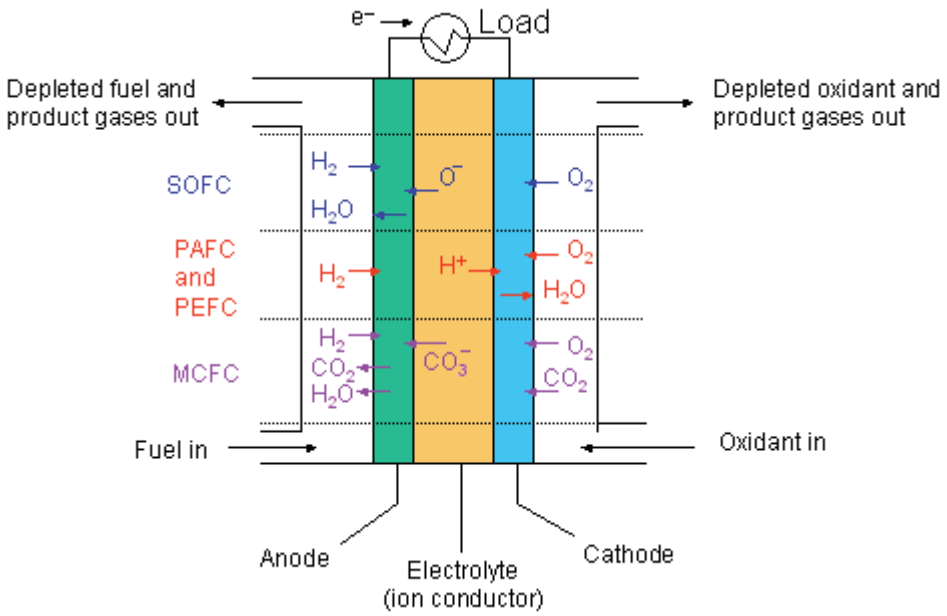

Fig. 2.1. Schematic drawing of Fuel Cells.

2.1.1. Types of fuel cells

Fig. 2.1 shows the operating principle of fuel cell for every type of fuel cell that is generally characterized by the electrolyte material. The electrolyte is the bridge for the ion exchange that generates electrical current. There are 5 types of fuel cells,[2-4, 7-9] which is listed in Table 2.1:

Table 2.1. Types of Fuel Cell

Type	Electrolyte	Operating temp.
Proton Exchange Membrane Fuel Cell (PEMFC)	Polymer Membrane	30-140°C
Alkaline Fuel Cell (AFC)	Potassium Hydroxide	150-200°C
Phosphoric Acid Fuel Cell (PFAC)	Phosphoric Acid	180-200°C
Molten Carbonate Fuel Cell (MCFC)	Lithium/Potassium Carbonate	650°C
Solid Oxide Fuel Cell (SOFC)	Yittria Stabilized Zirconia	1000°C

There is no single type of fuel cell that shadows others. But due to the low operating temperature, PEMFC is very attractive for automotive and portable applications.

2.1.2. Thermodynamic and kinetic considerations of fuel cell

The reversible cell electromotive force (emf) or $E_{0,cell}$ is defined as the difference between standard reduction potentials of the cathode and anode reactions ($E_{0,cathode}$ and $E_{0,anode}$). The actual value varies with the particular reactions that happen on both electrodes. For example for a PEMFC fueled with hydrogen the reversible cell emf is 1.23 V, and the Gibbs free energy change at standard conditions of the overall fuel cell reaction is always negative, representing a spontaneous process. This is the thermodynamic consideration of fuel cell process.[2-4, 7-9]

Ideally the cell voltage in fuel cell is independent of the current drawn, but because of the irreversibility or polarization that could develop during fuel cell operation, a completely reversible cell voltage can not be achieved. Overpotential is defined as the voltage difference between the reversible cell voltage based on the fuel cell reactions and the actual cell voltage at certain current density (total current divided by active electrode area). In fuel cells and most electrochemical system,[2-4, 7-9] the sources of overpotential are:

1. Losses due to the electrode kinetics limitation (activation overpotential), which are dominant at low current densities. For example, the sluggish kinetics of oxygen reduction reaction at the cathode has already caused 0.2 V open circuit potential loss.
2. Resistive losses from the electrodes and electrolyte (ohmic overpotential). These losses are prominent at intermediate current densities (~100 to 500 mA/cm^2)

3. Losses due to mass transport limitation in the gas-diffusion layer (concentration overpotential), which will dominate the potential loss at high current densities.

These overpotentials collectively cause the decrease of the actual cell voltage with the increase of the current density. A typical polarization curve (cell voltage vs. current density) for a PEMFC fueled with hydrogen is shown in Fig. 2.2.

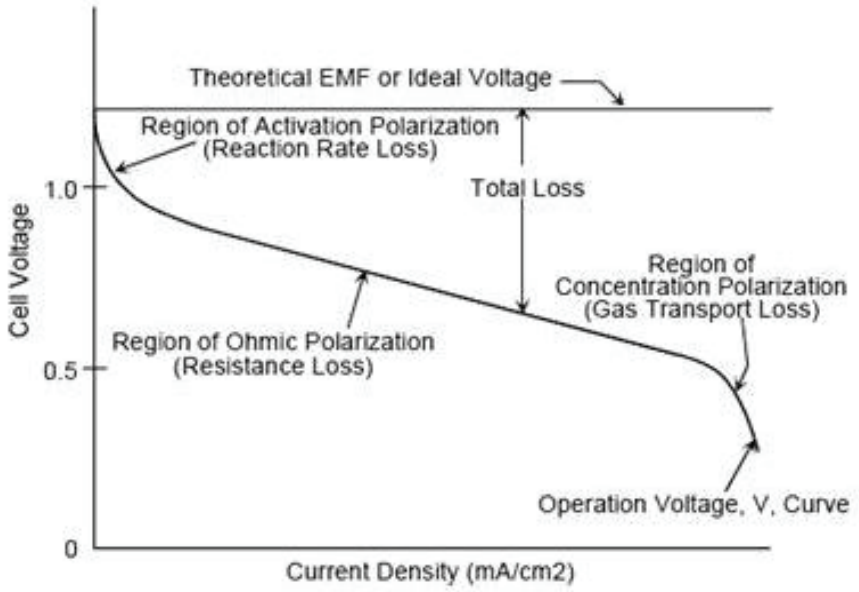

Fig. 2.2. Polarization curve of PEMFC fueled with H_2.

2.2. Proton exchange membrane fuel cell (PEMFC)

Proton Exchange Membrane (PEM) fuel cells are typically classified based on the fuel being used such as hydrogen based, Direct Methanol Fuel Cell (DMFC) and Direct Formic Acid Fuel Cell (DFAFC). Although hydrogen fuel cell has high efficiency and high power densities, the use of hydrogen always triggers safety concerns due to the difficulty in storing highly flammable gaseous H_2. On the other hand, methanol fueled fuel cells have advantages due to the storage easiness and fuel availability, but the

problem of slow anodic kinetics and high methanol crossover limit their potential use to low power density applications, such as portable appliances.[2-4, 7]

2.2.1. Methanol oxidation reaction (MOR)

Liquid fuels and/or oxidants can be used in a PEMFC. A type of PEMFC, the direct methanol fuel cell (DMFC), uses liquid methanol as the fuel. Methanol has a relatively high net energy density (5.26 kWh kg^{-1}) which exceeds that of pure H_2 (2.3 kWh kg^{-1}).[8, 10, 11] Methanol as a liquid fuel also has an important advantage in that the infrastructure for supporting a liquid fuel is already in place in terms of fuel pumping stations and fuel transportation, making the refueling of a liquid fuel cell easy and readily available. DMFC does suffer drawbacks. One of the most prevalent is the need for better catalysts for the anode, where methanol electro-oxidation is carried out. The electro-oxidation of methanol proceeds via a variety of intermediates, depending on the reaction conditions, thereby lowering the efficiency of the fuel cell and, in most cases, poisoning the catalyst surface with strongly bound carbon containing intermediate poisons, mainly carbon monoxide (CO).[8, 10]

The pathway of methanol oxidation has proven to be very complex on a smooth Pt_{poly} surface.[12-17] The complete oxidation of methanol in acid media is a $6e^-$ oxidation forming CO_2 as shown in the equation below for methanol electro-oxidation in acidic media:

$$CH_3OH + H_2O \rightarrow CO_2 + 6H^+ + 6e^-$$

While the complete oxidation of methanol yields CO_2 as the final product, at a bulk Pt_{poly} surface, the complete $6e^-$ oxidation seldom takes place unless a relatively high potential is applied. In the case of Pt the electrooxidation happens at 0.6 V. There are numerous intermediate products, including adsorbed poisons, formed during methanol oxidation. It

was suggested that methanol oxidation takes place in several steps, forming different species due to dissociation of the molecule[11, 18]:

$$CH_3OH \rightarrow Pt\text{-}CH_2OH + H^+ + e^-$$

$$Pt\text{-}CH_2OH \rightarrow Pt\text{-}CHOH + H^+ + e^-$$

$$Pt\text{-}CHOH \rightarrow Pt\text{-}COH + H^+ + e^-$$

$$Pt\text{-}COH \rightarrow Pt\text{-}CO + H^+ + e^-$$

Finally the strongly adsorbed CO on Pt sites will react with adsorbed OH to form CO_2 through Langmuir-Hinselwood mechanism as shown in the equation below:

$$Pt\text{-}CO + Pt\text{-}OH \rightarrow CO_2 + 2Pt + + H^+ + e^-$$

From the description of the mechanism of the oxidation of methanol given above, it is clear that modification of the adsorbed OH coverage is vital to the improvement of the overall oxidation performance, since the CO is strongly adsorbed on Pt sites and is difficult to oxidize at low potential.

2.2.2. Formic acid oxidation reaction

The formic acid electro-oxidation has attracted a lot of attention in the past decade because of the potential advantages of a direct formic acid fuel cell over a DMFC. The advantages are firstly formic acid normally exists as liquid at room temperature. Secondly, formic acid is non-explosive especially when dissolved in water, which makes the distribution, handling and storage easy, as compared to methanol and hydrogen. Thirdly, direct formic acid fuel cell does not suffer from the formic acid cross-over through the electrolyte membrane due to the anodic repulsion of formate anions and PEM.[19-22] Fourthly, it has a theoretical emf of 1.45V albeit with a lower power density of 1.74 kWh/kg with respect to methanol.[19-30]

It has been generally accepted that formic acid oxidation occurs via a dual path mechanism,[31, 32] i.e., a main dehydrogenation path involving reactive intermediate and a parallel path dehydration path involving adsorbed CO as a poisoning species, as shown on Fig. 2.3.

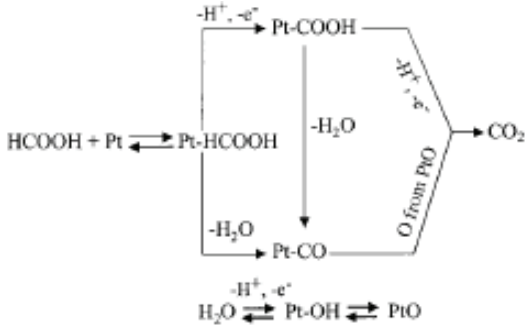

Fig. 2.3. Dual path mechanism for formic acid oxidation on the surface of Pt electrode.

While the dominating pathway on the Pt surface is the dissociative adsorption (dehydration) pathway that formed CO as the intermediate that eventually blocked the Pt sites. "The CO_{ads} can only be oxidized when Pt sites react with adsorbed water to form the Pt-OH. This shows that the desired pathway is the dehydrogenation that leads to the formation of CO_2 through reactive intermediates. Recently, it has been discovered by in situ time resolved Fourier transform infrared spectroscopy that formate (HCOO) is the reactive intermediate in the dehydrogenation pathway, instead of carboxylic acid (COOH) species."[33-36,157] From the description of the mechanism of the formic acid electrooxidation given, it is clear that a new type of catalyst that has high selectivity towards the dehydrogenation pathways is essential to the improvement of the overall oxidation performance since CO_{ads} can only be oxidized at high potentials.

2.2.3. Oxygen reduction reaction

Oxygen reduction is one of the most extensively studied electrochemical reactions due to its significance in both natural and industrial processes. Oxygen reduction is the

cathodic reaction in H_2/O_2 fuel cell, direct methanol fuel cell and direct formic acid fuel cell. However the slow kinetics of this reaction is an impediment in their development. Improvements in the efficiency of the oxygen reduction reaction would lead to an improvement in the overall efficiency of fuel cells.[2, 4, 7, 8]

The oxygen reduction reaction is a multi-electron reaction that may include a large number of intermediates and rate-determining steps involving various pathways. Although it is not the intent of this work to elaborate the mechanistic route of oxygen reduction reaction, it is useful to describe these mechanisms.[2, 4, 7]

The reduction of oxygen in acidic medium may proceed by two overall pathways:

1. The direct 4-electron pathway

   $O_2 + 4H^+ + 4e^- \rightarrow 2H_2O \quad E^o=1.229$ V

2. The peroxide pathway

   $O_2 + 2H^+ + 2e^- \rightarrow H_2O_2 \quad E^o=0.67$ V

   Followed by either the reduction of peroxide

   $H_2O_2 + 2H^+ + 2e^- \rightarrow 2H_2O \quad E^o=1.77$ V

   Or the decomposition of peroxide

   $2H_2O_2 \rightarrow 2H_2O + O_2$

Depending on the electrode material, oxygen reduction reaction may proceed by either pathway 1 or 2 or by a parallel pathway. Oxygen reduction reaction on Pt predominantly occurs via pathway 1.[2, 4, 7]

2.3. Electrocatalysts

At the heart of the PEMFC is the so-called membrane electrode assembly (MEA), which consists of two gas diffusion electrodes with catalyst layer sandwiched between a

proton exchange membrane. Typically, these components are made separately and then hot-pressed together under pressure. The most prominent cost of PEMFC lies on the electrocatalyst, where the most active catalysts are noble metals mainly Pt. That is why to commercialize PEMFC it is very important to reduce the high cost of catalyst without scarifying the activity.

2.3.1. Electrocatalysts for methanol oxidation reaction

For methanol oxidation reaction, Pt is still considered as the best catalyst because of its high intrinsic activity. The existence of CO is decreasing the Pt active site for MOR and this CO can bind strongly on the Pt active sites. The CO exists in the fuel because it can be generated with the existence of C and O atoms in methanol. This CO can be linearly bonded or bridge bonded to the Pt surface so that most of the active species are blocked. To overcome this low electrocatalytic activity of Pt, some approaches have been investigated mainly by incorporating ruthenium or tin. [12, 16, 17, 37-49]

It is reported that Ru can increase the rate of methanol adsorption, where the maximum CO adsorption can be reached more quickly on PtRu surface compared to a pure Pt surface at the same potential. Besides, due to the higher CO tolerance of PtRu, Ru's presence can lead to a faster CO oxidation than on pure Pt. According to the bifunctional mechanism, OH species can be generated on the Ru species from the water activation at low potential and oxidize the adsorbed CO species.[12, 16, 17, 37-39, 50, 51] Another possible explanation for the enhanced CO tolerance comes from the electronic effect where the electronic state of Pt is changed by the addition of Ru, leading to weaker Pt-CO bond.[52-54] It is possible that both mechanisms may work together. But recently

Wieckowski showed that the effect due to bifunctional mechanism was four times larger than the electronic (ligand) effect.[55]

The optimization of the atomic ratio of Pt/Ru, the structure of Pt/Ru, and the addition of a third alloying metal have been considered.[40, 41, 44, 45, 56-66] What is of great interest is the optimum Pt/Ru ratio. Some researchers believe that for methanol oxidation 1:1 Pt/Ru atomic ratio is optimal, [67, 68] while others proposed a ratio close to 80:20.[69, 70] This discrepancy likely comes from the different surface atomic compositions. Recently by depositing Ru atoms onto a smooth Pt electrode, Wieckowski group has found that the optimum Ru coverage for methanol oxidation is close to 40-50%.[54, 71]

2.3.2. Electrocatalysts for formic acid oxidation reaction

As mentioned in the previous chapter, the mechanism of formic acid oxidation in acid solution on the surfaces of Pt and Pt-group metal proceeds via a dual pathway mechanism, which is originally proposed by Capon and Parsons.[31, 32, 72, 73] Besides on Pt electrodes, the oxidation of formic acid was also for instance studied on single crystal Pt electrode, on rhodium, palladium, and gold.[73] Because Pt surfaces still suffer from the poisoning of CO_{ads}, the search for surface modifiers that can enhance the catalytic activity of Pt has been ongoing for decades. A variety of examples can be found in the review of Parsons and Vander-Noot[32] (prior to 1988) and Yu and Pickup[22] (before 2008). For example, ad-atoms such as Au, Mo, Ru, Cu, Ag, Ge, Sn, Pb, As, Sb, Bi, Se, or Te, have been tested as sources of possible catalytic enhancement.[20, 23, 27-29, 74-93] In particular, the modification by Pd as Pd ‘‘decorated’’ polycrystalline Pt surfaces, a Pt/Pd alloy, and

electrolytically deposited Pd on Pt single crystals have produced an enhanced reactivity.[76, 81, 87]

The ideal roles of the ad-atoms are to optimize the adsorption of HCOOH while oxidizing the poisoning species CO_{ads} and increasing the selectivity towards the dehydrogenation pathway where the poisonous species CO_{ads} does not form. The modification of Pt surfaces with ad-atoms such as Pb, Bi, Se and Te have produced an increase in the reactivity, where the enhancement induced by the ad-atoms has been explained by a ‘‘third body effect’’, that is the third body prevents chemisorbed CO, the surface poison, to form on the catalyst surface.[94]

2.3.3. Electrocatalysts for ORR

As already mentioned the ORR suffers from poor kinetics and this results in high polarization loss. The improvement of the overall fuel cell efficiency requires the finding of highly active catalysts more active than that of Pt/C. But the further requirements for the electrocatalysts like stability in harsh corrosive environment make noble metals most suitable and among them Pt shows the lowest overpotential. Therefore it is obvious why Pt has been used for the last two decades as the ORR catalyst. [95-97]

In order to search for an improved ORR catalyst with high noble metal loading while still maintaining the advantageous properties of Pt, such as relatively low overpotential, high stability, a variety of binary and even ternary Pt alloy catalysts have been investigated, where most of the alloyed metals with Pt are transition metals such as Co, Ni, Cu, Cr, Mo and Fe.[95-109] However all these transition metals dissolve from the electrocatalyst during fuel cell operation because of the strong tendency of transition metals to leave metal alloy crystal and form metal ions in acidic environment.

2.3.4. Advances in the preparation of core-shell electrocatalysts

In 1970, Turkevich et al had successfully grown Au on Pd nanoparticles to obtain Au-layered Pd nanoparticles;[110] this was the first attempt to prepare core-shell bimetallic nanoparticles ever reported. While in 1991, Schmidt et al prepared ligand stabilized Au-Pd and Au-Pt bimetallic nanoparticles by a successive reduction method; they did EDX measurement to prove the shell was rich with Pt or Pd;[111, 112] this was the first successful experiment with strong evidence that the core-shell structure was formed. Even though the core-shell structure has received much attention on heterogeneous catalysis, sensors and magnetic materials, not until in 2005 core-shell structure was introduced as a novel structure in electrocatalyst for fuel cell reaction.

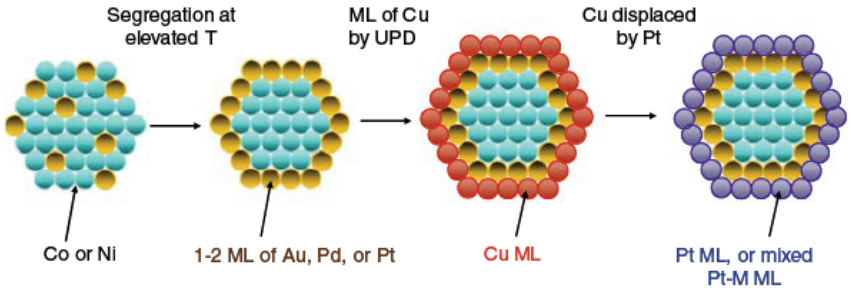

Scheme 2.1 Model for synthesizing Pt monolayer catalysts on non-noble metal-noble metal core-shell nanoparticles as proposed by Adzic group.

The first core-shell electrocatalyst for fuel cell reaction was reported by Adzic group.[113-124] They prepared a Pt monolayer on noble metal or non-noble metal nanoparticles and used them for O_2 reduction (see scheme 2.1). The electrocatalysts showed a very high activity toward O_2 reduction even though they only contain very small amount of Pt as the active metal. The Pt monolayer was prepared by galvanic displacement of a Cu monolayer deposited at underpotential. Geometric effects in the Pt monolayer and the effects of Pt-OH coverage, revealed by electrochemical data, X-ray

diffraction, and X-ray absorption spectroscopy data, appear to be the source of the enhanced catalytic activity. Although they obtained a very promising result, the size of the core nanoparticles was far too big so that a fully comparable activity to common electrocatalyst Pt/C can not be established because of the large difference in the active surface area. Moreover, the method they used here is an electrochemical method where it is less effective and less feasible compared to wet chemistry approach in terms of mass production of metal nanoparticles,.

Chapter 3

Pt_{shell}-Au_{core} electrocatalyst for methanol electro-oxidation

(Some parts of this chapter have been published in Ref. 157. The publisher, Elsevier, allows the inclusion of this article in the author's thesis.)

3.1. Introduction

Bimetallic Core-shell nanoparticles have attracted a lot attention due to their unique structure and activity for catalysts, sensors, magnetic materials and so on.[111, 112, 125, 126] "The enhanced activity of core-shell structure is related to the underlying interface between the core and shell metals where the core metal modifies the electronic properties of the shell metal.[113, 120, 124, 127-130] Another advantage of core-shell structure is the reduced usage of shell metal by replacing the buried core atoms of expensive metal nanoparticles with a different metal, as only surface atoms are directly involved in the catalysis. One important example is gold and platinum bimetallic nanoparticles. In fuel cell applications, Pt is regarded as the most important metal due to its high activity toward the electrooxidation of fuels such as hydrogen, ethanol and methanol. Due to its limited nature reserve and high cost, the usage of Pt in fuel cell application has to be reduced before this technology can be commercialized.[98]

One of the most promising ways to reduce the amount of Pt is by replacing the buried core metal with another metal to form the so-called core-shell structure.[160] Adzic group is one of the first groups introducing the use of Cu UPD and subsequent replacement with Pt to prepare Pt-based core-shell structure.[116, 119, 120] Recently this approach has been extended by Papadimitriou et al by surface replacement of the electrodeposited non-noble metal (Cu, Co, Ni and Fe) on glassy carbon with noble metals

(Pt and Au).[131-133] Such a novel structure exhibits high electrocatalytic activity for oxygen reduction reaction (ORR) and methanol oxidation reaction with significantly less amount of Pt being used compared to conventional Pt/C. However these two approaches use electrochemical methods which is not feasible for mass production of nanoparticles.

In this chapter, our objective is to synthesize a well defined nanoscale Au_{core}-Pt_{shell} on carbon support with a controlled shell thickness and improved Pt utilization as a novel electrocatalyst for fuel cell reaction. The core-shell structure is realized via a successive reduction strategy and by carefully choosing an appropriate reducing agent. The formation of core-shell structure is suggested by various techniques, including TEM, XRD, UV-vis, TGA, EDX and electrochemical technique. By controlling the shell thickness the enhancing effects of Au can be probed based on the layer thickness of Pt.

3.2. Experimental and characterization methods

3.2.1. Materials

Hydrogen tetrachloroaurate (III) trihydrate, hydrogen hexachloroplatinate (IV) hydrate and sodium borohydride were purchased from Aldrich; sodium citrate tribasic dihydrate from Fluka; hydroxylammonium chloride from Merck; sulphuric acid and methanol from Merck.

3.2.2. Preparation of Au seed

The Au seed preparation was based on the protocol developed by Grabar et al.[134] Briefly, 1 mL of 1% aqueous $HAuCl_4 \cdot 3H_2O$ was added to 100 mL of H_2O with vigorous stirring, followed by the addition of 1 mL of 1% aqueous $Na_3C_6H_5O_7$ (freshly prepared) one minute later. After an additional one minute, 1 mL of 0.075% $NaBH_4$ (freshly

prepared) in 1% $Na_3C_6H_5O_7$ was added. The stirring was continued for 5 minutes and then the Au colloidal seed was stored at 4°C until needed. [157]

3.2.3. Reduction and growth of Pt on Au surface and subsequent assembly on carbon support

Briefly, a certain amount of 0.1% aqueous H_2PtCl_6 and 0.1% aqueous $NH_2OH{\cdot}HCl$ was mixed with 100 mL water under vigorous stirring and heated to 60°C for 3 hours. A 5 fold molar ratio of $NH_2OH{\cdot}HCl$ over H_2PtCl_6 was chosen to ensure a complete reduction of H_2PtCl_6. No color change was observed during this period. Then the gold seed solution was added and the temperature was held constant at 60°C for 2 hours. After 2 hours the solution was cooled to room temperature. The deposition of the nanoparticles on carbon black was realized by mixing the as prepared nanoparticles solution with slurry of carbon black Vulcan XC-72. Briefly, a certain amount of carbon was mixed with 5 mL water and sonicated for 5 minutes with an ultrasonicator. After that, it was added to the nanoparticle solution prepared above and followed by continuous stirring overnight. The suspension was then filtered and washed with copious water. The final product was then obtained by vacuum drying at 70°C for 12 hours. [157]

3.2.4. Characterization and electrochemical measurements

X-ray diffraction (XRD) measurements were performed on a D8 Bruker AXS X-ray diffractometer using Cu Kα radiation 0.1542 nm at 40kV, 20mA, with a continuous scanning from 20° to 90° at a scan rate of 0.025°/s. The samples for XRD analysis were put on a Si (911) sample holder. The UV-vis spectra of the Au and PtAu hydrosols were measured by a Shimadzu UV2450 spectrometer equipped with quartz cells. The concentration of Au in Au hydrosol and Pt-Au hydrosols was 8×10^{-2} mM. Particle size

and morphology of samples were observed using JEOL 3010 transmission electron microscopy (TEM) at 200kV. The samples were dispersed in ethanol under sonication and then dropped onto a carbon-coated copper grid, followed by the evaporation of the solvent in air at room temperature. Thermogravimetric analysis (TGA) was performed on a TA instrument SDT Q600 to determine the total metal loading on carbon black. Typical samples weighed ~5 mg were heated on a platinum pan with a flow of 100mL/min of air under constant heating rate of 10^{o}C/min. The composition analysis using energy dispersive X-ray spectroscopy (EDX) was performed using a scanning electron microscopy JEOL JSM-6390LA operating at 20 kV. The electrochemical signals were recorded with Autolab PGSTAT302 potentiostat (Eco Chemie, Netherlands). The blank voltammograms were studied in deaerated 0.5 M H_2SO_4 and methanol oxidation was carried out in deaerated 1 M CH_3OH + 0.5 M H_2SO_4. High-purity nitrogen was used for solution deaeration. Electrode potentials were measured and reported against a saturated calomel electrode (SCE) placed close to the working electrode. The counter electrode was Pt wire. The working electrode was prepared based on a protocol developed by Schmidt et al.[135] 10μL of catalyst ink was deposited via a microsyringe onto the surface of a glassy carbon disk (Pine instrument, 5 mm diameter, 0.196 cm^2). The catalyst ink was produced by dispersing 8.0 mg of 20% Au/C, Pt/C and PtAu/C with ultrasonicator in 4.0 ml ethanol for 20 minutes. After drying the catalyst ink, another 10μL of 0.05% Nafion solution (diluted from 5% commercial solution with isopropanol) was dropped on top of the disk to fix the catalyst powders. [157]

3.2.5. Preparation of conventional Pt/C

Pt/C was prepared based on previous procedure[136] with slight modifications such as 20% Pt loading instead of 10 % and the whole preparation was done without Ar environment. Briefly, 80 mg of carbon black was suspended in 100 mL ethylene glycol solution; then 54 mg of $H_2PtCl_6.6H_2O$ dissolved in 50 mL ethylene glycol was added to the solution dropwise. NaOH (2.5 M in ethylene glycol) was added to adjust the pH of the solution to above 13 and then the solution was heated at 140^{o}C for 3 hours under reflux. The solid was filtered and washed with copious DI water and then dried at 70^{o}C overnight."[157]

3.3. Results and discussion

3.3.1. Au nanoparticles as the seed

Au seeds with average size of 4.8 nm were synthesized based on the previous reported protocol by Grabar et al. [134] The overall chemical reactions for the preparation of this Au hydrosol are given below:

$$NaBH_4 + HAuCl_4 + 3H_2O \rightarrow Au + H_3BO_3 + 3HCl + NaCl + 2.5H_2$$

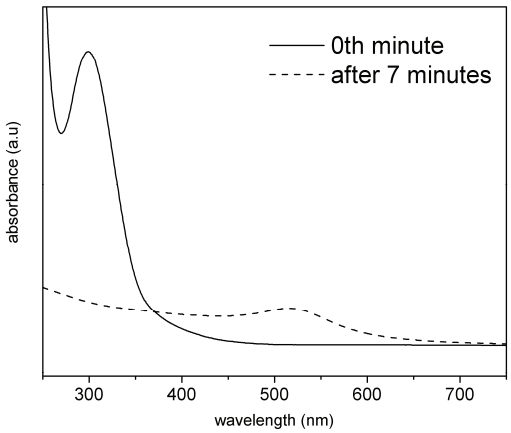

Fig. 3.1. UV-vis spectra of $HAuCl_4$ aqueous solution before (0th minute) and after reaction (after 7 minutes).

During the experiment, the color of the solution changed quite fast after adding the $NaBH_4$ from slightly yellow into dark wine. This shows that $HAuCl_4$ is readily reduced by $NaBH_4$ at room temperature. The successful reduction of the $AuCl_4^-$ to Au hydrosol was verified by UV-vis spectroscopy. As shown in Fig. 3.1, the strong absorption peak at 294 nm is attributed to the absorption of $AuCl_4^-$ near the red region wavelength.[137, 138] Before the reaction this peak could be observed but after only 7 minutes of reaction (dash line), this absorption peak vanished. Instead, a weak absorption peak at 511 nm that belongs to Au hydrosol was observed.[137, 138] This shows that the reaction time and the amount of reducing agent ($NaBH_4$) are enough to reduce all the $AuCl^{4-}$ to Au zerovalent.

The Au nanoparticles were further characterized using TEM. The TEM image of Au nanoparticles on carbon black and the particle size distribution are shown in Fig. 3.2. "It can be seen that the Au shape is spherical and dispersed well on carbon black with a mean diameter of 4.8 nm.

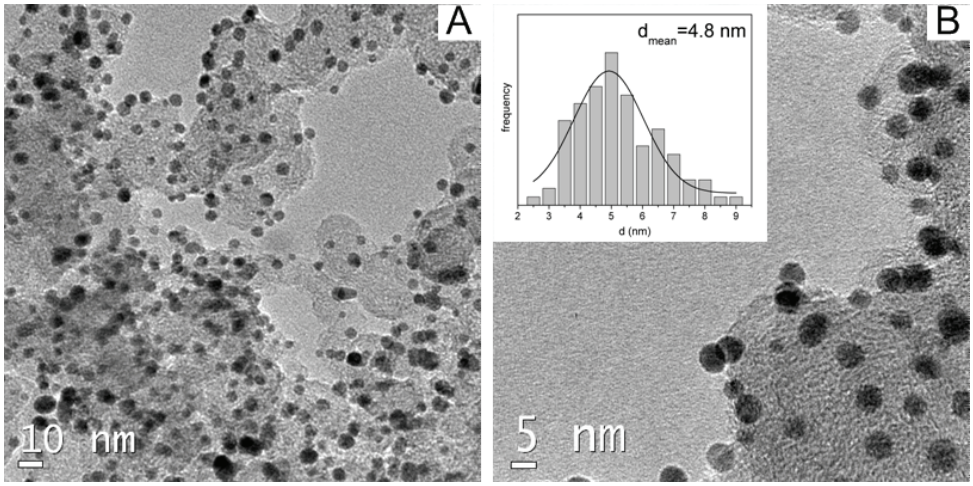

Fig. 3.2. TEM images of Au nanoparticles on carbon black, A) large section; B) small section. The inset in B shows the particle size distribution.

3.3.2. Pt_{shell}-Au_{core} electrocatalysts

To deposit platinum on the surface of Au, $NH_2OH{\cdot}HCl$ was carefully chosen as the reducing agent because it has been known that $NH_2OH{\cdot}HCl$ acts only as a growth agent in slightly acid environment without forming a new nucleus.[110-112] During the heating pre-treatment where H_2PtCl_6 aqueous solution and $NH_2OH{\cdot}HCl$ aqueous solution were mixed, neither color change nor precipitation was observed. This strongly suggests that $NH_2OH{\cdot}HCl$ only acts as the growth agent in the presence of preformed nucleus. The addition sequence is of critical importance in the experiment, e.g. adding of Au seeds into the solution during preheating stage will lead to the coarsening of Au seeds. The one reported in this work gave the most uniform dispersion.

The final size of the Pt-Au nanoparticles based on the nominal Pt/Au ratio in the precursor solutions can be calculated according to this relation.[125, 139]

$$D=D_{core}\left(1+\frac{V_{Pt}[Pt]}{V_{Au}[Au]}\right)^{\frac{1}{3}}$$

Table 3.1. Properties of nanoparticles prepared with different Pt/Au mole ratios."

Pt/Au mole ratio	measured particle size (nm)	calculated particle size (nm)	calculated shell thickness (nm)	Pt specific surface area normalized by that of Pt/C
0	4.8	-	-	-
1:2	5.4	5.43	0.31	3.2
1:1	6	5.94	0.57	4.9
2:1	7	6.75	0.98	3.2
3:1	7.5	7.41	1.30	1.9
4:1	8.2	7.97	1.58	1.3

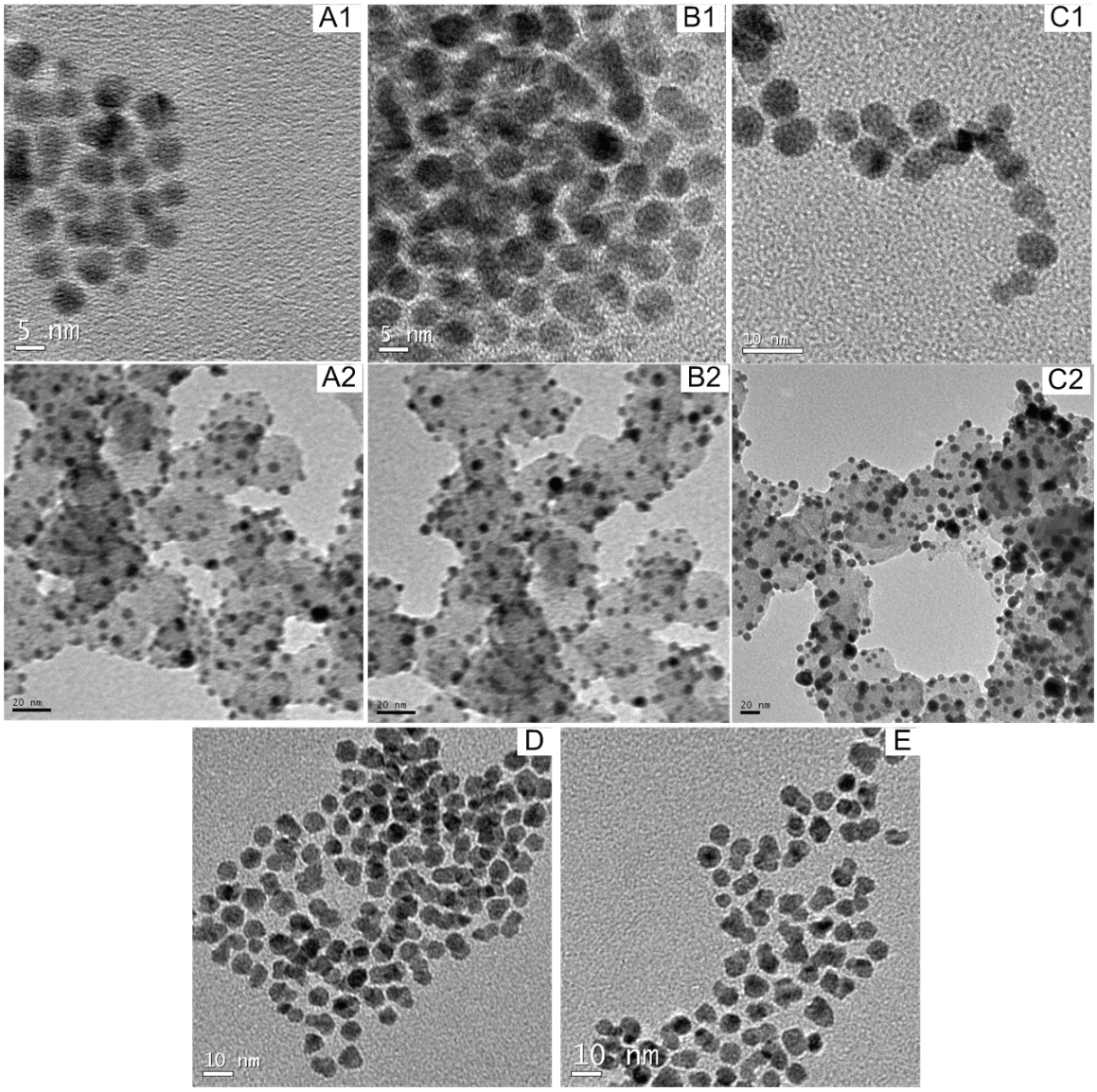

Fig. 3.3. TEM images of the representative samples: A1) Pt/Au=1:2 hydrosol; A2) Pt/Au=1:2 on carbon; B1) Pt/Au=1:1 hydrosol; B2) Pt/Au=1:1 on carbon; C1) Pt/Au=2:1 hydrosol; C2) Pt/Au=2:1 on carbon; D) Pt/Au=3:1 hydrosol; E) Pt/Au=4:1 hydrosol.

Where D_{core} is the diameter of Au seeds as determined by TEM analysis, the V_m's are the mole volumes and the []'s are the overall concentrations of the two metals involved. "By changing the precursor Pt-Au mole ratio and keeping the amount of Au seeds constant, the Pt shell thickness can be controlled and estimated by $(D-D_{core})/2$. Table 3.1 shows the calculated average particle size, shell thickness and specific surface area of Pt normalized with that of Pt/C for different ratios of Pt/Au." [157]

TEM was first conducted to examine the particle size and morphology of the PtAu catalysts. Fig. 3.3 shows typical TEM pictures of the PtAu nanoparticles hydrosols and PtAu nanoparticles supported on carbon black with various mole ratios. The catalyst preparation included the assembly of the nanoparticles on carbon black. It can be seen from Fig.3.3. (Part A2, B2 and C2) that the as prepared nanoparticles can be easily loaded onto carbon black. It can also be seen that all the prepared catalysts are well dispersed without agglomeration, as a result of the stabilizing effect of the acetate ions, since nanoparticles have the ability to adsorb negatively charge ions.

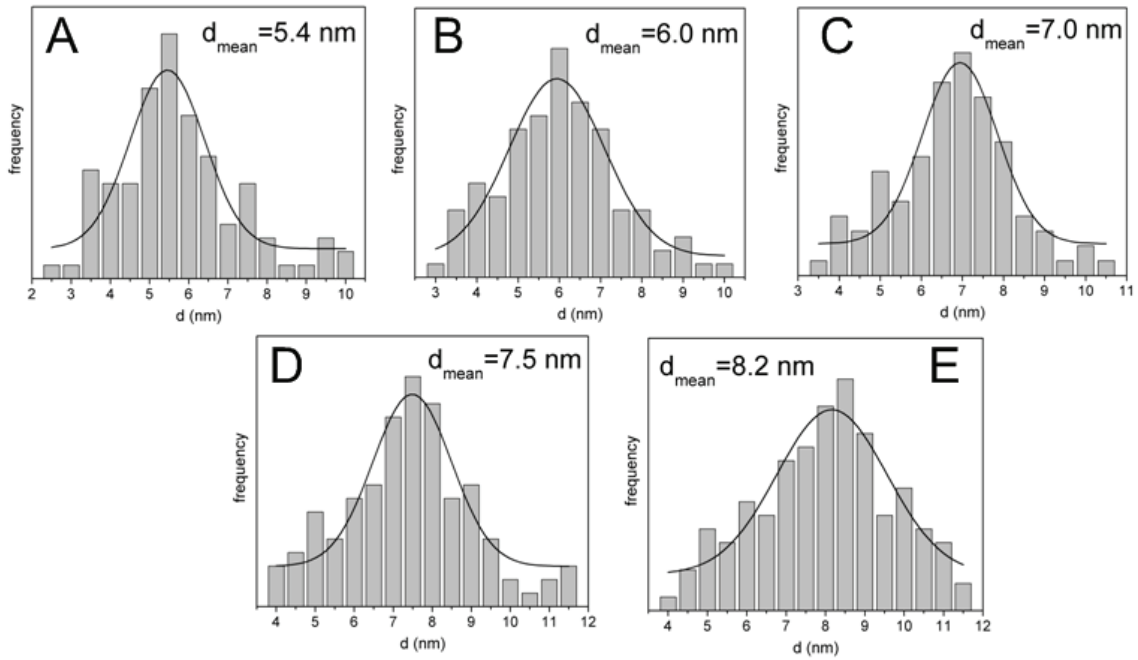

Fig. 3.4. Particle size distribution based on TEM of representative samples: A) Pt/Au=1:2; B) Pt/Au=1:1; C) Pt/Au=2:1; D) Pt/Au=3:1; E) Pt/Au=4:1.

"The stack diagrams of the particle size distribution (Fig. 3.4) include analysis of several different catalyst regions and quantification of the size of roughly 400 particles per catalyst. They reflect quantitatively the uniformity of the distribution with their distinct mean particle diameter. It becomes evident that with the increase of Pt/Au mole ratio, the mean particle size of the nanoparticles also increases. The measured mean

particle size for all the ratios agrees quite well with the calculated value as listed in Table 3.1. The core and shell components on PtAu nanoparticles are not easily differentiable because Au and Pt exhibit the same imaging contrast and have the same crystal structure. But the size increment before and after Pt deposition can be clearly seen. This, together with the similarity between measured mean particle size and calculated size, indicate that the Pt grows on the surface of Au, not forming its own nucleus." [157,160]

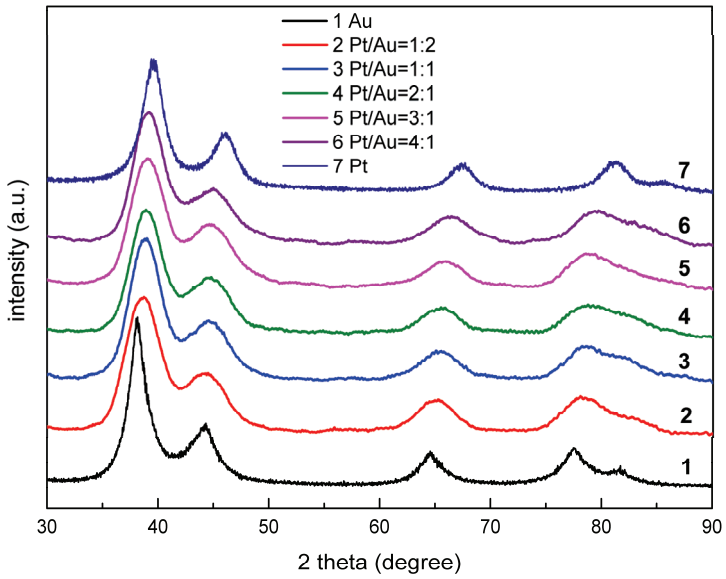

Fig. 3.5. XRD patterns of Au/C, Pt/C and various PtAu/C.

XRD spectra of the monometallic Au/C and Pt/C nanoparticles and the PtAu/C bimetallic nanoparticles are shown in Fig. 3.5. The characteristic peaks of fcc Au (2θ=38.2°, 44.4 ° and 64.6 °) and fcc Pt (2θ=39.8 °, 46.2 ° and 67.6 °) marked by their indices (111), (200) and (220) were observed for the monometallic catalysts. While for PtAu/C at the lowest Pt/Au ratio (1:2), the spectra resemble the core metal spectra. But a closer look at the diffraction peaks of Pt/Au=1:2 reveals that the corresponding peak widths are not symmetric and the intensity was increased in the middle position between the pure Au peaks and pure Pt peaks, for example at 2 theta range of 64°-66° besides the

Au (220) peak at 64.6° another peak at 65.3° could also be seen. This observation suggests the presence of Pt phase on Au nanoparticles. Since there are 2 different phases on the PtAu nanoparticles, the Scherrer formula using XRD data can not be used to estimate the average particle size which can be obviously seen from the width of the peaks of PtAu nanoparticles where they are all broader compared to that of Au/C. [157]

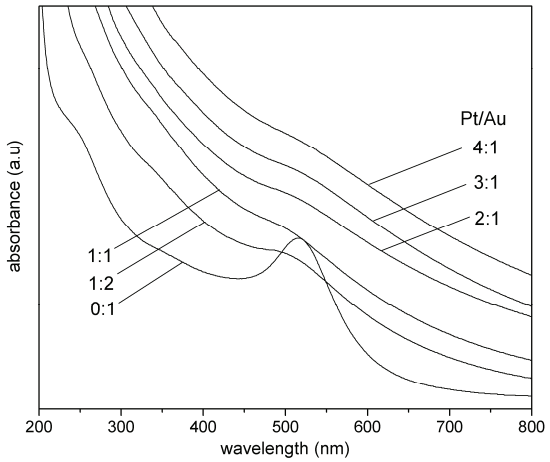

Fig. 3.6. UV-vis spectra of PtAu hydrosols with different Pt/Au mole ratios.

"Absorption spectra of Au hydrosol and Pt-Au hydrosols are shown on Fig. 3.6. The absorption peak at 511 nm due to the surface plasmon resonance of Au can be clearly observed for Au hydrosol. The continuous increase of the absorption intensity at lower wavelength with the increase of Pt/Au ratio is attributed to the increasing amount of Pt deposited on Au.[139, 140] For the PtAu hydrosol with 1:2 mole ratio, the Au plasmon absorption peaks become damped and shifted to a lower wavelength located at c.a 500 nm. This indicates that almost all the Au surface has been covered with Pt. While for the Pt/Au ratio 1:1 and higher, the Au plasmon absorption peak can be considered to be vanished. This suppression with the increase of Pt-Au ratio indicates a continuous increase in the shell thickness, consistent with the TEM analysis. [157]

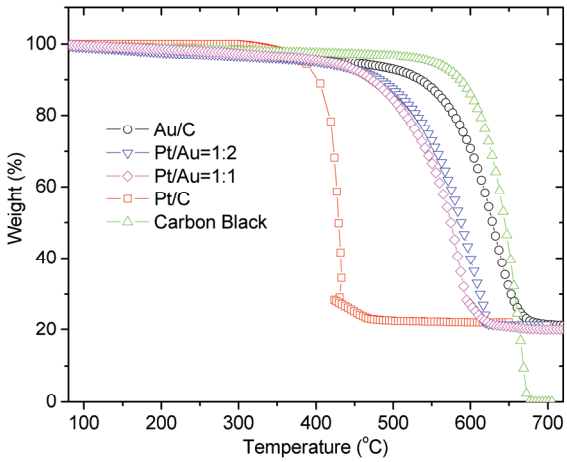

Fig. 3.7. TGA curves for Au/C, Pt/C, various PtAu/C and carbon black

To verify the loading of the nanoparticles on carbon black and the atomic compositions, TGA experiment and EDX experiment were conducted and the results are shown in Fig. 3.7 and 3.8 respectively. From the mass change in Fig. 3.7, all the metal loadings are close to the nominal loading (20%) showing the successful reduction of all the metal precursors and subsequent deposition onto carbon black.

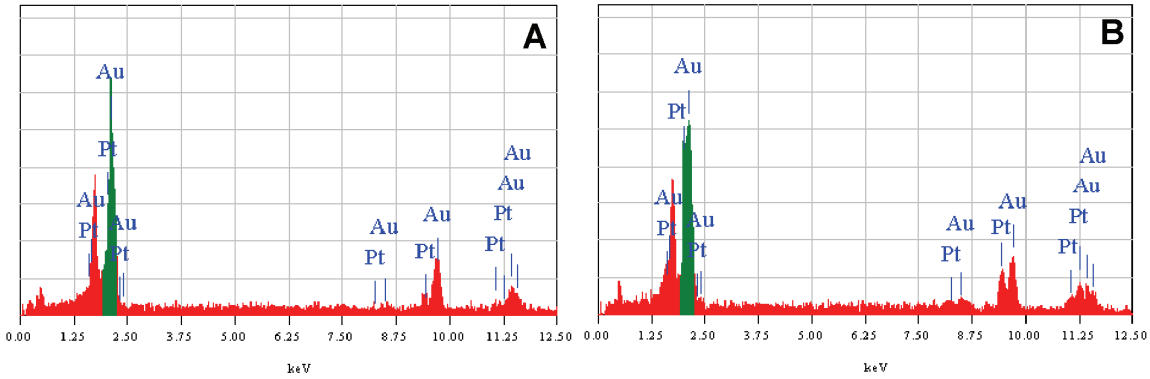

Fig. 3.8. The EDX spectrum of A) Pt/Au=1:2 and B) Pt/Au=1:1

The EDX spectrum in Fig. 3.8 confirms the presence of Pt and Au in Pt/Au=1;2 and Pt/Au=1:1. By quantitative EDX analysis, the corresponding average Pt/Au mole ratios are 1:2.1 and 1:0.98 for Pt/Au=1:2 and Pt/Au=1:1 respectively, which are quite close to the nominal ratios.

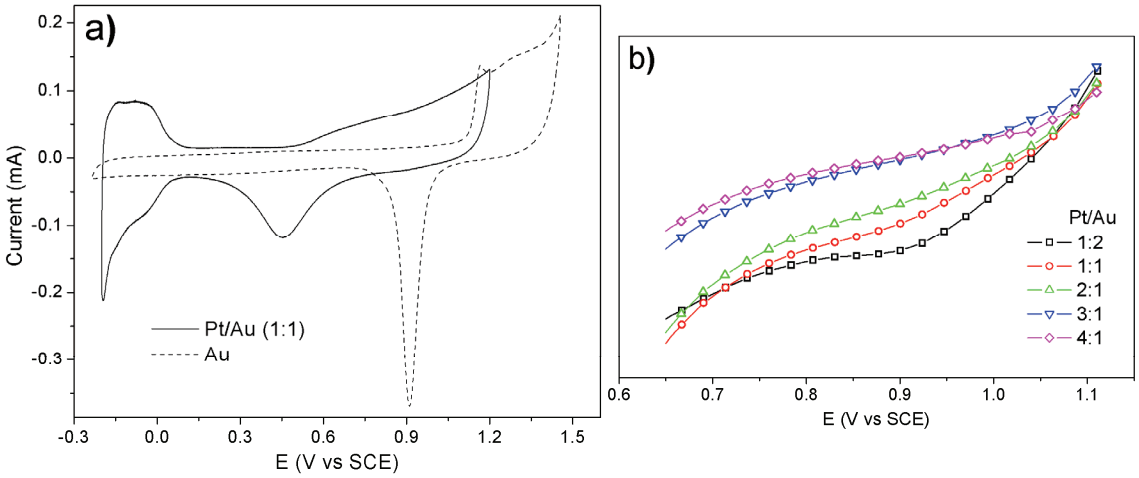

Fig. 3.9. a) CV of Au/C and PtAu/C (1:1) and b) cathodic scan of the CV of PtAu/C with different mole ratios in the range of 0.6-1.2 V. Scan rate 50mV.s^{-1}, in 0.5 M H_2SO_4.

Solid evidence for the homogeneity of the Pt coating comes from cyclic voltammetry (CV) as it can be regarded as a surface sensitive technique that only detects the electrochemical properties of surface atoms rather than bulk atoms. Fig. 3.9 shows the representative cyclic voltammograms for Au/C and PtAu/C. For Au/C the upper limit potential was 1.45 V while for PtAu/C was 1.2 V. The Au/C scan showed a typical voltammetric response of Au surface in acidic condition, including the oxide formation at c.a 1.1 V, oxide stripping at ~ 0.9 V and a flat, double layer region until 1 V.[141] For the PtAu/C (1:1) the above Au features are not observed. Instead, the typical features of Pt are observed which are: the broad oxidation peak, the sharp reduction peak at ~ 0.5 V and the hydrogen adsorption desorption peaks at low potential. This indicates that the entire Au surface has already been covered with Pt.[142, 143] To prevent the Pt anodic dissolution that can change the quality of the Pt coating, the upper limit potential for the PtAu/C was lower compared to Au/C, but it is still high enough for the observation of Au oxidation as indicated in Fig. 3.9.

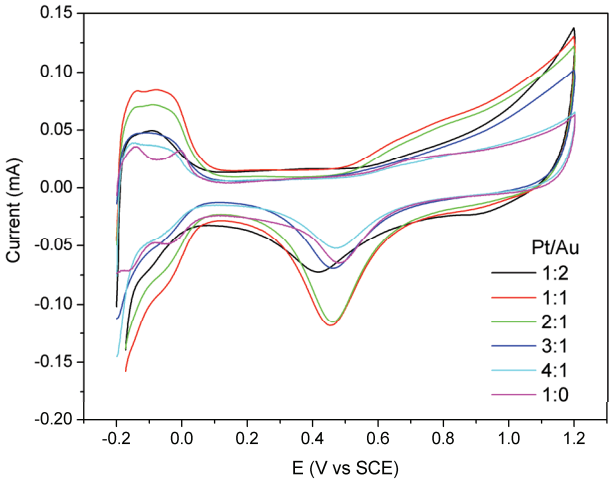

Fig. 3.10. CV of 20% Pt/C and PtAu/C with different mole ratios in 0.5 M H_2SO_4 at 50 mVs^{-1}.

Even more interesting is the quality of the Pt coating with various Pt/Au mole ratios as analyzed from CV result. To make a clear observation of the plots, only the cathodic scans of selected potential range of interest are presented. As shown in Fig. 3.9 part b, for the Pt-Au ratio of 1:2, the Au oxide reduction peak at 0.9 V still can be observed. This shows that there are some exposed Au sites, which is consistent with the UV-Vis observation. While for the higher Pt/Au ratio, the Au oxide peak is not observed, suggesting a complete shell of Pt has already covered the Au surface. The calculated shell thickness for the ratio of 1:2 is 0.31 nm which is bigger than the Pt atomic diameter of 0.278 nm.[144] If the growth of Pt on Au seed is epitaxial, this ratio should be enough to form a complete monolayer of Pt. The still observed Au suggests that the Pt growth is not fully epitaxial, although Pt and Au all have cubic closed pack structure. Probably Pt clusters or islands were formed first on the Au seed surface. Further growth with the increase of the Pt/Au ratio then fill the gaps between these islands to form a complete coverage. This suggests that the Pt surface has stronger activity compared to the Au surface for the reduction of $PtCl_6^{2}$.

To demonstrate the improved utilization of Pt in the core-shell structure compared with conventional Pt/C, the Pt electrochemical surface area (ECSA) of all the catalysts in Fig. 3.10, was measured by integrating the hydrogen desorption region. The specific surface area was then obtained by dividing the ECSA with Pt weight and reported in Table 3.1 after normalization to the value of the Pt/C. It can be seen that all core shell catalysts show improved specific surface area than Pt/C because of the improved Pt dispersion, although the latter has much smaller size.

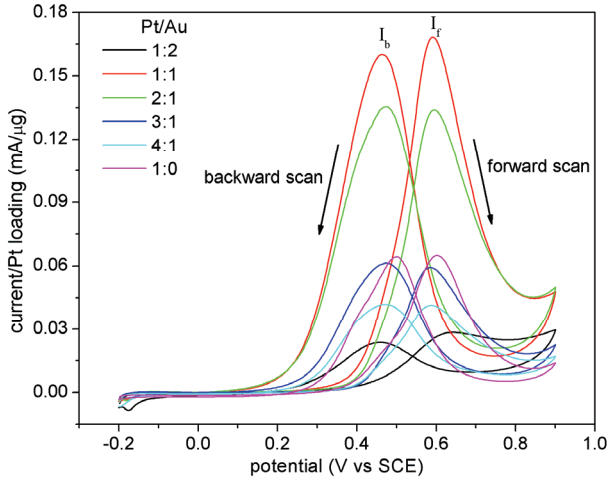

Fig. 3.11. CV of Pt/C and PtAu/C with different mole ratios at 10 mVs^{-1} in 1 M CH_3OH + 0.5 M H_2SO_4

The electrocatalytic activities of PtAu/C were tested in aqueous solution of 1 M CH_3OH + 0.5 M H_2SO_4 at room temperature and normalized with the Pt loading (Fig. 3.11). The specific catalytic activity of Pt, represented by the forward peak current, decreases with the increase of Pt-Au ratio, in agreement with the trend of normalized measured specific area in Fig. 3.10 and calculated values in Table 3.1. Considering that only surface atoms are active as catalyst for reaction, this can be explained by the fact that surface atomic ratios of Pt is higher with thinner shell (lower Pt/Au ratio). As a result

of this improved dispersion, the specific activity of Pt at Pt/Au ratio of 2:1 and 1:1 are two to three times better than Pt/C. While for the higher mole ratios, the activities were almost the same or slightly lower compare to Pt/C because of the comparable specific surface area (Table 3.1). As for the PtAu/C (1:2), much lower activity was observed. This may be explained by the fact that not enough continuous Pt atoms available to conduct the dehydrogenation of methanol on the surface of Au, since several continuous atoms of Pt (neighbouring sites) are needed for the methanol oxidation.[145] Another explanation may come by the fact that at this mole ratio some of the Au sites are still exposed and based on the DFT calculation, this exposed Au surface leads to a stronger CO adsorption on Pt sites that block the continuous dehydrogenation reaction.[146] A closer look at the peak potential on the forward scan indicates that PtAu/C catalysts that form a complete Pt shell show a negative shift compared to that of Pt/C (see Table 3.2). This shows that Au as the core metals has a positive effect for the methanol oxidation, when the Pt overlayer forms a complete shell.

Table 3.2. Forward peak potentials and I_f/I_b ratios of Pt/C and various PtAu/C

Catalyst	Peak potential (V)	I_f/I_b ratio
Pt/C	0.60	1.01
PtAu/C (1:2)	na[a]	na[a]
PtAu/C (1:1)	0.58	1.06
PtAu/C (2:1)	0.58	0.98
PtAu/C (3:1)	0.58	0.97
PtAu/C (4:1)	0.58	0.98

[a]: not applicable because the forward peak is not apparent.

Another important factor for evaluating an electrocatalyst activity for methanol electrooxidation is its resistance to carbonaceous species accumulation. This can be identified by the ratio of forward peak current density (I_f) to the backward peak current density (I_b), where a higher I_f/I_b means the electrocatalyst is less susceptible to poisoning. This value is 1.06 for PtAu/C (1:1), while for the rest PtAu/C and Pt/C this value is lower

and close to 1 as shown in table 3.2. The enhanced activity and a greater resistance to carbonaceous species accumulation for PtAu/C (1:1) compared to other PtAu/C and Pt/C indicates that the activity of PtAu/C towards methanol oxidation is highly dependent on the Pt shell thickness, where a thin shell is superior to the others.

3.4. Conclusions

In summary, Pt_{shell}-Au_{core}/C with a controlled shell thickness was successfully synthesized based on a successive reduction strategy. The formation of core-shell structure has been suggested by various techniques including TEM, XRD, UV-vis, TGA, EDX and electrochemical techniques. The electrocatalytic activity was tested using methanol oxidation reaction as a probe. Core-shell catalysts with a complete and thin shell of Pt on Au shows an enhanced catalytic activity than Pt/C, as a result of improved Pt utilization."

Chapter 4

Highly efficient submonolayer Pt-decorated Au nanoparticles for formic acid electro-oxidation

(Some parts of this chapter have been published in Ref. 159, 160. The publisher, Elsevier, allows the inclusion of these articles in the author's thesis.)

4.1. Introduction

"Recently intense research has focused on alternative energy technologies that can reduce the dependence on fossil fuels and also reduce the pollution from these fossil fuels. Fuel cells are one of the most promising candidates and have the potential to be used in various applications. For small portable applications, small organic molecules with considerable hydrogen to carbon ratio like methanol, ethanol and formic acid are the potential fuels because the handling and storage of these liquid fuels are easier and safer compared to pure H_2.[10, 32] But these molecules also have some disadvantages where self poisoning and slow reaction kinetics limit their fuel cell performance.[32, 98] With Pt as the most commonly used metal for the catalyst material and with methanol and formic acid as the fuels, it was shown that the intermediate CO_{ads} is the species that poisons the catalytically active electrode surface even at low potentials.[31, 32, 147-149]

To improve the catalyst performance, combinations of Pt and other metals has been studied extensively. Pt based alloy catalyst such as PtRu, PtFe, PtPd, PtBi have been studied and it is generally accepted that the enhancement of the activity of these metals compared to pure Pt is due to the bifunctional and/or electronic effect.[150-156] However the effect of alloying is limited by many parameters and most importantly the usage of Pt for these alloy catalysts is still considered too much for commercial applications. For

example PtRu alloy with 1:1 mole ratio and PtFe alloy with 1:1 mole ratio showed the highest catalytic activity for methanol and formic acid oxidation respectively.[153, 154]

In this chapter as a continuation of last chapter's work on Pt_{shell}-Au_{core}/C,[157] we report the synthesis of a novel electrocatalyst, submonolayer Pt-decorated Au nanoparticles on carbon black support using a wet chemistry approach.[158-160] This catalyst shows a significantly improved activity toward formic acid oxidation with much lower Pt loading compared to Pt/C where it facilitates the direct oxidation of formic acid and suppresses the formation of CO_{ads}. In this study, the Pt-decorated Au catalyst with different Pt:Au mole ratios were prepared to study the effect of different Pt/Au composition and we address the origin of the high activity for formic acid oxidation using electrochemical methods. In order to study the inhibition of self poisoning during the reaction and establish the origin of the enhancement, a series of cyclic voltammogram experiments for formic acid and methanol oxidation were conducted. Finally, electrochemical impedance spectroscopy (EIS) was performed to elucidate the formic acid oxidation mechanism and an unusual electrochemical impedance spectrum without pseudo-inductive behavior was observed. Based on these results a new mechanism is proposed.

4.2. Experimental and characterization methods

4.2.1. Chemicals

Hydrogen tetrachloroaurate (III) trihydrate ($HAuCl_4 \cdot 3H_2O$), hydrogen hexachloroplatinate (IV) hydrate ($H_2PtCl_6 \cdot 6H_2O$) and sodium borohydride ($NaBH_4$) were obtained from Aldrich; isopropanol and sodium citrate tribasic dehydrate ($Na_3C_6H_5O_7$) from Fluka; hydroxylammonium chloride ($NH_2OH \cdot HCl$), sulphuric acid, formic acid and

methanol from Merck. All the chemicals were used as received. DI water was processed by Mili-Q water purification system.

4.2.2. Preparation techniques

Au seeds preparation was based on the Au preparation reported in chapter 3.2.2.[134, 157-160] While the preparation of the decorated nanoparticles was based on the procedures reported in chapter 3.2.3, but with lower Pt/Au mole ratios.[158-160] By changing the Pt:Au mole ratio (based on the metal precursors mole ratio) which is less than the ratio needed to form a complete monolayer shell, a controllable Au surface coverage by Pt can be achieved. For comparison, in-house made Pt/C with 20% Pt loading was prepared based on the ethylene glycol method (chapter 3.2.5).[136]

4.2.3. Characterization

Specimens for TEM were prepared by ultrasonically suspending the as-prepared nanoparticles with ethanol, then dropping a small amount of the dispersion onto clean copper grids and drying it in air. Samples were examined using JEOL 3010 transmission electron microscopy operated at 200kV. The UV-vis spectra of the Au and PtAu hydrosols were measured by a Shimadzu UV2450 spectrometer equipped with quartz cells. The concentration of Au in Au hydrosol and Pt-Au hydrosols was 8×10^{-2} mM. All the samples were transferred to the cell immediately after cooling down to room temperature. Thermogravimetric analysis was performed on a TA instrument SDT Q600 to determine the total metal loading on carbon black. Typical samples weighed ~5 mg were heated on a platinum pan with a flow of 100mL/min of air under constant heating rate of 10^{o}C/min. The compositional analysis using energy dispersive X-ray spectroscopy

(EDX) was performed using a scanning electron microscopy JEOL JSM-6390LA operating at 20 kV. [159,160]

4.2.4. Electrochemical measurements

All the electrochemical performance tests were carried out at room temperature condition (25^{o}C) and were performed in a rotating disk electrode system using Autolab PGSTAT302 potentiostat. Electrode potentials were measured and reported against saturated calomel electrode and Pt wire was used as the counter electrode. The preparation of the working electrode was based on the thin film method.[135] Briefly 8 mg of the sample was mixed with 4 ml of water and sonicated to form a homogeneous ink, then 10μL of the ink was deposited using microsyringe onto a glassy carbon electrode (GCE) with 5 mm diameter to yield a total metal loading of 4μg. The GCE was dried inside an oven operating at 80^{o}C. After that, 10μL of 0.05% Nafion solution (diluted from 5% solution using isopropanol) was dropped on top of the disk to fix the catalyst powder. All the solutions were deaerated using pure N_2 for at least 20 minutes prior to any measurement. Before the activity test, the electrode was cycled at 50 mV s^{-1} between -0.2 to 0.9 V in 0.5 M H_2SO_4 for at least 20 scans. To determine the Pt electrochemical active surface area (ECSA) the electrode was cycled between -0.2 to 1.2 V for 5 scans and then the 5th scan was used to determine the hydrogen adsorption desorption charge. After that the electrode was transferred to the cell containing 0.5 M H_2SO_4 + 0.5 M HCOOH electrolyte solution. Subsequently, 20 scans were recorded at 10 mV s^{-1} in the potential range -0.2 to 0.9 V with a rotating rate of 1000 rpm to prevent the accumulation of CO_2 bubbles on the disk surface. For the methanol oxidation activity test, 0.5 M H_2SO_4 + 1 M CH_3OH aqueous solution was used as the electrolyte. As for the CO stripping

experiment, the CO was adsorbed onto the working electrode by bubbling the 0.5 M H_2SO_4 electrolyte with CO for 10 minutes while holding the electrode potential at -0.15 V, the electrolyte was then purged with N_2 for 30 minutes before the CO stripping curve was taken.

The surface poisoning of the catalyst under open circuit potential in 0.5 M HCOOH was studied based on the technique described by Clavilier and co-workers.[161] Briefly, after catalyst activation in 0.5 M H_2SO_4 within the potential range of -0.2 to 1 V, the electrode was removed from the cell and immersed in 0.5 M HCOOH solution for 3 minutes. The electrode was then transferred to deaerated pure water and rotated to clean the excess HCOOH from the vicinity of the electrode and then immersed back into 0.5 M H_2SO_4 solution at -0.1 V. After that the oxidation of the poisonous intermediate formed from the HCOOH solution was achieved upon scanning the electrode within the potential range of -0.2 to 1 V.

As for the EIS measurement, the electrode was first activated in the supporting electrolyte then transferred to the 0.5 M H_2SO_4 + 0.5 M HCOOH solution. Before starting the EIS measurement, the system was given 15 minutes to reach a pseudo steady state at each specific potential before collecting the EIS data. The spectra were recorded between 10 kHz and 10 mHz at 10 points per decade with the amplitude (rms value) of the ac signal 10 mV. During the EIS measurement the electrode was rotated at 1000 rpm. The EIS spectra were recorded using a built-in frequency respond analyzer (Eco Chemie, Netherlands). [157-160]

4.3. Results and discussion

4.3.1. TEM analysis

The Au nanoparticles on carbon black Vulcan XC-72 and the PtAu hydrosols were characterized using high resolution-TEM (HRTEM). The image of Au nanoparticles dispersed on carbon black is shown in the previous chapter (Fig. 3.2). While the TEM images of various PtAu starting from Pt/Au ratio of 1:3 to 1:10 are shown in Fig. 4.1. It can be seen that the average diameter of the PtAu hydrosols is around 5 nm which is close to the mean diameter of Au nanoparticles. The same protocol has also been used to synthesize Pt_{shell}-Au_{core} nanoparticles.[157] The obtained average particle size agrees well with the theoretical calculation by assuming the growth of Pt onto Au cores. This proves that, for Pt-Au hydrosols prepared with this protocol, all the Pt would deposit on Au surfaces without forming individual Pt nanoparticles. Moreover, the complete Pt shell covering the Au nanoparticles was obtained at Pt:Au mole ratio 1:1.[157] This then indicates that in this work (with low Pt:Au ratios) the Pt atoms were deposited as a submonolayer to form the decorated structure. At higher magnification as shown in Fig. 4.1 (part A1 and E1), the most frequently observed lattice fringes fit well with the Au (111) surface while the distinct difference between the Au and Pt fringe on the edge of the particle cannot be observed. This might be due to the small difference between the Au and Pt lattice constant.[162]

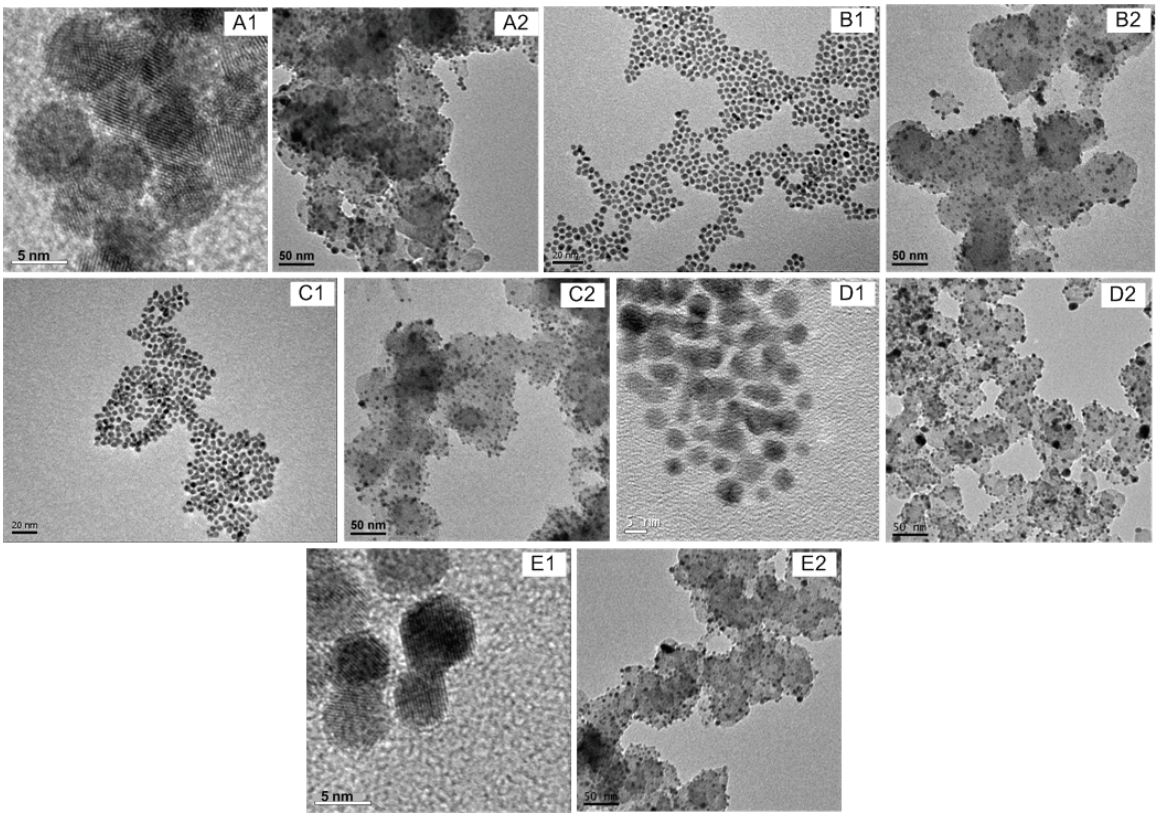

Fig. 4.1. TEM images of the representative samples: A1) Pt/Au=1:3 hydrosol; A2) Pt/Au=1:3 on carbon; B1) Pt/Au=1:4 hydrosol; B2) Pt/Au=1:4 on carbon; C1) Pt/Au=1:6 hydrosol; C2) Pt/Au=1:6 on carbon; D1) Pt/Au=1:8 hydrosol; D2) Pt/Au=1:8 on carbon; E1) Pt/Au=1:10 hydrosol; E2) Pt/Au=1:10 on carbon.

4.3.2. UV-vis analysis

The absorption spectra of Au and PtAu hydrosols are shown in Fig. 4.2. The absorption peak at 511 nm belonging to the Au surface plasmon can be clearly observed for the Au hydrosol. The PtAu hydrosols also show the same Au plasmon absorption peak characteristic, but the intensity become lower and peak location also shifts to the lower wavelength region. These trends suggest that the Pt atoms were deposited on the Au surface that leads to the increase of the Au surface coverage by Pt and gradual suppression of absorption peak with the increase of Pt:Au mole ratio.[126, 138, 139, 157, 159, 160, 163]

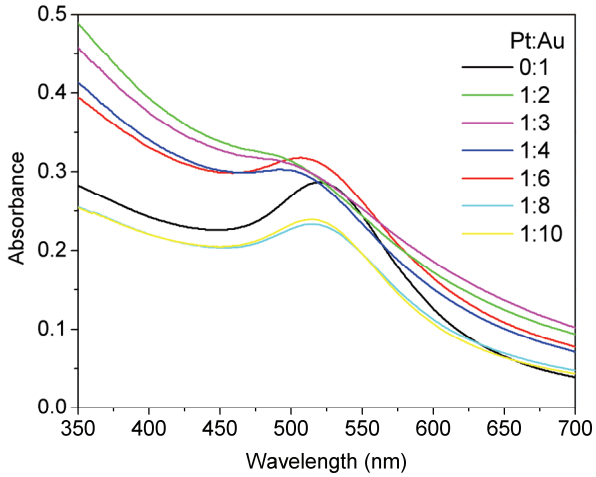

Fig. 4.2. UV-vis absorption spectra of Au hydrosol and PtAu hydrosols.

Furthermore, the appearance of Au plasmon peak reveals that some of the Au surface is still not covered by Pt, proving the formation of a decorated structure. Liz-Marzan et al. have reported that based on the modified Mie theory for Au_{core}-Pt_{shell} case, the Au plasmon absorption peak became suppressed with the increase of surface coverage and finally vanished when a complete Pt monolayer was formed.[137, 138, 140, 164, 165] This is in good agreement with our experimental result. Because the Au plasmon absorption is related directly to the exposed Au surface area, we suggest that by comparing the Au plasmon peak area from the UV-Vis spectrum, the surface coverage of Au by Pt can be semi quantitatively predicted. The estimated surface coverage changes from 8% to 87% when Pt/Au ratio changes from 1:10 to 1:2 (see Table 4.1). As a comparison we also calculated the Au surface coverage by Pt using the assumption of epitaxial growth of Pt on Au.[139] The surface coverage using the UV-Vis absorption corresponds well with the calculation assuming epitaxial growth at high Pt:Au mole ratios. At low ratios, the coverage from UV-Vis absorption shows lower value, probably due to the weaker capability of discrete Pt atoms to block plasmon resonance. The estimated surface

coverage reveals the disordering Pt structure on the Au nanocrystals surface that will be further elucidated in the next session.

Table 4.1. Au surface coverage by Pt.

Pt:Au	Au plasmon area[a]	Surface coverage[b]	Surface coverage[c]
0:1	8.28	0%	0%
1:10	7.83	8%	19%
1:8	7.45	10%	24%
1:6	6.70	20%	31%
1:4	4.95	40%	46%
1:3	2.27	73%	60%
1:2	1.11	87%	87%

[a]: Integration of the area under the peak starting from 400 to 600 nm after background subtraction
[b]: based on Au plasmon area
[c]: assuming epitaxial growth of Pt on Au surface

4.3.3. XRD analysis

All the XRD spectra for the Pt-decorated Au resemble the Au spectra where all the (111), (200), (220) and (311) can be observed (see Fig. 4.3). This indicates that only monolayer or sub-monolayer of Pt was deposited on Au without forming individual Pt particles, otherwise the XRD spectrum would have replicated the Au and Pt peaks as of physical mixture.[138, 140] The absence of Pt peaks implies that the size of the Pt clusters on the surface of Au is smaller than the detecting capability of XRD (~ 1 nm)."[163] This XRD analysis agrees well with the TEM observation. However a closer look at the diffraction peaks of various PtAu/C reveals that the peak widths are not symmetric and the intensity slightly increase in the middle position between pure Pt peaks and Au peaks, which in accordance with the XRD analysis in chapter 3 indicating the present of Au and Pt phases.

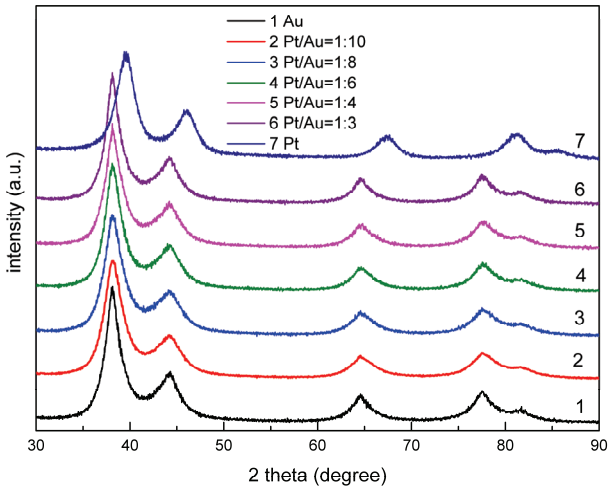

Fig. 4.3. XRD patterns of Au/C, Pt/C and various PtAu/C.

4.3.4. TGA analysis

The total metal loading of the nanoparticles on carbon black was determined by using thermogravimetric analysis (TGA) and the results are shown in Fig. 4.4. It can be seen from Fig. 4.4 part A that carbon black starts to oxidize at ~550^{o}C and the addition of Pt lowers the oxidization temperature to ~430^{o}C indicating a catalyzing mechanism where the Pt nanoparticles promote the oxidation of carbon black at low temperature.[166] While for Au/C, the oxidization temperature is roughly the same with that of carbon black (the difference in the onset temperature is around 50^{o}C). But with the addition of Pt, the oxidation temperatures of various PtAu/C shift negatively and lie in between the oxidation temperature of Pt/C and Au/C indicating that the Au-based electrocatalysts have greater stability against oxidation compared to Pt/C.[122] The weight loss profiles for PtAu/C with different Pt/Au ratios are quite similar (see inset in Fig. 4.4 part B) suggesting that Pt/Au ratio does not affect much on the oxidation of carbon black, at least in the Pt/Au ratio used in this study. From the mass change observed in Fig. 4.3, the

actual total metal loadings are quite close to the nominal loading (20%) indicating a complete reduction of Au and Pt and subsequent deposition on carbon black.[167]

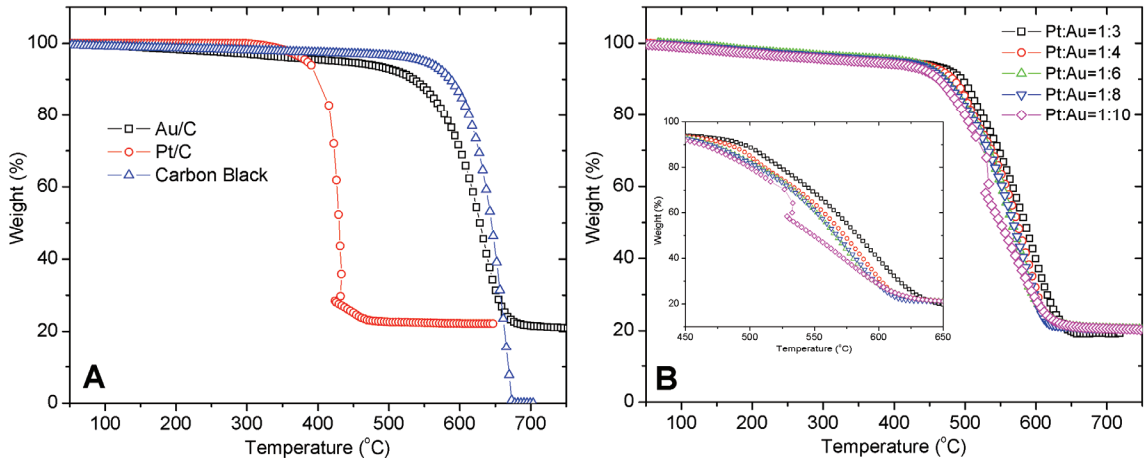

Fig. 4.4. TGA curves of A) Au/C, Pt/C and carbon black and B) various PtAu/C.

4.3.5. EDX analysis

The Pt/Au mole ratios were verified using energy-dispersive X-ray spectrometry and the results are shown in Fig. 4.5. The samples were the residue obtained after TGA analysis. It can be seen that Pt and Au are presents in all the samples and the intensity of Pt increases with the increase of Pt/Au mole ratio showing the successful reduction of H_2PtCl_6 by $NH_2OH.HCl$. Quantitatively the Pt/Au mole ratios are quite close with the nominal Pt/Au mole ratios being 1:7.7, 1:5.7, 1:3.9 and 1:3.1 for Pt/Au=1:8, Pt/Au=1/Au=1:6, Pt/Au=1:4 and Pt/Au=1:3 respectively.

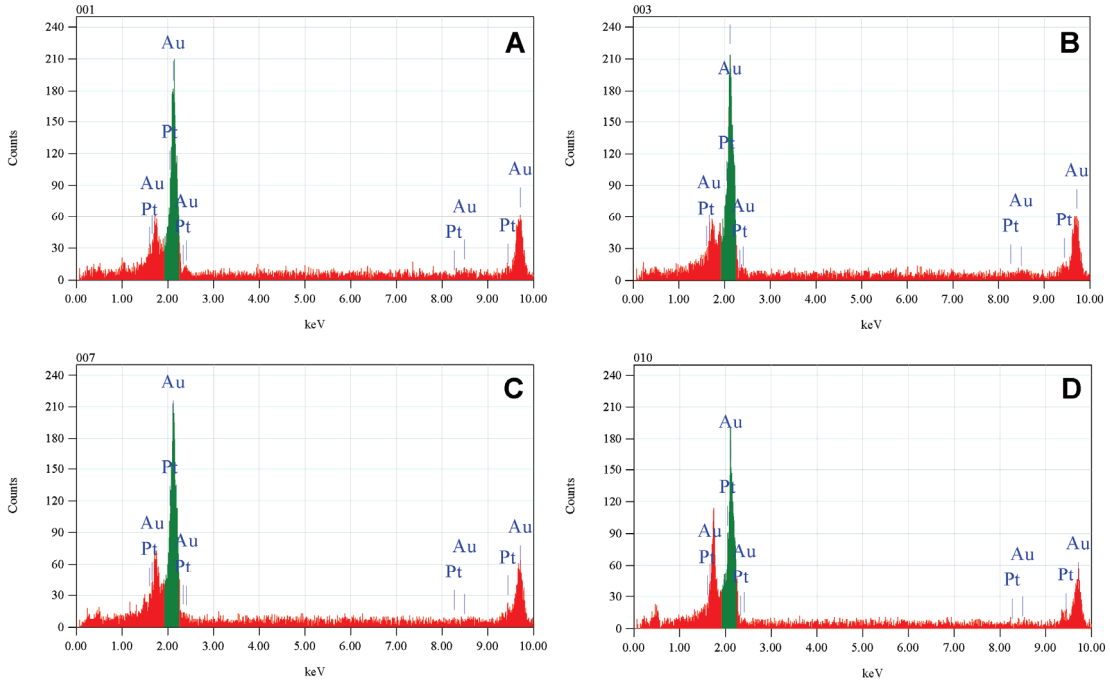

Fig. 4.5. EDX spectra of A) Pt/Au=1:8; B) Pt/Au=1:6; C) Pt/Au=1:4 and D) Pt/Au=1:3.

4.3.6. Voltammetric analysis

"The solid evidence of the formation of the decorated structure is further supported by electrochemical measurement as it can be regarded as a surface sensitive technique that allows only the characterization of the surface atoms rather than the bulk atoms. The cyclic voltammograms were recorded in deaerated 0.5 M H_2SO_4 solution and the results are represented in Fig. 4.6.

The inset in Fig. 4.6 shows the typical Au characteristic in acidic condition where broad double layer until 1 V, oxide formation starting from ~1 V and oxide reduction peak at ~0.9 V are observed.[168] However, for the PtAu/C with different mole ratios, the above features become less pronounced with the increase of the Pt:Au ratio. Instead, a sharp cathodic peak around 0.3 to 0.4 V and a nearly symmetrical anodic and cathodic peak in the low potential region are observed. Such characteristic is similar to Pt

characteristic in acidic media where the sharp cathodic peak can be attributed to the Pt oxide reduction peak and the similar peaks at the low potential are due to the hydrogen adsorption and desorption.

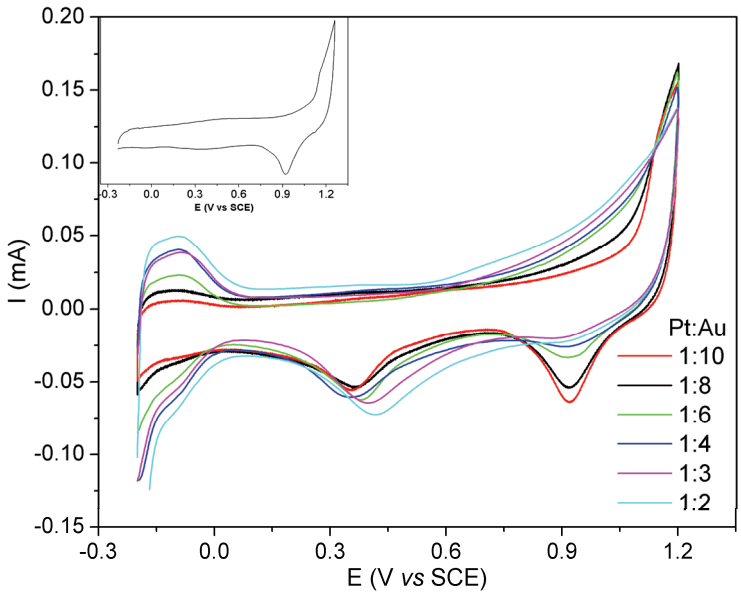

Fig. 4.6. CV of various PtAu/C in 0.5 M H_2SO_4 at 50 mV s^{-1}. The inset shows the CV of Au/C.

A closer look at the evolution of the Au oxide reduction peak at ~0.9 V for Pt:Au with different mole ratios reveals that with the increase of Pt:Au ratio the peak become suppressed and we have showed in the chapter 3 that when the Pt:Au ratio is raised to 1:1 and higher, the Au oxide reduction peak completely vanished.[157] This corroborates well with the TEM and UV-Vis analysis where all the Pt atoms were deposited on the Au surface without forming its own nucleus, and some parts of the Au surface were still exposed giving the decorated structure. A further observation at the Pt oxide reduction peak in Fig. 4.6 shows that the higher the Pt:Au ratio, the Pt oxide reduction peak shifts to higher potential. With the increase of Pt:Au ratio from 1:10 to 1:2, the Pt oxide reduction peak moves from 0.33 V to 0.44 V. To understand this, we may consider the electron chemical potential of metal reflected as work function. The values of the work

function of Pt and Au are 5.40 eV and 5.32 eV respectively.[144] When Pt and Au are in intimate contact, electrons will flow from Au to Pt until the electron chemical potentials on both metals are equal. At lower Pt:Au ratios, the Pt entities on the Au surface have more negative charge per atom which makes Pt atoms more difficult to obtain electrons (reduction peak shifts to a lower potential) compared to higher Pt:Au ratios and Pt (Pt oxide reduction peak located at 0.5 V). This indicates a stronger bonding between Pt and oxygen containing species. Similar conclusion can be made from the widely accepted d-band model proposed by Nørskov.[127-129] When Pt monolayer is deposited on Au surface, there is an upper shift in d-band center to maintain a constant filling of the d-band, which leads to a higher adsorption energy of adsorbate, oxygen containing species in this case.

4.3.7. Formic acid electro-oxidation

The activity of these catalysts was measured in deaerated 0.5 M H_2SO_4 + 0.5 M HCOOH electrolyte solution. As shown in Fig. 4.7, the measured current was normalized by the Pt ECSA which was obtained by integrating the area under the hydrogen desorption peak of CVs in 0.5 M H_2SO_4 (after the double layer charge correction) and a hydrogen charge/Pt surface area conversion factor of 210 μC cm^{-2} was used to obtain the specific ECSA. It is clear that Au/C is catalytically inactive towards formic acid oxidation under the experimental conditions studied here that is why the result is not shown.[159]

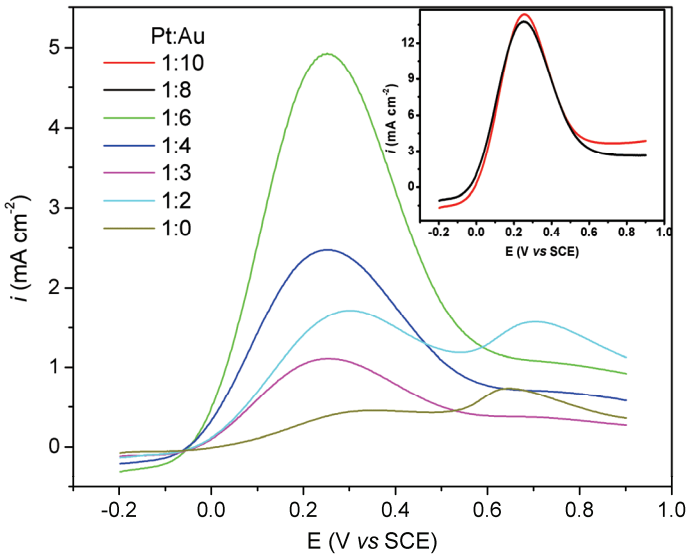

Fig. 4.7. Anodic scan of Pt/C and PtAu/C with different mole ratios at 10 mV s^{-1} and 1000 rpm in 0.5 M H_2SO_4 + 0.5 M HCOOH (for clarity the inset shows the anodic scan of Pt:Au 1:8 and 1:10)

It has been known that formic acid electro-oxidation on Pt occurs through a dual parallel reaction pathways in which the desired pathway (dehydrogenation) leads to the formation of CO_2 through reactive intermediates whereas the second pathway (dissociative adsorption) leads to the formation and accumulation of poisonous intermediates that prevents the complete oxidation of the formic acid.[31, 32, 148] Several investigations using Pt electrode showed that CO_{ads} is the primary poisonous intermediate, while recently it has been discovered using in situ time resolved Fourier transform infrared spectroscopy that formate (HCOO) instead of carboxylic acid (COOH) species is the reactive intermediate in the dehydrogenation pathway.[33-36] For Pt/C as shown in Fig. 4.7, two peaks were observed in the forward scan, at ~0.35 V and 0.65 V respectively. The first peak at ~0.35 V is related with the direct oxidation of HCOOH to form CO_2 while the second peak at ~0.65 V corresponds to the oxidation of the poisonous species CO_{ads} to form CO_2. At low potential range, the Pt sites are partially poisoned by

CO_{ads} from the dissociative adsorption step. The measured current then mainly comes from the formic acid oxidation on the unoccupied Pt sites through the dehydrogenation pathway. The peak current indicates the level of Pt surface poisoning by CO_{ads}. At high potential the CO_{ads} is oxidized by Pt-OH species that starts to form at around 0.5 V during the forward scan, which releases most Pt sites for formic acid oxidation. As for the backward scan (cathodic scan), most of the poisonous intermediates have been oxidized at high potential and formic acid oxidation then can proceed on clean Pt surface through the dehydrogenation pathway. Therefore, a big peak was observed. Because the anodic scan allows the formation and build up of the poisonous intermediate, we focused our observation on the evolution of the anodic scans. It is worth noting that the current density for the Pt/C we obtained in this study was slightly lower compared to previous study by Lovic et al, as an example the peak current density for the CO_{ads} oxidation formed from HCOOH at 0.7 V is around 1.2 mA cm^{-2}, while for this work it is around 0.75 mA cm^{-2}.[169] This might be the result of lower scan rate (10 mV s^{-1} *vs* 50 mV s^{-1}), lower platinum loading (20 wt% *vs* 50 wt%) and higher H_2SO_4 concentration (0.5 M *vs* 0.1 M) used in this work.

Surprisingly, the decorated catalysts starting from Pt:Au 1:2 showed different behaviors compared with Pt/C towards formic acid oxidation, where the first peak becomes higher and the peak potential and onset potential of this peak shifts negatively. At higher potential, the second peak that corresponds to the oxidation of CO_{ads} becomes diminished with the decrease of the Pt:Au mole ratio and this peak can not be observed anymore at Pt:Au 1:4 and lower ratio. Moreover for the Pt-decorated Au with lower Pt:Au ratios, the current measured during the anodic (between 0.2 to 0.3 V) and cathodic

scans do not appreciably differ, suggesting a low inhibition rate, i.e the suppression of CO_{ads} formation.[94, 158-160, 170] On the contrary, Pt/C showed a big difference between anodic and cathodic scans, signifying the severe poisoning of the active sites by CO. Furthermore, the onset potential of the direct oxidation pathway for the Pt-decorated Au is lower compared with Pt/C indicating that the formic acid is easier to oxidize on the surface of the decorated catalyst. The results obtained for the decorated structure with different Pt:Au mole ratio indicate that the poison formation is dependant with the Au coverage by Pt as tabulated in Table 4.1.

To further prove that the poisonous intermediate formation reactions have been inhibited on this decorated structure, we conducted the poison formation reaction on open circuit potential and the results are shown in Fig. 4.8. [160] The first positive sweep is the stripping of the chemisorbed poisonous species. It can be seen for the Pt/C, there's a big sharp oxidation peak at ~0.53 V that is ascribed to the oxidation of CO_{ads} formed from the dissociative adsorption of formic acid.[31, 147, 161] While this peak still can be seen for the core-shell structure (Pt:Au=1:1), for the decorated structure, the peak becomes smaller and finally vanished at low Pt:Au mole ratio, indicating less poisoning and eventually no poisoning of the catalyst by CO_{ads} with the decrease of the Pt:Au mole ratio. It can also be observed that the peak position shifts positively from Pt/C to Pt:Au (1:2). This can be explained by the increased Pt-CO bond strength due to the up-shift in the d-band center of the Pt atoms.[127-129]

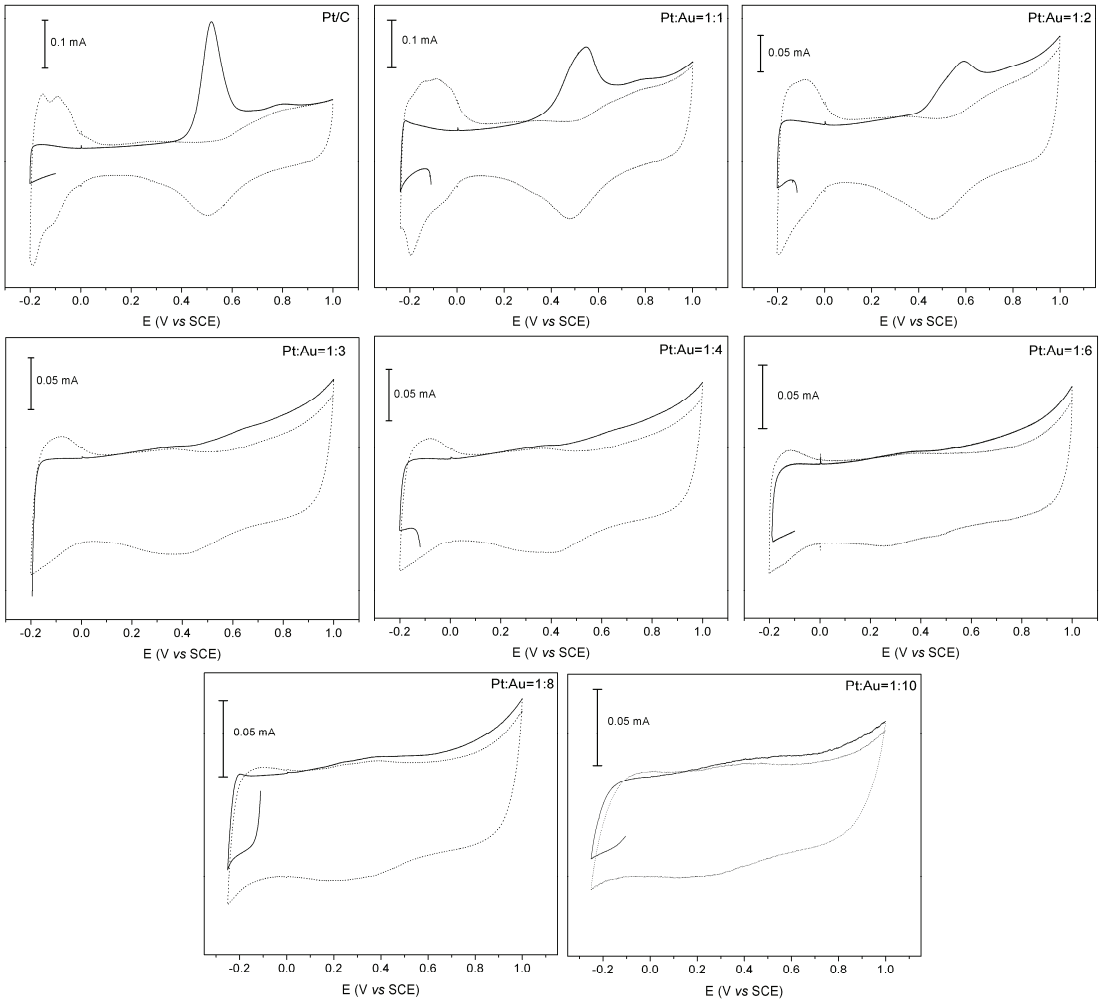

Fig. 4.8. Poison stripping experiment on Pt/C and PtAu/C with various Pt:Au mole ratios. The poisonous species was adsorbed from 0.5 M HCOOH and the poison stripping was conducted at 50 mVs^{-1} in 0.5 M H_2SO_4. The full line shows the first positive sweep while the dotted line shows the subsequent sweeps, upon removal of the poisonous species.

The blocking of dissociation pathway can be rationalized with the Au surface coverage by Pt which can be determined from UV-Vis spectra and calculated using the epitaxial growth assumption. If there is a two dimensional growth as assumed by the epitaxial growth of Pt on Au surface, the most probable stable structure of Pt at low Pt:Au mole ratio that have Pt coverage of 0.33 is $(\sqrt{3} \times \sqrt{3})R30^0$ as revealed by the electrochemical scanning tunneling microscopy measurement on the spontaneous

deposition of Pt on Au (111).[171] This atomic arrangement reveals that Pt atoms on the Au surface are isolated from each other at low coverage. Even at a higher Pt:Au ratio, it is believed that the Pt ensemble will still show the same disordering with Pt atoms existing as small isolated islands, presumably 2 to 3 atoms. It has been shown that the formic acid dissociative adsorption pathway is a site demanding reaction, where more than two ensemble Pt sites are needed[151, 170, 172] (see Scheme 4.1 [159]). In contrast, the dehydrogenation pathway of formic acid oxidation does not require the presence of continuous neighboring Pt sites.[170, 173] So a continuous decrease of Pt coverage on Au surface, i.e., decreasing availability of Pt adjacent atoms, leads to a decrease in the dehydration rate and an eventual blocking of the CO formation (the disappearance of the second oxidation peak at ~0.63 V), while the dehydrogenation reaction can still occur without being affected. So it is reasonable to conclude that the inhibition of the poisonous intermediate formation from formic acid dissociative adsorption pathway is likely due to less amount of Pt ensemble sites that the Pt-decorated Au catalyst possesses. This analysis suggests that a single Pt atom or a small island of Pt is advantageous for the direct oxidation of formic acid.

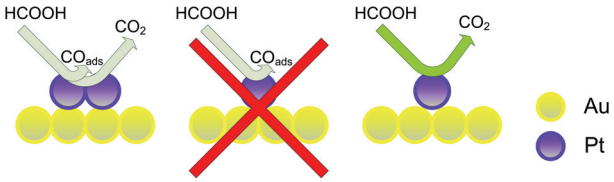

Scheme 4.1. Illustration of the catalytic reactions of formic acid oxidation (dehydration and dehydrogenation) on the Pt-decorated Au surface.

While direct formic acid oxidation is not a site demanding reaction, methanol oxidation requires an ensemble of minimum number of neighboring Pt atoms to proceed.[145, 170] To further prove the role of the ensemble effect on this decorated

structure, methanol oxidation was conducted and the results are shown in Fig. 4.9. It is clear that the Pt:Au with a mole ratio 1:1 that exhibit a complete shell (Pt_{shell}-Au_{core}) shows similar catalytic activity like Pt/C for methanol oxidation, but with less amount of Pt used.[157] Furthermore, it can be seen that the hydrogen adsorption-desorption area of Pt/C and Pt:Au 1:1 (core-shell) decreased greatly when 1 M CH_3OH + 0.5 M H_2SO_4 was used as the electrolyte. But it is not the case for the decorated structure, as hardly any change was observed on Pt-decorated Au with different mole ratios. [160]

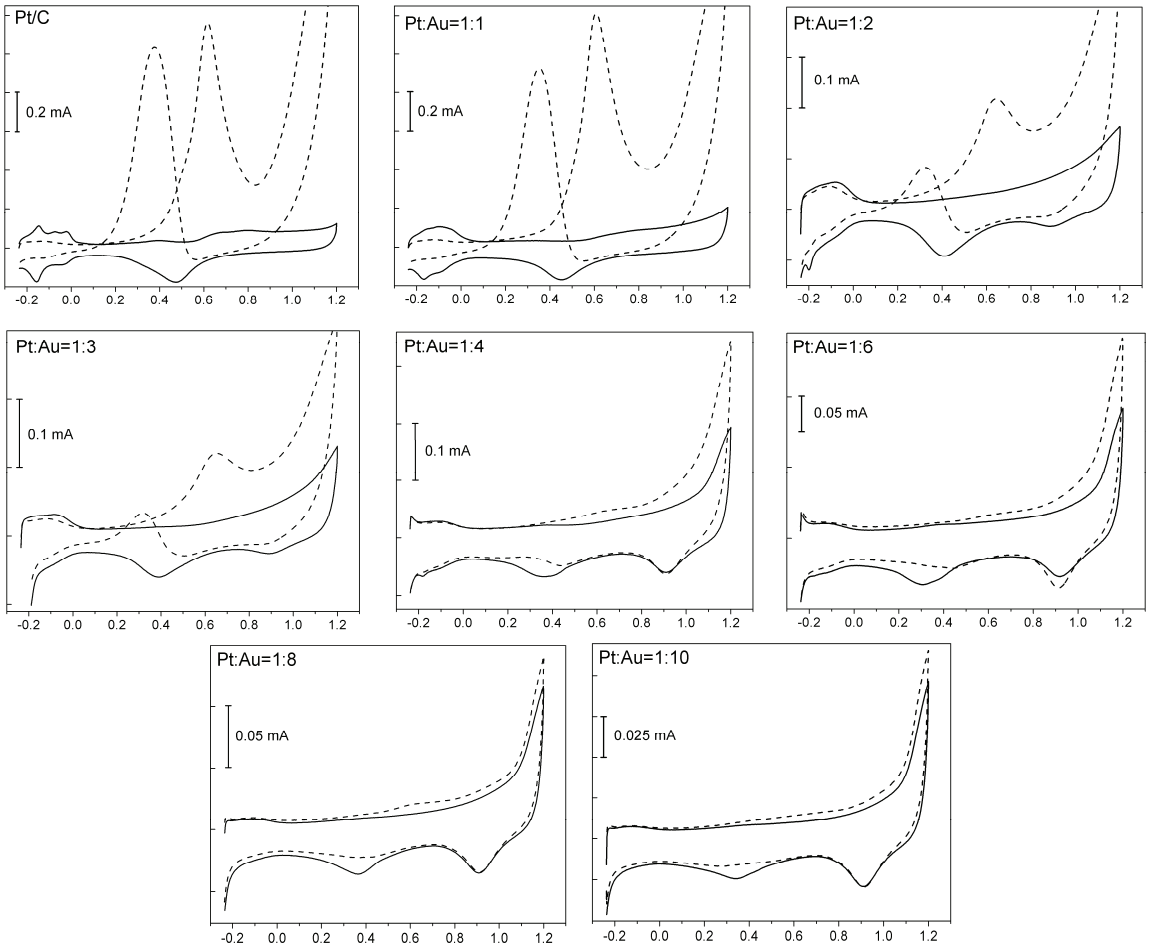

Fig. 4.9. CV curves of Pt/C and PtAu/C (core-shell and decorated) with different mole ratios in N_2 saturated 0.5 M H_2SO_4 (full line). Dash line is in 1 M CH_3OH + 0.5 M H_2SO_4. Scan rate: 50 mV s^{-1}.

The comparison of the full line cyclic voltammograms with and without methanol clearly reveals that less methanol can dissociate to form the intermediate and subsequently oxidize to form CO_2 on the decorated structure compared with Pt/C and core-shell structure, which was indicated by the less blocking of hydrogen adsorption-desorption area on the Pt-decorated Au. In addition, with the decrease of Pt:Au ratio, lower methanol electro-oxidation current was observed. At Pt:Au mole ratio of 1:4 or lower, no considerable methanol electro-oxidation peaks were observed. The inactivity of this Pt-decorated Au for methanol electro-oxidation at low Pt:Au mole ratio is another evidence of the ensemble effect as previously proven by Du and Tong[145] and this further prove that the ensemble effect plays a big role as the origin of the inhibition of poison intermediate formation for formic acid electro-oxidation on this Pt-decorated Au structure.

To verify the increased Pt-CO bond strength on the PtAu electrocatalysts, CO stripping experiment was conducted and the results are shown in Fig. 4.10 (only anodic sweeps are shown for simplicity)." [157] By knowing that Au surface does not adsorb CO at all, all CO oxidation waves observed can be assigned to the existence of Pt on the Au surface. As a reference the CO stripping curve for Pt/C is also shown. The inset in Fig. 4.8 shows the corresponding CO stripping peak potentials as a function of Pt/Au mole ratios.

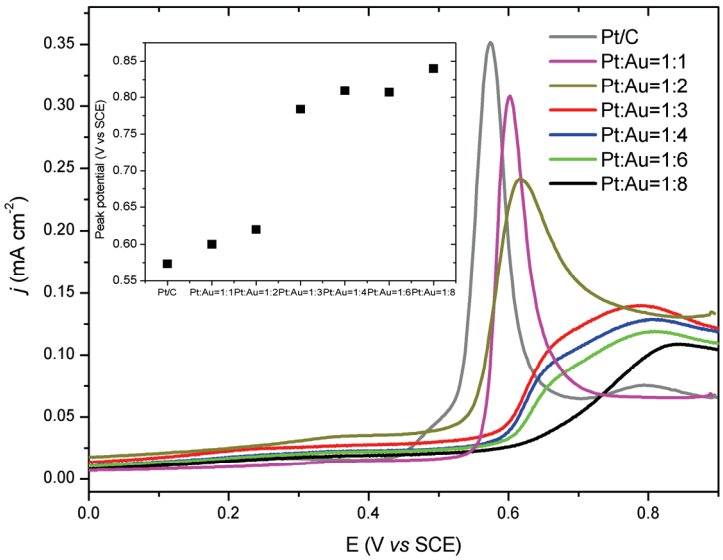

Fig. 4.10. CO stripping curves for Pt/C and various PtAu/C in CO-saturated 0.5 M H_2SO_4. The inset shows the corresponding peak potentials as a function of Pt/Au mole ratios.

It can be observed obviously that the CO stripping peak potentials of all the PtAu/C are shifted to higher potentials compared to that of Pt/C, indicating a stronger Pt-CO bond strength in accordance with the d-band centre model proposed by Norskov, which attributes the bond strengthening to an up-shift of Pt d-band centre.[127-129, 174] Furthermore the up-shift of the Pt d-band centre also explain the strengthened bonding between Pt and oxygen containing species, as indicated by the negative shift of the Pt oxide reduction peak as seen in Fig. 4.6.

The most striking observation in Fig. 4.10 is that the CO stripping peaks at the Pt/Au ratio of 1:3, 1:4, 1:6 and 1:8 appear at ~0.8 V, far away from the Pt/C, Pt/Au=1:1 and Pt/Au=1:2 at around ~0.6 V. The peak curves also are much broad. The sudden positive peak potential jump at Pt/Au=1:3 surprisingly is in accordance with the trend in formic acid electro-oxidation and poison stripping experiment where the Pt/Au=1:3 and lower do not show any formation of CO_{ads} during the formic acid oxidation and poison stripping experiment. These facts indicate that the Pt sites in the Pt/Au=1-3 is unique

which have high activity for formic acid oxidation but low activity for methanol oxidation and low activity for CO oxidation and when the Pt/Au mole ratio becomes lower, the Pt sites become inactive for methanol oxidation.[145]

"The improvement at high Pt:Au ratio of 1:2 (close to 87% coverage) indicates that there are other possible origins for the improvement besides the CO blocking mechanism due to the ensemble effect. "Electronic effect" could be one possible origin i.e the difference between the work function of the Pt adatom and the Au nanoparticles as the substrate that may increase the reactivity of Pt entities on Au surface. As we previously mentioned, this electronic effect can be observed on cathodic shift of the Pt oxide reduction peaks. This behavior has also been observed for Pt (111) adsorbed with Bi adatom, PtBi alloy and Pt on Au(111), where for the Bi on Pt(111) case, an increase on the formic acid electro-oxidation specific activity of almost 40 times higher than Pt(111) was observed and for Pt on Au(111) case, an increase on the reactivity toward CO bonding and formic acid oxidation compared with clean Pt was observed.[175-180] Moreover, the enhanced specific activity may also be attributed to the superior activity of the Pt atoms that reside on the steps and edges of Au surface compared to Pt atoms on the terrace. At the initial stages, *i.e* low Pt:Au ratio, Pt will be deposited on the steps and edges of Au surface instead on the upper terrace due to the higher adsorption energy that kink sites possess.[181]

From the above analysis, it can be proposed that the initial growth of Pt on Au nanoparticles using this synthetic procedure occurs on the high population of corner or edge of Au nanocrystal surface, which leads to small isolated Pt atoms. The subsequent Pt atoms will deposit on the lower terrace forming a small Pt island (mainly 2 to 3 atoms

wide). Then further growth will eventually form a complete layer covering the Au surface with the deposition of Pt on the upper terrace. Additionally, small fraction of the Au atoms on the surface may be displaced by Pt as was observed in other study.[174]

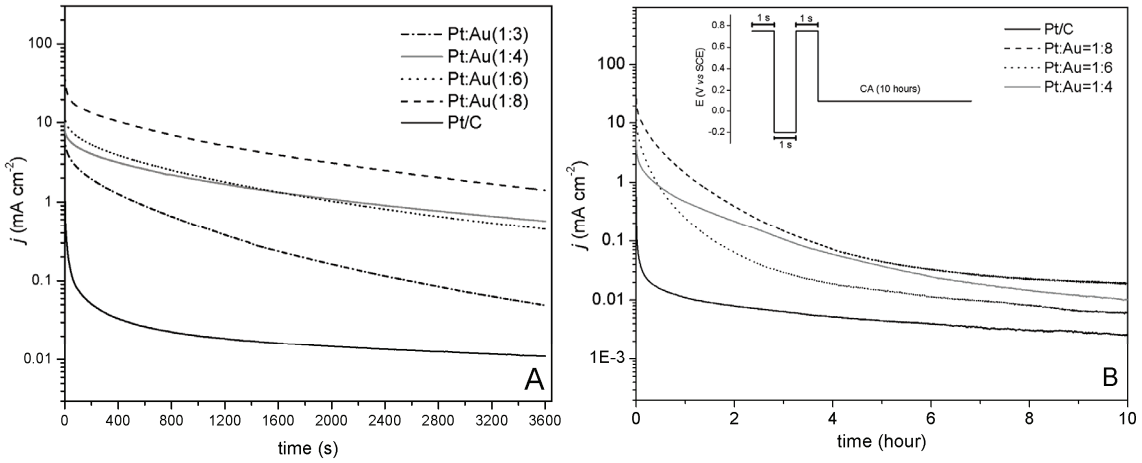

Fig. 4.11. Chronoamperometric plots for formic acid oxidation at 0.1 V and 1000 rpm in 0.5 M H_2SO_4 + 0.5 M HCOOH for Pt/C and various PtAu/C for A) 1 hour and B) 10 hours. The inset in part B shows the pretreatment steps.

To characterize the durability of these catalysts, we conducted chronoamperometric experiment and the results are shown in Fig. 4.11. The current density vs time data represent more accurate information on the relative activities and stabilities of the Pt-decorated Au electrodes. It is found that at 0.1 V, initially the current densities of PtAu/C with Pt:Au ratio of 1:6 and 1:8 are almost two orders of magnitude higher compared to Pt/C. However, the current density decreases and stabilizes over the experimental period of time. After a period of 1 hour, the current density for Pt:Au ratio of 1:3 dropped almost two order of magniture, indicating the instability of Pt:Au=1:3 that might be due to the accumulation of CO_{ads} formed after a certain period of time, but it is not the case for Pt:Au ratio of 1:4, 1:6 and 1:8, where the current density drop is not as significant as that of Pt:Au ratio 1:3. And after a period of 10 hours, the current densities are 2.6 μA cm^{-2}, 10.2 μA cm^{-2}, 6.1 μA cm^{-2} and 21.1 μA cm^{-2} for Pt/C and PtAu/C with

Pt:Au ratio of 1:4, 1:6 and 1:8 respectively. Clearly, one order of magnitude enhancement still can be achieved after a long period of time. At the beginning, it can be seen that the current decays very rapidly for the Pt/C electrode even though the pretreatment steps can remove the CO_{ads} and ensure a clean Pt surface before the chronoamperometry experiment commences.[182] This initial decay is due to the fast accumulation of CO_{ads} on the clean Pt surfaces from the dissociative adsorption pathway that block the continuos formic acid oxidation.[182, 183]

4.3.8. The electrochemical impedance spectra analysis

It is important to understand the reaction mechanism of formic acid electro-oxidation on the Pt-decorated Au surface. While the conventional electrochemical methods including cylic voltammetry methods can only be used to characterize the performance of the catalyst with little insight into the mechanism, EIS is a good tool to study the intrinsic reaction mechanism of formic acid oxidation on this decorated structure. To further elucidate the mechanism, a series of EIS experiments were conducted using PtAu/C with Pt:Au mole ratio 1:6 as the electrode and the results are shown in Fig. 4.12. A similar impedance trend was observed on the Pt/C and PtPd/C cases for formic acid electro-oxidation.[21]

It can be seen from Fig. 4.12 part A, that the impedance arcs are located within the first quadrant for electrode potentials lower than 0.3 V and the diameter of the arc abruptly decreases from -0.1 to 0.1 V and then increase gradually from 0.1 to 0.25 V (the same trend can also be observed from the evolution of the phase angle at low frequencies shown in the bode plot). The large arc at -0.1 V suggests a slow reaction rate of the direct oxidation of formic acid at this potential but with only an increase of 50 mV to -0.05 V,

the arc diameter abruptly decreases which coincidentally happens at the same potential as the onset potential of the electro-oxidation of formic acid as shown in Fig. 4.7. This indicates a faster direct oxidation rate and with the increase of the electrode potential the charge transfer resistance for the dehydrogenation of formic acid electro-oxidation becomes smaller.

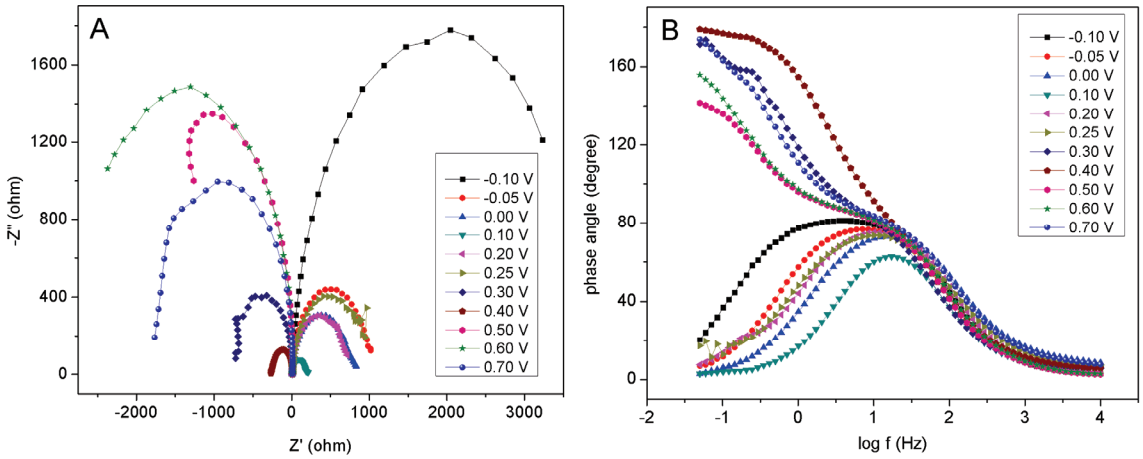

Fig. 4.12. Nyquist plots (A) and Bode plots (B) of the Pt:Au 1:6 in 0.5 M HCOOH + 0.5 M H_2SO_4 at various electrode potentials. The electrode rotation is 1000 rpm.

With a further increase of the potential from 0.25 to 0.3 V, the impedance arc moves from the first quadrant to second quadrant implying the passivation of the electrode surface. This trend can also be observed on the bode plot at low frequencies, where the phase angles are larger than 90^o at potentials $\geq$ 0.3 V, indicating the presence of a negative charge transfer resistance as a consequence of the electrode surface passivation.[184] This electrode surface passivation usually attributed due to the reversible formation of oxygen containing species on Pt, presumably chemisorbed hydroxyl species. But this is not the case for the Pt-decorated Au. From the observation of the anodic current in 0.5 M H_2SO_4 as shown in Fig. 4.6, the surface oxidation on Pt decorated Au catalyst commences at higher potential than Pt/C and continues to shift to higher potential

with the decrease of the Pt:Au mole ratio, roughly ≥ 0.5 V for Pt:Au mole ratio of 1:6. The observed passivation at 0.3 V then is not due to the surface oxidation. This observation corroborates well with the positive shift of the onset potential for the formation of Pt surface oxide and the potential of the CO stripping peak with the decrease of the Pt coverage on Pt-decorated Au electrode as shown in the CO stripping experiment in Fig. 4.10 and as reported by Du and Tong.[145] We suggest that this passivation at low potential is due to the adsorbed water instead of the adsorbed hydroxyl species. With the increase of potential, the adsorbed water-metal interaction increases which causes the dissociation of H_2O at the surface to form the adsorbed hydroxyl (OH^-) species.[185]

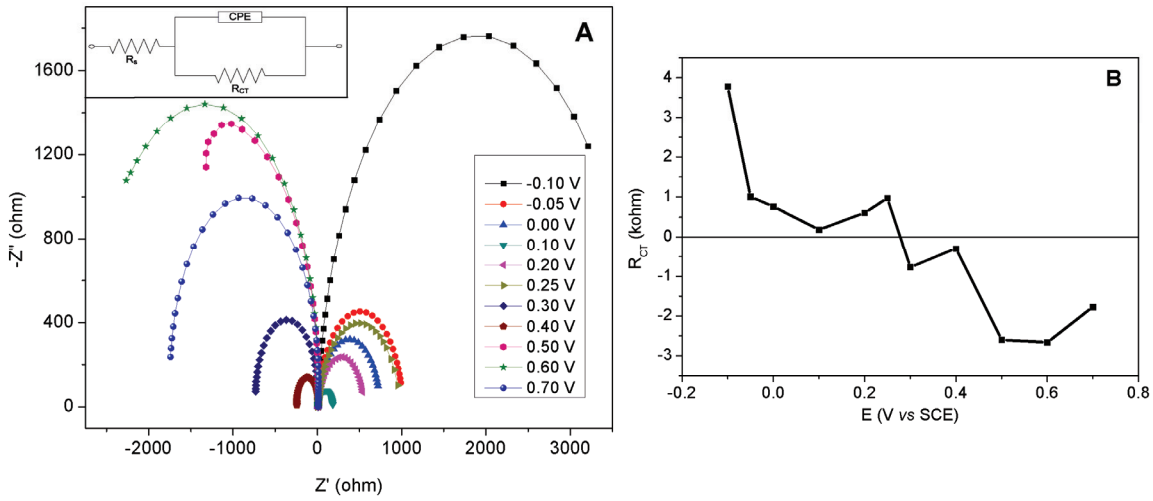

Fig. 4.13. A) Fitting results of the experimental data in Fig. 4.12 by using the equivalent circuit model shown in the inset. B) The dependence of R_{CT} on electrode potentials for the PtAu/C with Pt/Au mole ratio 1:6 as determined by fitting the experimental data based on the equivalent circuit model.

As shown in Fig. 4.12 part A above 0.3 V, the observed arc diameter first decreases from 0.3 to 0.4 V, then increases from 0.4 to 0.6 V. To elucidate the unusual behavior of EIS for the formic acid electro-oxidation on this decorated structure, we used the equivalent circuit model shown in the inset of Fig. 4.13 to fit the experimental data. This equivalent circuit model has been widely used to fit the experimental impedance

spectra that show only one primary semicircle in the complex plane representation.[152, 153, 184] It can be seen that the model fits well with the experimental data as shown in Fig. 4.13 part A and the variation of the charge transfer resistance (R_{CT}) as a function of electrode potential is shown in Fig. 4.13 part B." [157]

"If there's no adsorbed intermediate, the R_{CT} will increase continuously due to the strong interaction of adsorbed water on the Pt sites. The lack of clear trend for R_{CT} in the potential range above 0.25 V indicates the presence of adsorbed intermediate."[157] In the previous part we have shown that CO is not the adsorbed intermediate and formic acid will oxidize through the dehydrogenation pathway, so most likely the adsorbed intermediate is the reactive intermediate formed in the direct oxidation pathway, i.e. formate (HCOO-). The inconsistent trend on the charge transfer resistance as a function of potential might be related with the oscillatory phenomenon observed on Pt electrodes under potentiostatic and galvanostatic conditions.[186, 187] Based on the above explanation, we propose a mechanism for the formic acid electro-oxidation on the Pt-decorated Au surface: [160]

$$Pt + HCOOH \rightleftharpoons Pt\text{-}(HCOOH)_{ads} \quad (1)$$

$$Pt\text{-}(HCOOH)_{ads} \rightarrow Pt\text{-}(HCOO)_{ads} + H^+ + e^- \quad (2)$$

$$Pt\text{-}(HCOO)_{ads} \rightarrow Pt + CO_2 + H^+ + e^- \quad (3)$$

$$Pt + H_2O \rightleftharpoons Pt\text{-}(H_2O)_{ads} \quad (4)$$

$$Pt\text{-}(H_2O)_{ads} + HCOOH \rightleftharpoons Pt(HCOOH)_{ads} + H_2O \quad (5)$$

$$Pt\text{-}(H_2O)_{ads} + Pt\text{-}(HCOO)_{ads} \rightarrow 2Pt + CO_2 + H_2O + H^+ + e^- \quad (6)$$

At low potential region ($\leq$ 0.25 V) the formic acid will oxidize directly on the Pt sites according to reaction 1-3. After the adsorption of formic acid molecule on a Pt site, formic acid undergoes dehydrogenation reaction through the reactive intermediate formate and finally forms CO_2 in two fast reaction steps. Above 0.25 V, formic acid has

to compete with water for the free Pt sites. It has been shown by Iwasita et al, that the water adsorption strength on Pt (111) increases with increasing potentials above 0.4 V_{RHE}, while the hydroxyl containing species can form on Pt (111) at potentials above 0.5 V_{RHE}.[185, 188] Being aware of the strong water interaction, between 0.25 V to 0.4 V we suggest that the adsorbed water formed on the Pt-decorated Au electrode will be displaced with formic acid molecules and vice versa as shown in step 5.[188] Moreover the possibility of the adsorbed water to react with the formate species can not be neglected as shown in step 6.[189] With further increasing potential (≥ 0.5 V) the adsorbed water dissociates to form the hydroxyl species. This oxygen-containing species occupies much more Pt sites and is adsorbed strongly that resulted in less free Pt site for the step 1 to proceeds. The adsorption competition between the formic acid and water (at low potential) and oxygen containing species (at high potential) for the Pt sites can be seen from the faradaic current of formic acid oxidation where above 0.3 V the activity decreases rapidly and reach a plateau above 0.6 V. [160]

4.4. Conclusions

We have reported the preparation of carbon supported Pt-decorated Au nanoparticles by successive reduction method. From the TEM, UV-Vis, TGA, EDX and voltammetry analyses, we conclude that a decorated structure with presumably single isolated Pt atoms at lower Pt/Au ratio or small island consist of 2-3 Pt atoms at higher Pt/Au ratio exist on the Au nanocrystals surface and such a unique Pt atom configuration is beneficial for the oxidation of formic acid at low potential but not advantageous for the oxidation of methanol. As for the specific activity towards formic acid electro-oxidation at 0.1 V, we found that this decorated structure can exhibit more than one order of

magnitude enhancement compared to conventional Pt/C. Such an enhancement is attributed to the inhibition of poisonous intermediate formation that shows this catalyst favor the dehydrogenation pathway due to the ensemble effect and the electronic effect that may increase the reactivity of the Pt entities on Au substrate. Based on the EIS measurement, we propose a reaction mechanism for the formic acid oxidation on this decorated structure."

Chapter 5

The effect of subsequent Au reduction on the Pt-decorated Au nanoparticles and different Au core sizes on the activity of Pt-decorated Au nanoparticles for formic acid oxidation

5.1. Introduction

Bimetallic electrocatalysts often exhibit incredible physicochemical properties by offering unique surface structure compared to single metal electrocatalysts.[125, 127, 139, 140, 153, 155, 157, 190-193] Special attention has been focused on Pt-based bimetallic catalysts and among them; Pt-Au bimetallic is gaining much interest due to alloying Pt with Au will improve the catalytic activity of Pt by modifying its d-band electronic structure.[127-129]

In the past decades, the rapid emerging sciences in nanotechnology have driven an intensive research in fabrication of PtAu bimetallic system and deliberately control the structures at the nanoscale level.[125, 140, 158, 193, 194] However, little attention has been paid to the systematic investigation of the activity-stability-size relationship[5, 6] on the activity of PtAu bimetallic system. In this chapter, we report the synthesis of Pt-decorated Au electrocatalysts based on seed-mediated growth with different Au core size and evaluate their activities and durability for formic acid oxidation. Subsequently, we optimize the structure of the Pt-decorated Au by subsequently reducing Au precursor onto the as-prepared Pt-decorated Au nanoparticles. This investigation is motivated by the results obtained from the effect of Au core sizes where the smallest Au core size shows the highest activity but with a short durability. With the hypothesis that the addition of Au atoms after the Pt precursor reduction could decreases the number of continuous Pt atoms

ensemble that is beneficial for the formic acid oxidation, the amount of Au added was varied systematically and it was found that indeed the dilution of the surface Pt sites by adding more Au on the decorated Au of a size 2 nm lead to a higher activity and longer durability compared to without adding Au.

5.2. Experimental and characterization methods

5.2.1. Synthesis of Au nanoparticles with different sizes

The synthesis of Au nanoparticles with a mean size of 2 nm using Tetrakis(hydroxymethyl)phosphonium chloride (THPC) as the reducing agent is based on the protocol reported by Duff group.[195-197] Briefly, 45.5 mL of distilled water was added to a continuously stirring vessel (beaker). Then 1.5 mL of 0.2 M sodium hydroxide (NaOH) was then added to the beaker. Subsequently, the reducing agent THPC (1 mL of a solution of 1.2 mL of 80% aqueous solution diluted to 100 mL with water) was added as a reducing agent. After 3 minutes, 2 mL of $HAuCl_4 \cdot 3H_20$ with concentration of 25 mM was added. The mixture was allowed to mix for 30 min to ensure complete reaction. The amount of Au nanoparticles produced was approximately 10mg.

The synthesis of Au nanoparticles with a mean size of 5 nm can be seen in chapters 3.2.2 and 4.2.2.

The synthesis of Au nanoparticles with a mean size of 10 nm is based on modified Frens method.[198] Briefly, 200 mL of an aqueous solution of 0.1 % sodium citrate was heated to boiling. Into this boiling solution was added 2 mL of 25 mM $HAuCl_4 \cdot 3H_20$ and the boiling was continued for 1 hour. The color of the solution first turned purple and on further boiling changed to red ruby indicating the formation of Au nanoparticles. Note that instead of boiling the $HAuCl_4 \cdot 3H_2O$ solution as in Frens method, we boiled the

sodium citrate solution first. This method has been reported to produce gold nanoparticles of the size 10 nm.

5.2.2. Synthesis of Pt-decorated Au nanoparticles with different Au core sizes

The reduction of Pt precursor onto the as-prepared Au nanoparticles with different size can be seen in the chapters 3.2.3 and 4.2.3. In this study the Pt:Au mole ratio is fixed at 1:8. "Briefly, a certain amount of 0.1% aqueous H_2PtCl_6 and 0.1% aqueous $NH_2OH{\cdot}HCl$ was mixed with 100 mL water under vigorous stirring and heated to 60^oC for 3 hours. No color change was observed during this period. Then the gold seed suspension was added and the temperature was held constant at 60^oC for 2 hours. After 2 hours the solution was cooled to room temperature. The deposition of nanoparticles on carbon black Vulcan XC-72 was realized by mixing a certain amount of carbon with 5 mL water and sonication for 5 minutes with an ultrasonicator. Then the resulting carbon slurry was added to the nanoparticles solution prepared above and a small amount of 0.2 M HCl was added to modify the pH to 5 to assist the deposition of nanoparticles onto carbon black and followed by continuous stirring overnight. The total metal loading was fixed at 20% weight. The suspension was then filtered and washed with copious water. The final product was then dried at 70^oC in vacuum condition for 12 hours." [157,160]

5.2.3. Synthesis of Pt-decorated Au nanoparticles with different Au filling gap coverage

For this study, Au nanoparticles (mean size of 2 nm) is used as the substrate and the initial Pt/Au mole ratio was chosen as 1:1 by reducing Pt precursor onto the 2 nm Au nanoparticles as reported in chapters 3.2.3 and 4.2.3 but with $NH_2OH.HCl$ to H_2PtCl_6 mole ratio of 10:1. Subsequently $HAuCl_4$ was added and reduced by the excess

$NH_2OH.HCl$ and the amount of was varied. Briefly, 10 mg of 2 nm Au nanoparticles in 50 mL DI water was mixed with heated 100 mL DI water at 60°C containing 26.6 mg of $H_2PtCl_6.6H_2O$ and 0.5 mmol of $NH_2OH.HCl$ for 3 hours to produced Pt-decorated Au with Pt/Au mole ratio of 1:1. After the solution cooled down to room temperature, a controlled amount of $HAuCl_4.3H_2O$ solution was added into the solution. For the 1st experiment, no $HAuCl_4.3H_2O$ solution was added, this sample will be called PtAu=1:1. In the 2nd experiment, 11 mg of $HAuCl_4.3H_2O$ in 50 mL H_2O was added and allowed to react overnight, this sample will be called <100%. For the 3rd experiment, 14 mg $HAuCl_4.3H_2O$ in 50 mL H_2O was added, this sample will be called 100%. And for the final experiment, 17 mg $HAuCl_4.3H_2O$ in 50 mL H_2O was added, this sample will be called >100%. Subsequently all the hydrosols were mixed with a certain amount of carbon black slurry to produce a total metal loading of 20% and 0.2 M HCl was used to modify the pH to 5 to assist the deposition of nanoparticles onto carbon black. "The suspension was then filtered and washed with copious water. The final product was then dried at 70°C in vacuum condition for 12 hours."[157]

5.2.4. Characterizations

"The morphology was observed using JEM-1400 (JEOL) operated at 100 kV. The X-ray diffraction patterns were collected using D8 Bruker AXS X-ray diffractometer using Cu Kα radiation at a potential of 40 mV and current of 40 mA using a step scan of 0.02° and holding time of 10 seconds. The UV-vis spectrum of the Au and PtAu hydrosols were measured by a Shimadzu UV2450 spectrometer equipped with quartz cells. The concentrations were all 8 x 10^{-2} mM. The compositional analysis using EDX was performed using a scanning electron microscopy JEOL JSM-6390LA. The

electrochemical signals were recorded using Autolab PGSTAT 302 at room temperature in 3 electrode configuration system. The potentials were measured and reported against a saturated Ag/AgCl electrode."[157] The electrochemical procedures for CO stripping and poison stripping experiments can be seen in chapter 4.2.4.

5.3. Results and discussion

5.3.1. The effect of different Au particle size on the activity of Pt-decorated Au electrocatalysts

Fig. 5.1 shows the typical TEM images of the Au nanoparticles with different size and the as-prepared Pt-decorated Au nanoparticles with the same Pt/Au mole ratio (1:8) on carbon black. It can be seen that with the reduction of small amount of Pt precursor, the mean size of the Pt-decorated Au is quite closed with the size of the respective Au nanoparticles, indicating the successful reduction of Pt precursor on the Au surfaces by $NH_2OH.HCl$. By counting at least 500 nanoparticles of each sample on different areas, the diameters of the catalysts particles were measured and the results are shown in Table 5.1.

Table 5.1. Comparisons of particle sizes of the various Au/C and Pt-decorated Au/C.

Samples	Measured particle size by TEM (nm)	Measured particle size by XRD (nm)
Au 2 nm	2.1 ± 1.1	2.2
PtAu 2 nm	2.3 ± 0.9	-
Au 5 nm	4.8 ± 2.5	4.6
PtAu 5 nm	5.1 ± 2.4	-
Au 10 nm	10.2 ± 3.1	10.8
PtAu 10 nm	10.4 ± 4.2	-

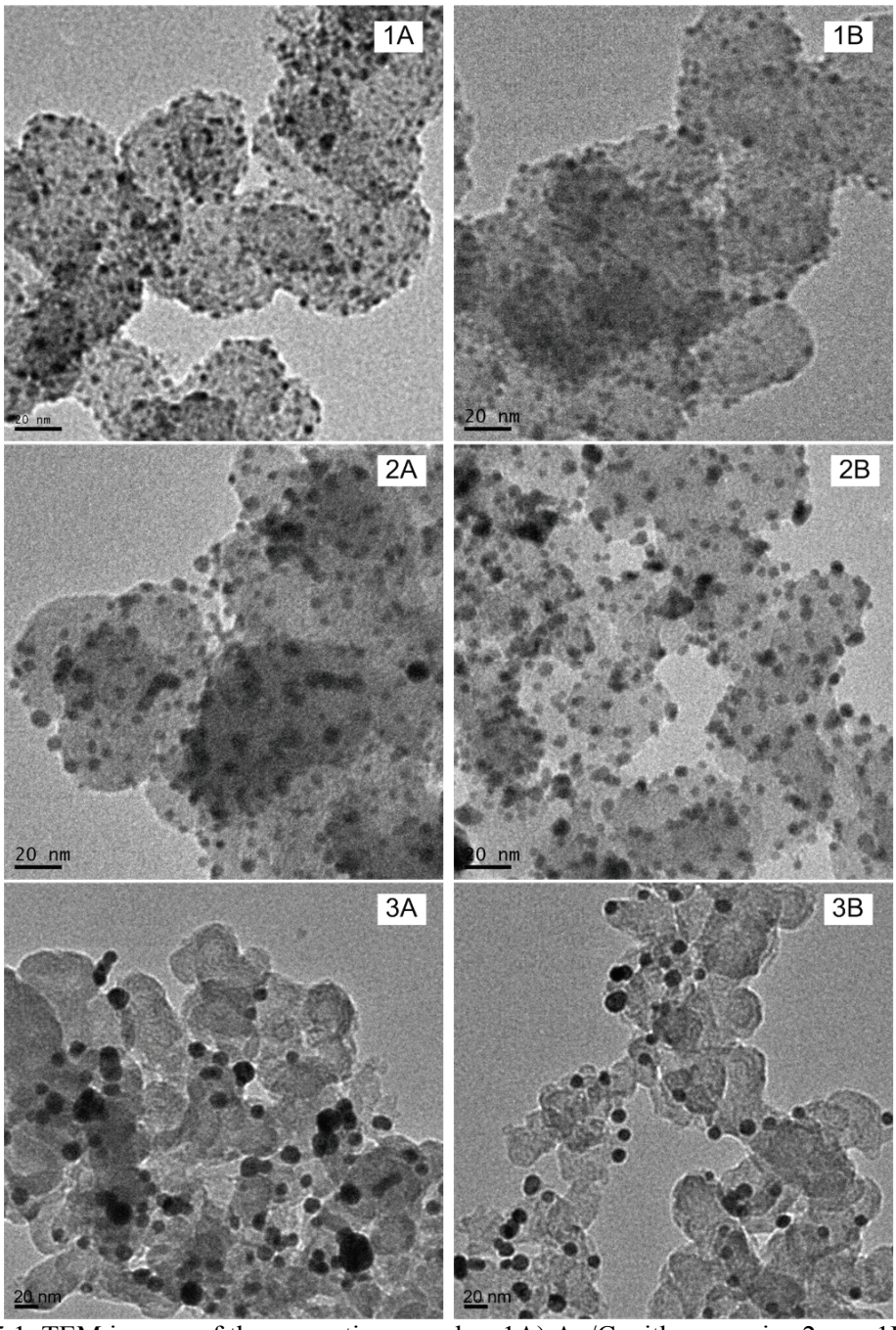

Fig. 5.1. TEM images of the respective samples: 1A) Au/C with mean size 2 nm; 1B) Pt-decorated Au with mean size 2 nm; 2A) Au/C with mean size 5 nm ;2B) Pt-decorated Au with mean size 5 nm ;3A) Au/C with mean size 10 nm ;3B) Pt-decorated Au with mean size 10 nm

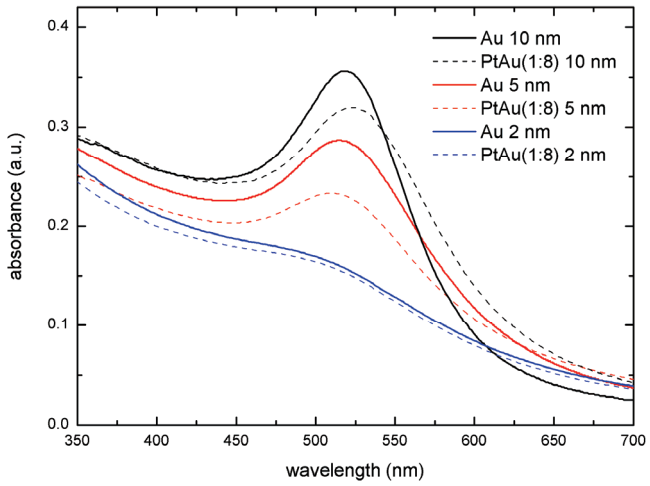

Fig. 5.2. UV-vis spectra of Au hydrosols with different Au sizes and their respective Pt-decorated Au hydrosols.

Au hydrosols exhibit strong plasmon resonance absorption that has been shown to be dependent on their particle size and shape. For roughly cubooctahedron Au nanoparticles, the plasmon peak usually falls between 515 and 530 nm. [199-201] Fig. 5.2 shows the UV-vis absorption spectra of the Au hydrosols with different particle size and the spectra of their respective Pt-decorated Au hydrosols. For the 2 nm Au and its Pt-decorated Au, there are no obvious plasmon peak which is in accordance with the results reported by Duff et al.[195, 197] But for the 5 nm Au and 10 nm Au hydrosols, there are strong plasmon absorption peak centered on ~520 nm. The absorbance increase is due to the progressive increase in the particle size where larger particles have larger molar extinction coefficient values. This observation agrees with the TEM analysis. When the Pt precursor is reduced on the respective Au nanoparticles, the plasmon absorption peaks decrease and become broader indicating the decreased exposed Au surface that suggest the successful reduction of Pt precursor onto the Au nanoparticles.

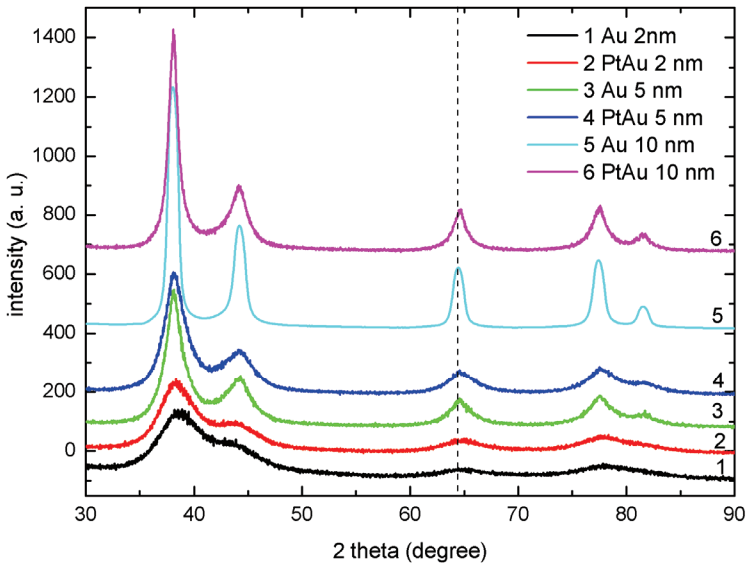

Fig. 5.3. XRD patterns of Au/C with different sizes and their respective Pt-decorated Au/C.

The XRD spectra of all the Au nanoparticles and the as-prepared Pt-decorated Au nanoparticles can be seen in Fig. 5.3. It can be seen that the spectra of all the Pt-decorated Au resemble the Au spectra, but the shape of the peaks are not symmetric and the intensity slightly increase in the middle position between pure Pt peaks and Au peaks, which in accordance with the XRD analysis in chapters 3 and 4 indicating the present of Au and Pt phases. The most striking difference can be observed on the peak width of Au 10 nm and PtAu 10 nm, where the widths of the PtAu 10 nm peak are broader than that of Au 10 nm indicating a much smaller particle size which is inconsistent with the TEM analysis, where the mean particles size of the respective Pt-decorated Au is close with that of Au. This discrepancy confirms that Scherrer formula utilizing XRD data can not be used to characterize the particle size of Pt-decorated Au structure.

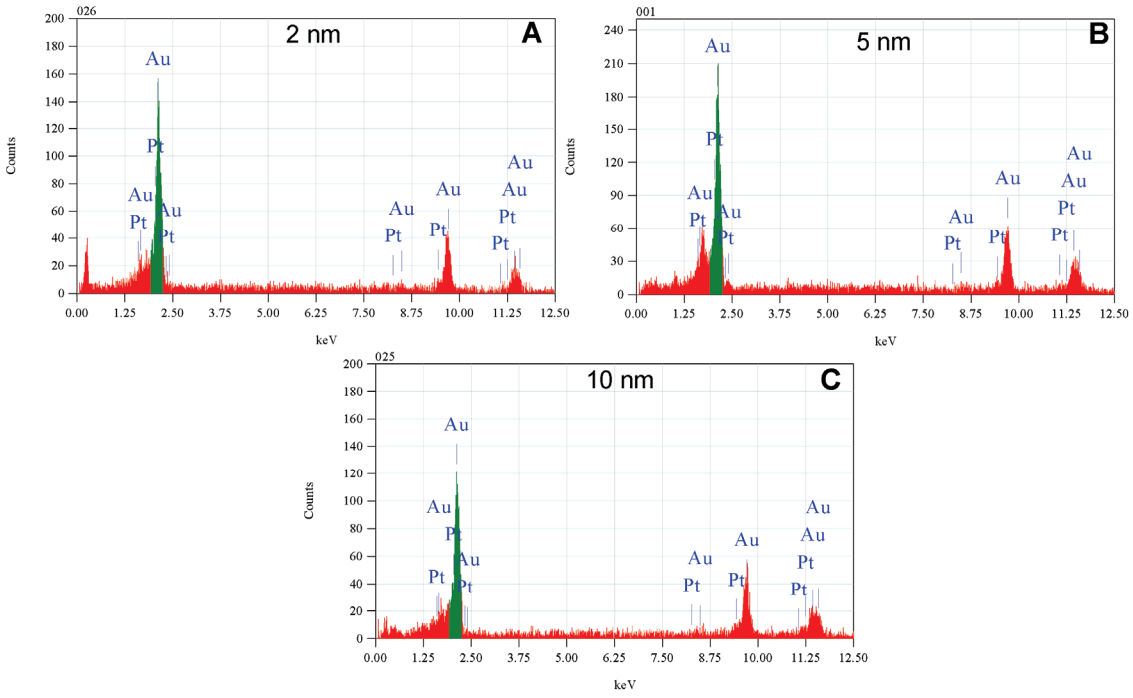

Fig. 5.4. EDX spectra of A) Pt-decorated Au with a size of 2 nm; B) Pt-decorated Au with a size of 5 nm; C) Pt-decorated Au with a size of 10 nm

To confirm the successful reduction of Pt precursor, EDX analysis was conducted and the results can be seen in Fig. 5.4. It can be seen that all the as-prepared Pt-decorated Au nanoparticles contain both Pt and Au and by quantitative analysis, the Pt/Au mole ratios of all the samples are closed with the intended ratio of 1:8 that verify the complete reduction of Au precursor and Pt precursor.

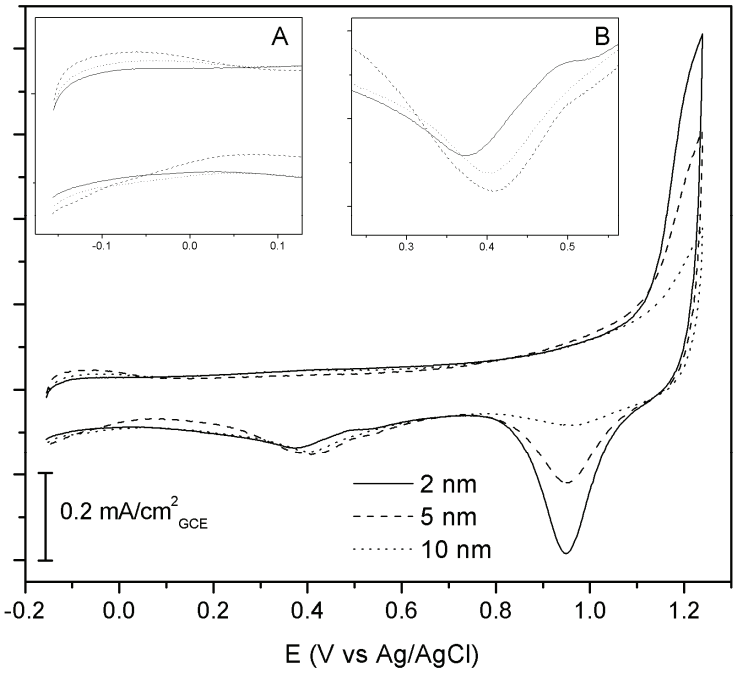

Fig. 5.5. CVs of Pt-decorated Au with different sizes in deaerated 0.5 M H_2SO_4 at 50 mVs^{-1}. Insets show the blow up region of A)-0.15 V to 0.12 V and B) 0.25 V to 0.55 V (cathodic scan)

Fig. 5.5 shows the cyclic voltammograms of the Pt-decorated Au nanoparticles with different size but with the same Pt/Au mole ratio. It can be seen in the inset on Fig. 5.6 "that after the decoration of Au nanoparticles by Pt, the well-defined hydrogen adsorption–desorption region and the Pt oxide reduction peaks appear which are the characteristics of Pt-based electrodes. The Au oxide reduction peaks at 0.95 V still can be observed for all the catalyst,"[160] but with the increase of size, the peak becomes smaller and the intensity becomes lower. Since the current is normalized with the glassy carbon electrode area and the total metal loading are all the same, the decrease in the Au oxide reduction peak with the increase of Au size is related with the Au surface area where the small Au nanoparticles has higher surface area. While the intensity of the Pt oxide

reduction peaks for all the catalysts are roughly the same, indicating that all the catalysts contains almost the same amount of Pt atoms available for electrocatalytic reactions.

The CVs also reveals that for the same Pt/Au mole ratio, the 2 nm Pt-decorated Au nanoparticles has higher oxophilicity compared to the other Pt-decorated Au nanoparticles that have bigger particle size (see inset B of Fig. 5.5). This suggests that the small Pt-decorated Au shows a stronger bonding between Pt and oxygen containing species compared with Pt-decorated Au with bigger particle size even though they have the same Pt/Au mole ratio.

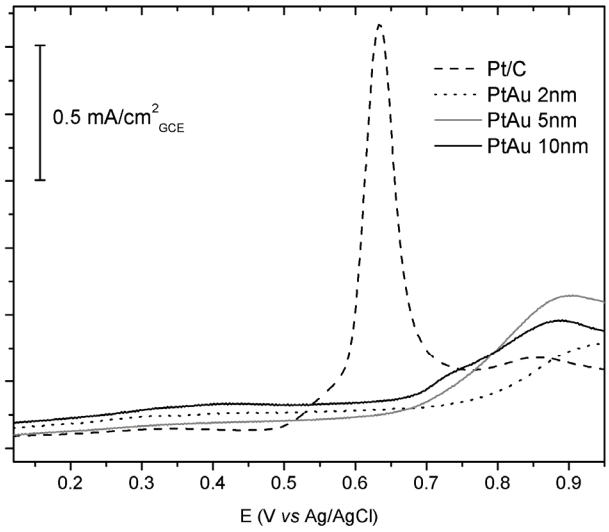

Fig. 5.6. CO stripping curves for Pt/C and various Pt-decorated Au with different sizes in CO-saturated 0.5 M H_2SO_4.

CO stripping experiment was further conducted to characterize the surface properties of the as-prepared Pt-decorated Au nanoparticles since CO adsorption is very sensitive to the surface structure and particle size. Fig. 5.6 shows the CO stripping curves of Pt/C and Pt-decorated Au nanoparticles with different size. It can be seen that all the Pt-decorated Au nanoparticles have higher CO stripping peak potentials and much broader peak compared to that of Pt/C. This positive potential peak confirms the stronger

Pt-CO bond on the surface of Pt-decorated Au as predicted by the Nørskov d-band centre model.[128, 129] More interestingly is with the size decrease of Pt-decorated Au nanoparticles, the CO stripping peak potentials shifts toward high potentials that suggest a stronger Pt-CO bonding on this catalysts which is in accordance with the CV in 0.5 M H_2SO_4 analysis where a stronger bond between Pt and oxygen containing species has been observed with the size decrease of Pt-decorated Au nanoparticles.

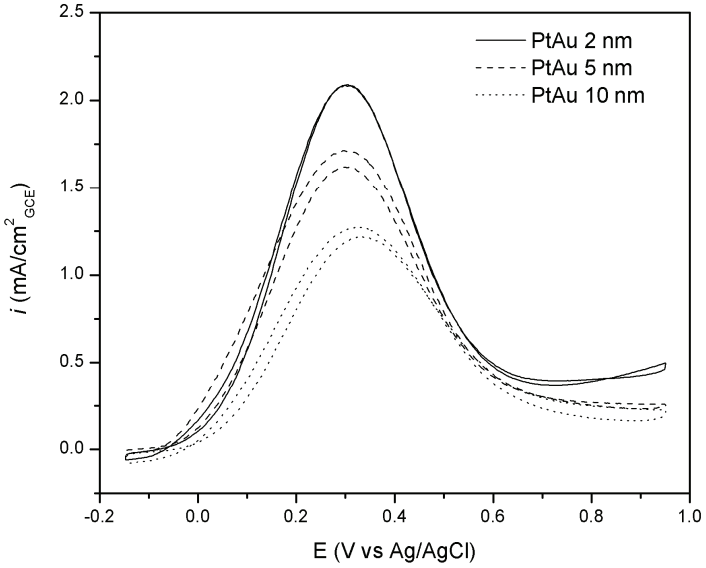

Fig. 5.7. CVs of Pt-decorated Au with different sizes at 10 mV s^{-1} and 1000 rpm in 0.5 M H_2SO_4 + 0.5 M HCOOH.

The activity of the as-prepared Pt-decorated Au nanoparticles as electrocatalysts were tested for formic acid oxidation. Fig. 5.7 shows the CVs of Pt-decorated Au electrocatalyst with different size in 0.5 M H_2SO_4 + 0.5 M HCOOH. Obviously all the Pt-decorated Au oxidize formic acid through the dehydrogenation branch which can be seen that the forward and backward scans are not appreciably differ and only one peak observed at 0.3 V on the anodic scan, indicative of the dehydrogenation pathway. [159, 161] Interestingly, the current normalized with the glassy carbon electrode area increases with

the decrease of size which suggest that the catalytic activity actually increases with the decrease of particle size. In addition, the peak potential also decreases with the decrease of particle size, which suggest the higher catalytic activity the small Pt-decorated Au possess. This can be related with the 'electronic' effect as explained in chapter 4.3.7, in accordance with the CO stripping experiment and CV in 0.5 M H_2SO_4 analyses where the smaller the Pt-decorated Au size, the stronger the reactivity towards CO and oxygen containing species, respectively.

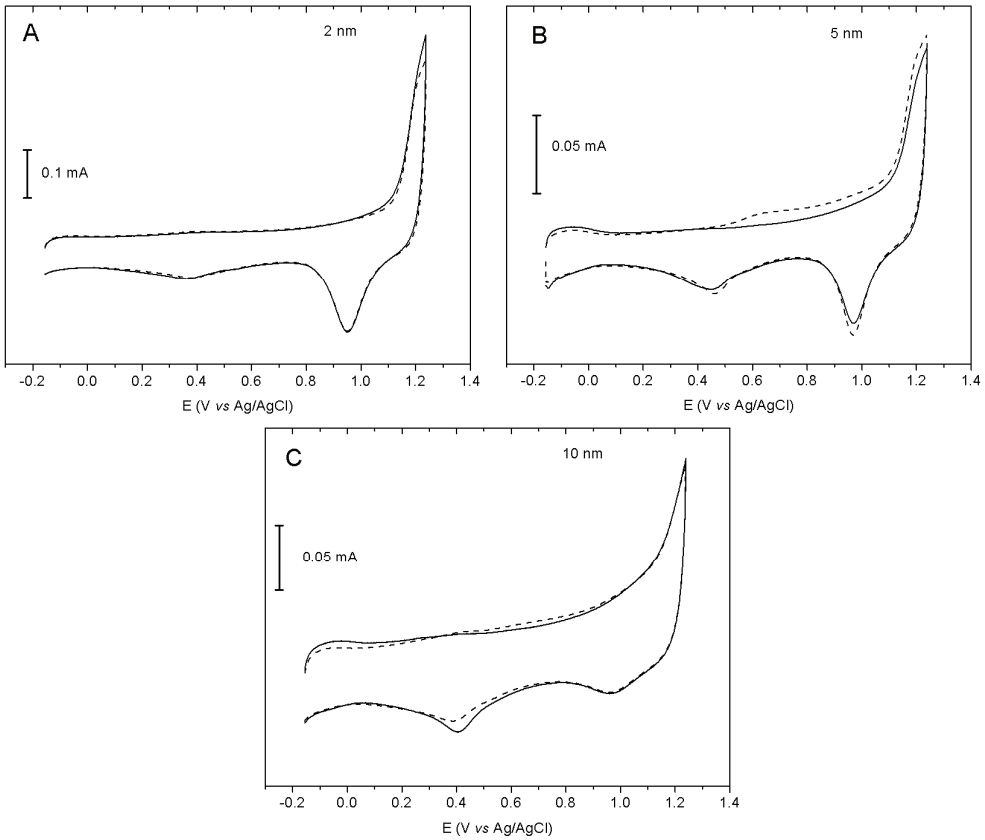

Fig. 5.8. CV curves of Pt-decorated Au with different size in N_2 saturated 0.5 M H_2SO_4 (full line). Dash line is in 1 M CH_3OH + 0.5 M H_2SO_4. Scan rate: 50 mV s^{-1}.

Fig. 5.8 shows the electro-activity of the Pt-decorated Au with different sizes towards methanol electrooxidation. It is clear that all the Pt-decorated Au have negligible

activity for methanol electrooxidation. This further confirms the 'ensemble' effect is the origin of the activity beside the 'electronic' effect, in accordance with the explanation in chapter 4.3.7.

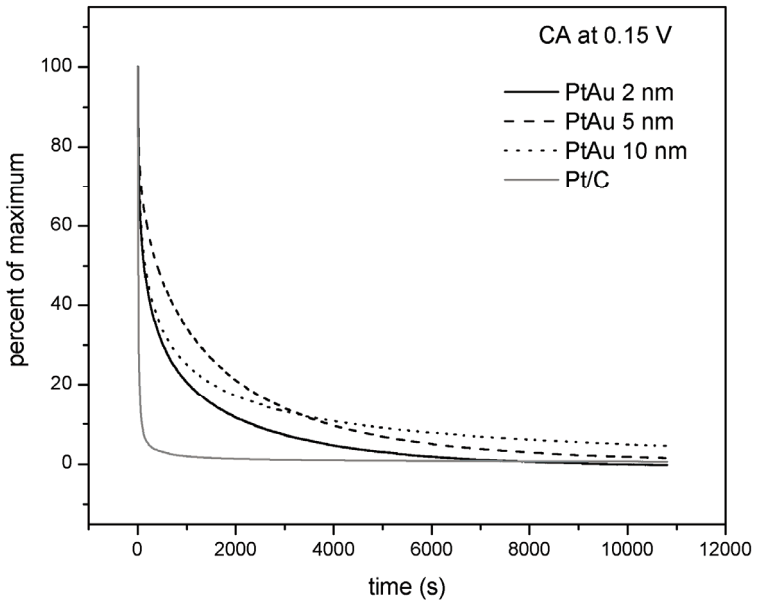

Fig. 5.9. Chronoamperometric plots for formic acid oxidation at 0.15 V and 1000 rpm in 0.5 M H_2SO_4 + 0.5 M HCOOH for Pt/C and Pt-decorated Au with different sizes.

The chronoamperometric plots of Pt/C and various Pt-decorated Au with different sizes are compared in Fig. 5.9. At a fixed potential of 0.15 V, formic acid can be oxidized on the catalyst surface and the poisonous intermediate CO_{ads} would gradually accumulate and occupy most of the Pt sites. A sharp decay in the activity for Pt/C is indicative of fast accumulation of CO_{ads} on the Pt sites. In contrast, for the cases of the Pt-decorated Au with different size, the decays are more gradual. Interestingly, the decay in activity after 3 hours is less severe for the 10 nm Pt-decorated Au and more severe for the 2 nm Pt-decorated Au and the 5 nm Pt-decorated Au lies in between. This observation suggests that despite the 2 nm Pt-decorated Au has higher initial activity, after prolonged formic acid oxidation, the activity decreases substantially.

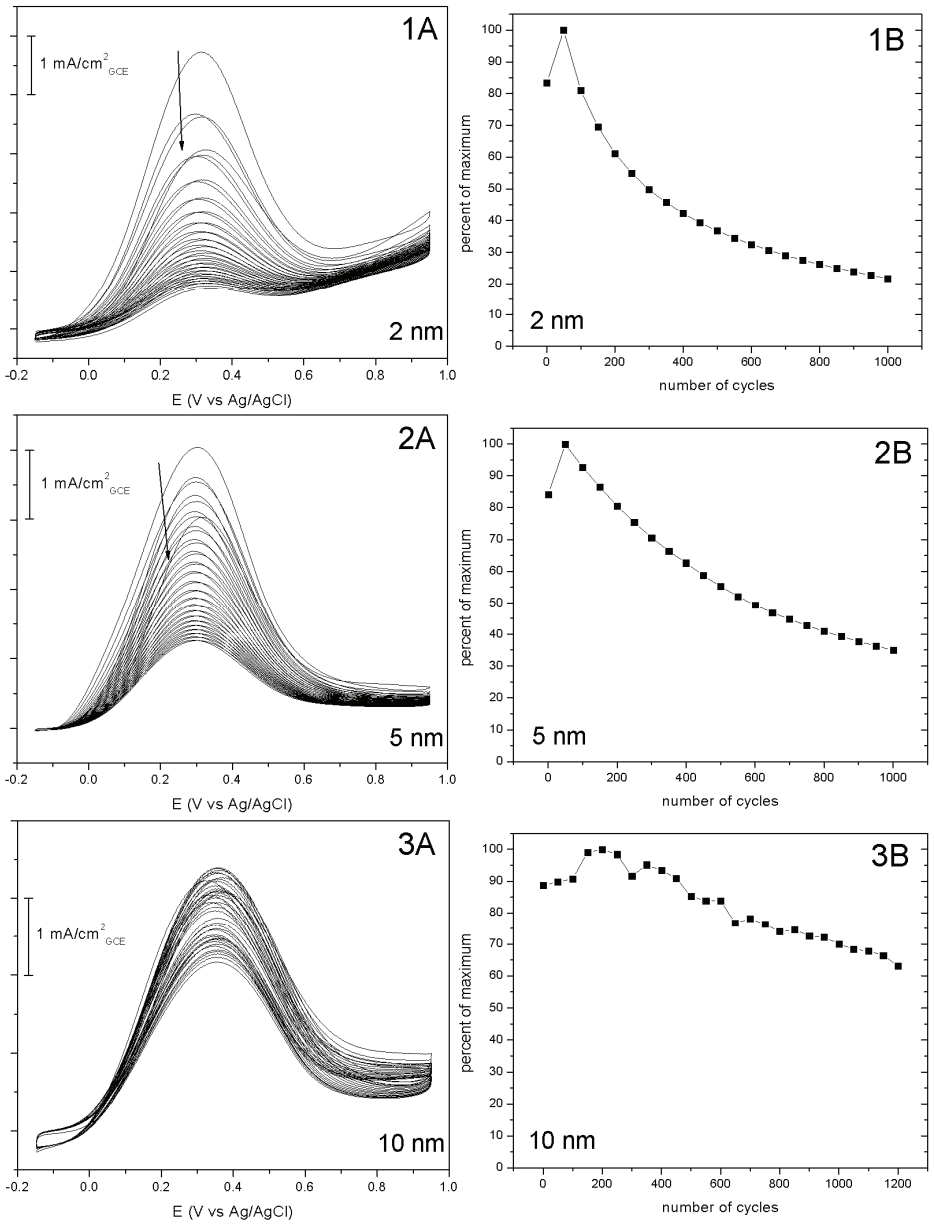

Fig. 5.10. Electrocatalysis stability of Pt-decorated Au catalysts during continuous CV cycles between -0.15 to 0.95 V in 0.5 M HCOOH + 0.5 M H_2SO_4 at 50 mV s^{-1} for 1) 2 nm Pt-decorated Au; 2) 5 nm Pt-decorated Au and 3) 10 nm Pt-decorated Au. Part A shows the CVs cycles for every 50 cycle while part B shows the normalized peak current at ~0.3 V as a function of cycle number.

Unlike the CA experiment that shows the durability of the electrocatalysts at a fixed potential, repeated CV cycles within appropriate potential range in acidic electrolyte is a good method to evaluate the degradation of an electrocatalysts.[190, 202] The

degradation tests were carried out by cycling the working electrode between -0.15 and 0.95 V at a scan rate 50 mV s^{-1} in deaerated 0.5 M HCOOH + 0.5 M H_2SO_4 and the results are presented in Fig. 5.10. The CV scans of 2 nm Pt-decorated Au shows a significant decrease in the activity, where it losses 80% of its initial maximum activity. But unexpectedly, the durability of the catalysts in terms of formic acid oxidation actually improves with the increase of particle size, where the activity of 5 nm Pt-decorated Au and the activity of 10 nm Pt-decorated Au decrease about 65% and 38% of their initial maximum activity, respectively.

To further study the durability of the electrocatalysts, the CV scans in 0.5 M H_2SO_4 of all the samples were examined before and after the repeated potential cycling in 0.5 M HCOOH + 0.5 M H_2SO_4 and the results are shown in Fig. 5.11.[190, 202] The 1st, 2nd and 20th CV scans after the durability test were plotted to show the dynamic of the CV shape. It is obvious that the major cause of the activity dropped is the loss of surface area (Pt surface area and Au surface area) especially for the 2 nm Pt-decorated Au, where a significant decrease in the Au-oxide reduction area before and after the potential cycling of more than 50 % can be observed. And with the increase of the particle size, the difference in the Au-oxide reduction area before and after potential cycling becomes less significant. This suggests that the 2 nm Pt-decorated Au losses most of the Au surface area. The possible modes of surface area losses of Pt and Au are the Pt dissolution, Ostwald ripening and aggregation due to the carbon corrosion.[203, 204] It is commonly known that the size of Pt nanoparticles will eventually increase to 8-10 nm after fuel cell operation, as a result of the migration and agglomeration.[203, 204] The increase in durability when the Pt-decorated Au particle size increase maybe due to the reason where big

particles are more resistant to dissolution, Ostwald ripening and aggregation due to carbon corrosion.

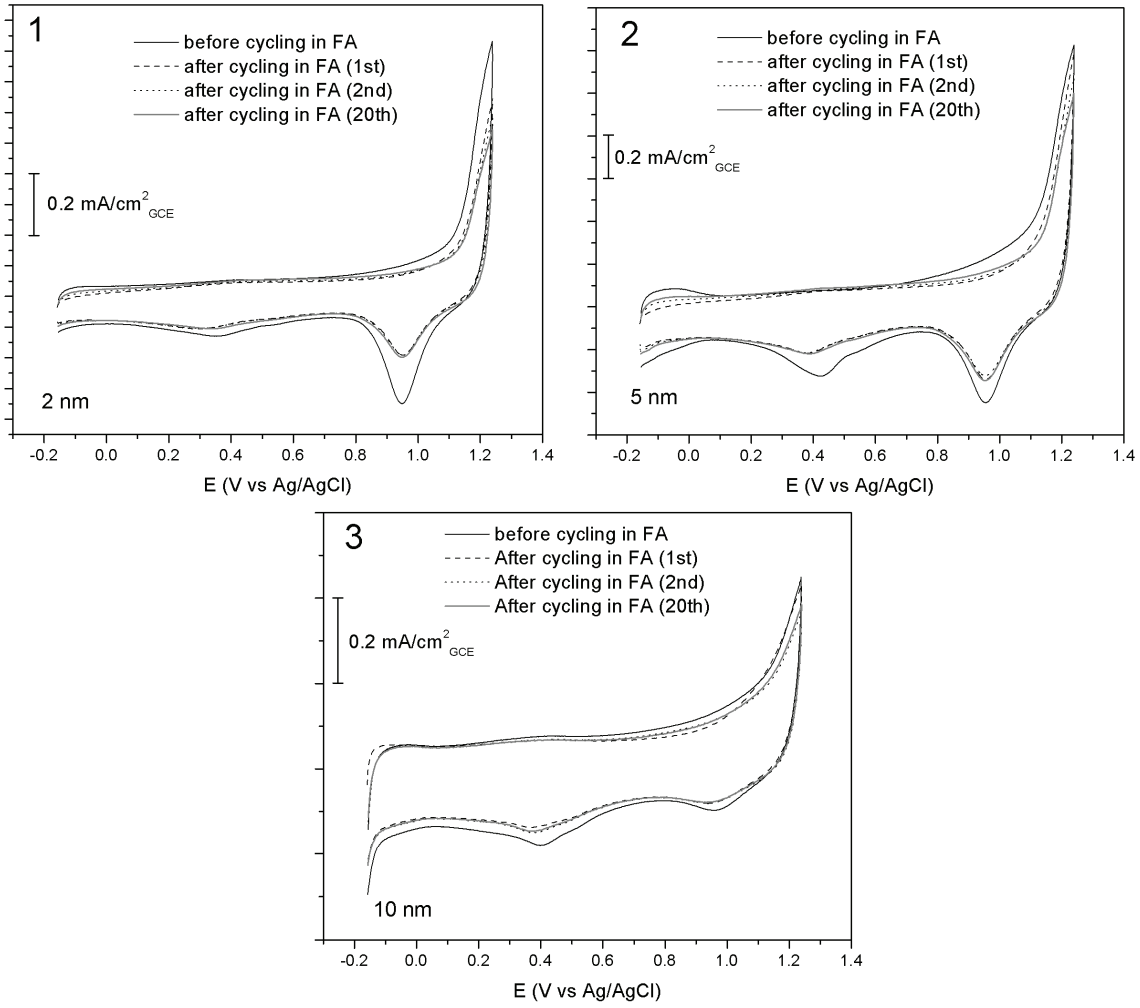

Fig. 5.11. CVs of Pt-decorated Au catalysts in 0.5 M H_2SO_4 at 50 mV s^{-1} before and after 1000 cycles in 0.5 M HCOOH + 0.5 M H_2SO_4 for 1) 2 nm Pt-decorated Au; 2) 5 nm Pt-decorated Au and 3) 10 nm Pt-decorated Au.

5.3.2. The effect of subsequent Au reduction on the Pt-decorated Au electrocatalyts

Motivated by the results in chapter 5.3.1, where the 2 nm Pt-decorated Au shows higher activity but lower durability towards formic acid oxidation compared to bigger Pt-decorated Au nanoparticles, we optimize the surface structure of Pt-decorated Au based on the 2 nm Au core size by subsequently reduced Au precursor onto the surface of 2 nm Pt-decorated Au to obtain a better stability. In this study the initial Pt/Au mole ratio was chosen to be 1:1, and subsequently the Au precursor was reduced. Our initial experiments shows that in order to obtain Pt_{shell}-Au_{core} nanoparticles with the 2 nm Au as the substrate, the Pt/Au mole ratio needed was 2:1. With the initial Pt/Au mole ratio of 1:1 and assuming that the growth is fully epitaxial, for the 2nd experiment (<100% sample) where the amount of $HAuCl_4.3H_2O$ added was 11 mg, it is expected that a submonolayer of Pt and Au formed on the 2 nm Au surface as shown in the Scheme 5.1 and when 14 mg (100% sample) and 17 mg (>100% sample) of $HAuCl_4.3H_2O$ were added, one monolayer and more than one monolayer of Pt and Au should formed, respectively. It is expected that as the results of reducing Au precursor onto the PtAu=1:1, the durability of the catalyst will be enhanced due the subsequently reduced Au precursor will fill in the gap between the Pt-islands that will prevent the formation of bigger Pt island.

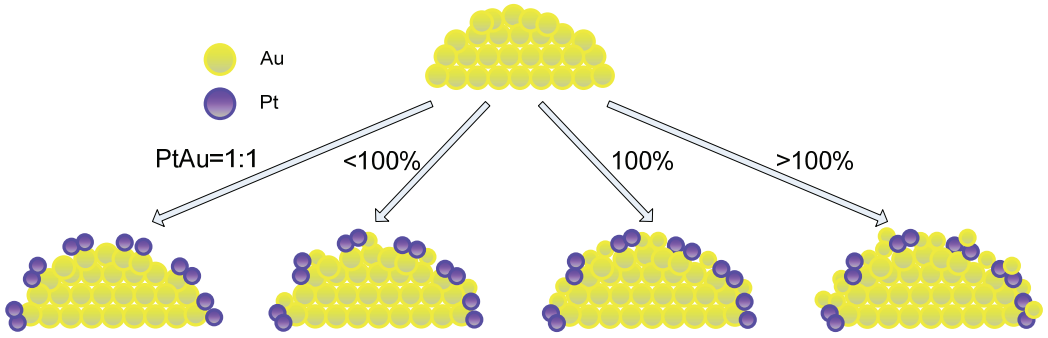

Scheme 5.1. The proposed growth mechanism of Pt and Au precursors onto the 2 nm Au nanoparticles.

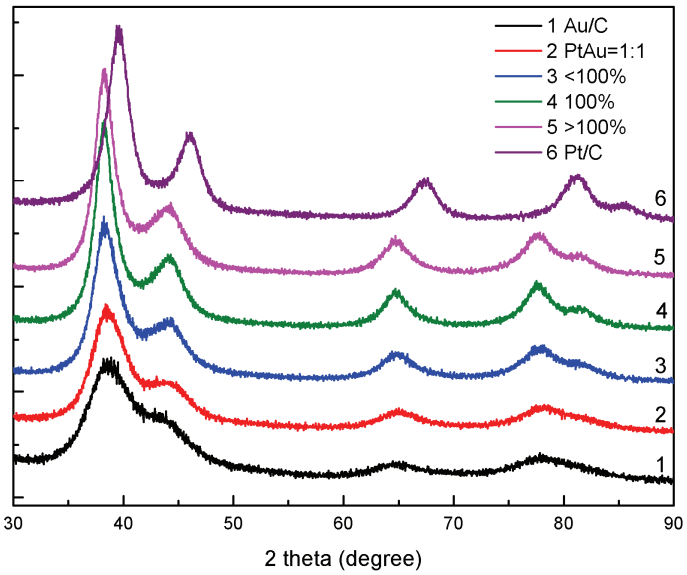

Fig. 5.12. XRD patterns of Au/C, Pt/C, PtAu=1:1, <100%, 100% and >100% samples.

Fig 5.12 shows the XRD patterns of all the samples. It can be seen that the PtAu=1:1, <100%, 100% and >100% only show the reflection peaks of face centered cubic Au, indicating that the amount of Pt entities in these samples are low and can not be detected by XRD. But as explained in the previous chapter, the peak width of XRD patterns containing Pt and Au with core-shell and decorated structure can not be used to determine the particle size. So that to determine the particle size, only TEM image analysis was used. By counting around 500 particles from 5 different areas, the mean particle size of the respective samples were constructed and tabulated in Table 5.2.

Table 5.2. Comparisons of particle sizes of the Au/C, <100%, 100%, >100% samples.

Samples	Measured particle size by TEM (nm)	Measured particle size by XRD (nm)
Au	2.1 ± 1.1	2.2
PtAu=1:1	2.9 ± 1.7	-
<100%	3.1 ± 2.1	-
100%	3.5 ± 2.5	-
>100%	3.6 ± 2.4	-

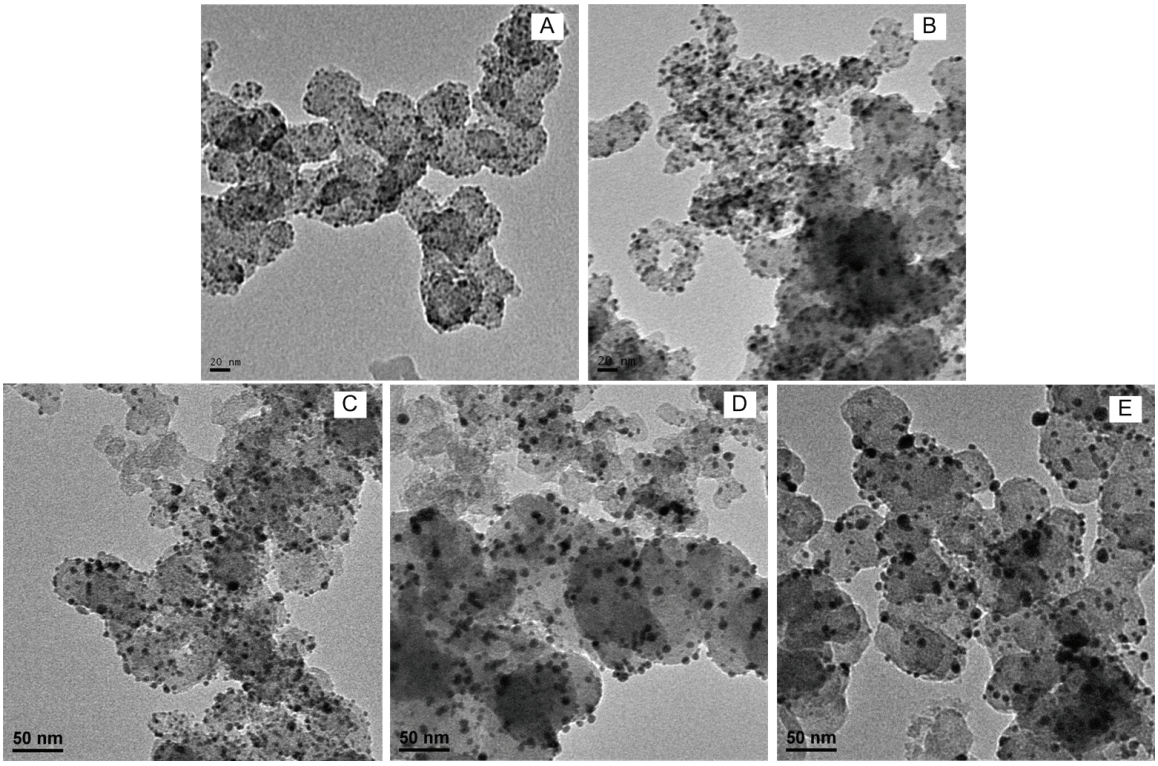

Fig. 5.13. TEM images of the respective samples; A) Au/C; B) PtAu=1:1; C) <100%; D) 100%; E) >100%.

Fig. 5.13 shows the TEM images of the Au/C, PtAu=1:1, <100%, 100% and >100%. It can be seen that the Au/C has high monodispersity with a mean particle size of 2.1 nm and dispersed very well on carbon black. The same conclusions can be observed for the PtAu=1:1 with a mean particle size of 2.9 nm which is close with that of Au/C, indicating the reduction of Pt precursor happens on the surface of the Au nanoparticles, forming a submonolayer of Pt. While the mean particle sizes of the <100%, 100% and >100% are quite close with that of PtAu=1:1 indicating the subsequent reduction of Au precursor onto the as prepared PtAu=1:1.

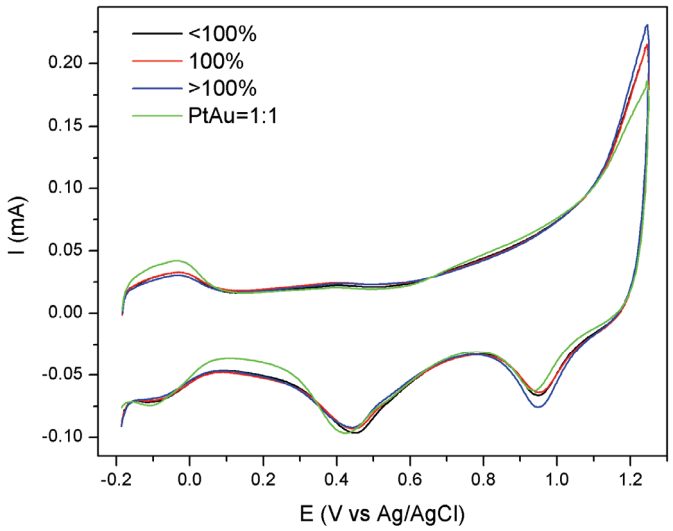

Fig. 5.14. CVs of PtAu=1:1, <100%, 100% and >100% samples in 0.5 M H_2SO_4 at 50 mVs^{-1}.

Fig. 5.14 compares the CV scans recorded in 0.5 M H_2SO_4 for the PtAu=1:1, <100%, 100% and >100%. It can be seen that all the samples exhibit the same characteristic like Pt/C (H_{UPD} area at low potentials and the Pt oxide reduction peak at 0.45 V) and Au/C (Au oxide reduction peak at 0.95 V) that confirms the surfaces are consist of Pt and Au crystals which is indicative of the formation of decorated structure.. Although the total metal loading of all the samples are the same, it can be seen that the PtAu=1:1 possess the highest Pt active area, as revealed by a larger H_{UPD} area compared to the other samples. In addition, the Au oxide reduction peak area also increases with the increase in the amount of Au deposited. This is because for the same total metal loading, the PtAu=1:1 contains more Pt atoms that mostly reside on the surface thus catalytically available for the electrocatalysis and with the increasing amount of Au precursor reduced, the Au surface area also increases.

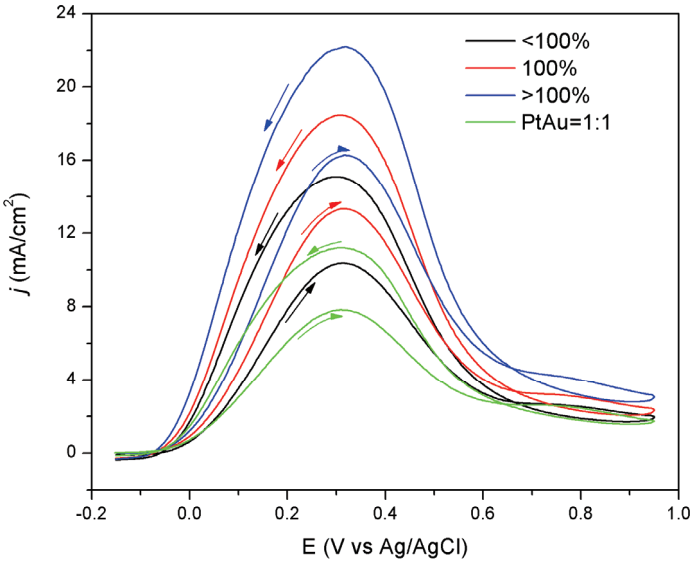

Fig. 5.15. CVs of PtAu=1:1, <100%, 100% and >100% samples in 0.5 M HCOOH + 0.5 M H_2SO_4 at 50 mVs^{-1}.

What is of interest is the unprecedented high activity this decorated structure exhibited for formic acid oxidation when more Au precursors are reduced onto the PtAu=1:1. Fig. 5.15 shows the voltammograms of PtAu=1:1, <100%, 100% and >100% in 0.5 M formic acid. It is unexpected that the addition of more Au onto the PtAu=1:1 actually increase the current density in the forward scan and backward scan, even though the addition of more Au decreases the catalytically active Pt surface sites. But for these samples, the forward scans always lower than the backward scans, indicating that CO_{ads} still formed on these catalysts on a lower extent compared with that of Pt/C. This conclusion can also be observed from the appearance of small discernible peak on the forward scan at ~0.78 V, indicating the CO_{ads} oxidation process by the Pt-oxygen containing species.

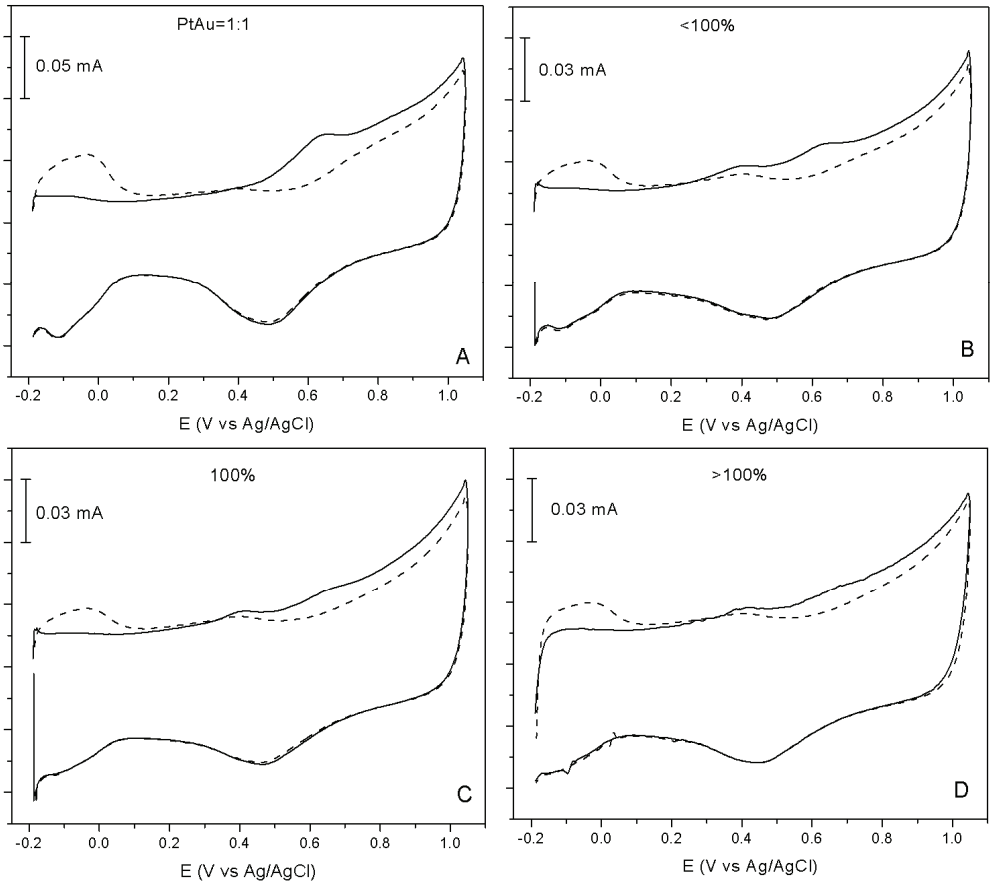

Fig. 5.16. Poison stripping experiment on A) PtAu=1:1, B) <100%, C) 100%, and D) >100% samples. The poisonous species was adsorbed from 0.5 M HCOOH and the poison stripping was conducted at 50 mVs^{-1} in 0.5 M H_2SO_4. The full line shows the first positive scan while the dotted line shows the subsequent scan, upon removal of the poisonous species.

To characterize the formation of CO_{ads} formed from the dehydration of HCOOH, the poison stripping experiment was conducted with the results presented in Fig. 5.16. The first forward scan is the stripping (oxidation) of the CO_{ads} formed from the dissociative adsorption of HCOOH. It is obvious that the PtAu=1:1 still shows a small peak in this first positive going scan that indicates CO still formed. But with the reduction of Au precursor, the peak becomes less discernible and almost disappear when the amount of Au precursor reduce was increased, suggesting that the addition of more Au

creates less number of ensemble sites that can produce CO during the electrooxidation of formic acid.

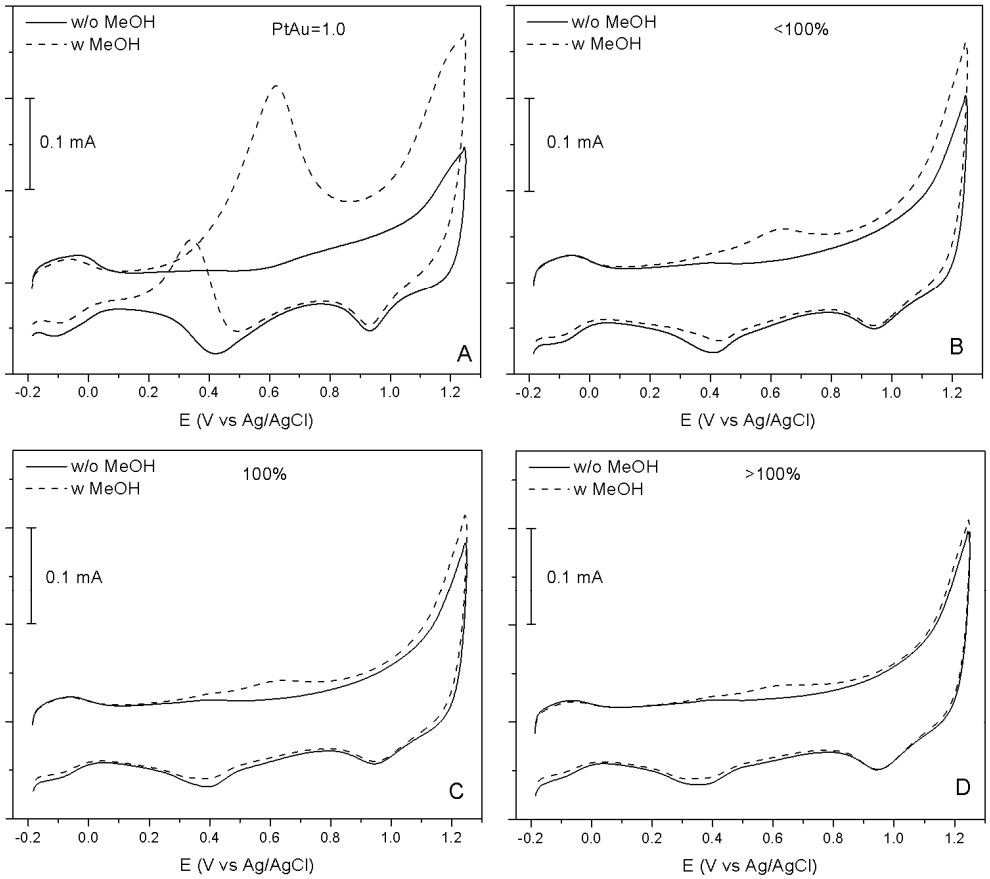

Fig. 5.17. CVs of A) PtAu=1:1, B) <100%, C) 100% and D) >100% samples in N_2 saturated 0.5 M H_2SO_4 (full line). Dash line is in 1 M CH_3OH + 0.5 M H_2SO_4. Scan rate: 50 mV s^{-1}.

To further prove that the addition of more Au on the PtAu=1:1 could form less continuous ensemble sites that is beneficial for the formic acid oxidation, we conducted methanol electrooxidation experiment and the results are shown in Fig. 5.17. It has been shown by DFT calculation that a continuous ensemble of at least 4 Pt atoms is needed in order for methanol oxidation could proceed.[170] By comparing the full line CVs with and without the presence of methanol, it is obvious that, when Au precursor is reduced onto the PtAu=1:1, less methanol can dissociate and oxidize on the Pt sites, indicating that the

addition of Au formed less continuous Pt ensemble sites needed for methanol oxidation. This conclusion also can be observed from the less blocking of the H_{UPD} area for the <100%, 100% and >100%.

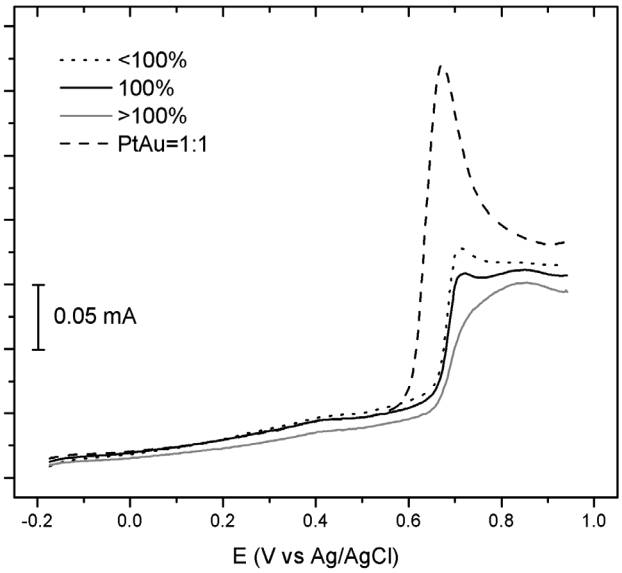

Fig. 5.18. CO stripping curves of PtAu=1:1, <100%, 100% and >100% samples in 0.5 M H_2SO_4 at 50 mVs^{-1}.

Besides the ensemble effect, we predict that electronic effect may play a role in the electro-activity improvement when Au precursor is reduced onto the PtAu=1:1. To verify this CO stripping experiments were conducted and the results are shown in Fig. 5.18. It can be seen that the addition of Au shifts the CO stripping peak potential and the CO stripping onset potential, indicating a stronger CO bond on Pt sites. This confirms that indeed the electronic effect may play a role in the increase of activity for the <100%, 100% and >100% samples compared with that of PtAu=1:1 sample. Closer look on the CO stripping curves reveals that the <100% and 100% samples consist of two poorly separated peaks, one at 0.71 V and the other at 0.85 V, which are believed to be related to the two types of Pt surface sites on the Au electrode surface as observed by Du et al.

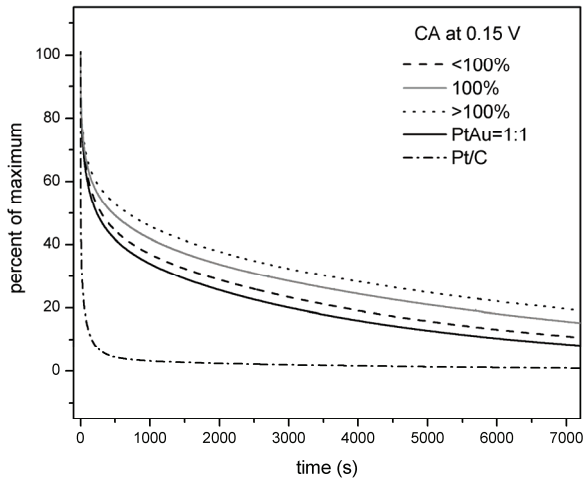

Fig. 5.19. Chronoamperometric plots for formic acid oxidation at 0.15 V and 1000 rpm in 0.5 M H_2SO_4 + 0.5 M HCOOH for Pt/C. PtAu=1:1, <100%, 100% and >100%.

The performance stability of the electrocatalysts for formic acid oxidation was investigated by chronoamperometry and the results are shown in Fig. 5.19. Steady state measurements were carried out at a constant potential of 0.15 V for 2 hours. While the Pt/C shows a fast decay in activity, the PtAu=1:1, <100%, 100% and >100% samples show a slow decay in current and after a period of 2 hours, the PtAu=1:1, <100%, 100% and >100% still can maintain 9%, 11%, 15% and 20% of their initial activity, respectively, indicating that the subsequent reduction of Au precursor onto the PtAu=1:1 sample does not just increase the specific activity but also increases the durability of the catalysts.

5.4. Conclusions

In this chapter, we have reported the effect of different particle sizes on the activity of Pt-decorated Au, where with the increase of size for the same Pt/Au mole ratio the durability of the catalysts toward formic acid electrooxidation actually increases, due to big particle size can mitigate the effect of particle aggregation. But it is found that the smallest Pt-decorated Au (2nm) in this study possess the highest activity toward formic

oxidation albeit with low durability. With this finding, the structure of the 2 nm Pt-decorated Au was optimize by subsequently reducing Au precursor onto the as prepared Pt-decorated Au with Pt/Au=1:1. The addition of Au resulted with the increase in the activity and durability of the Pt-decorated Au of the size 2 nm toward formic acid oxidation. It is hypothesized that the subsequent reduction of Au precursor will create less continuous Pt ensemble sites that are beneficial for the direct oxidation of formic acid.

Chapter 6

Synthesis and characterization of Co_{core}-Pt_{shell} electrocatalyst prepared by spontaneous replacement reaction for oxygen reduction reaction

6.1. Introduction

The search for better catalysts for oxygen reduction reaction for Proton Exchange Membrane Fuel Cells has been ongoing for decades. Platinum, known as the best catalyst so far, suffers from high overpotential for ORR and its high cost. In the last couple of years, it has been shown that by forming a monolayer-submonolayer of Pt on other metals, the Pt usage could be reduced considerably without sacrifying the activity.[114, 116, 119, 120] Such an approach is promising and must be studied further in order for the PEMFCs and direct methanol fuel cells to be commercialized.

The preparation of Pt monolayer electrocatalyts was first introduced by Adzic group by a spontaneous electroless replacement between Pt ion precursor and underpotentialy deposited Cu that previously was electrodeposited on the surface of another noble metal.[113, 119, 120] By carefully choosing the noble metal as the core metal, they show that the electro-activity of the Pt monolayer can be enhanced two to four times better than the commercial Pt/C.[115, 124] Such an enhancement was attributed to the structural and-or electronic effects. Existing techniques like microemulsion,[205-208] polyol reduction method[167, 209, 210] and thermal decomposition of carbonyl compounds[191, 211-213] have been successfully used to prepared transition metal nanoparticles alloyed with noble metals, but these techniques are either very costly in terms of the metal precursors and solvents used or not feasible for mass production of nanoparticles.

Another promising method to synthesize Pt-M core-shell nanoparticles supported on carbon is the deposition of the non-noble metals on previously formed Pt/C, followed by high temperature alloying [214-216] and continued by voltammetric surface dealloying.[217-220] However as the results of high temperature treatment, the metal particles will grow in size, as induced by the coalescence and sintering of the platinum nanoparticles. This will reduce the active surface area of Pt and also the electrochemical dissolution of the non-noble metal from the surface of the nanoparticles by voltammetric dealloying could poison the membrane layer. Recently, Pd based electrocatalyts modified with transition metals such as Co and W have been proposed to have comparable ORR activity with Pt/C but further study has shown that Pd based metals are a poor choice of electrocatalysts due to its lack of stability in electrochemical environments.[221-223]

Pure Pt on the outermost shell layer can also be created by heat treatment of Pt alloys or acid removal of the transition metals from the Pt alloys.[212, 224, 225] However, usually Pt-based alloys contain up to 80% Pt before the treatment and almost pure Pt after the treatment, especially for the case of acid removal. In this chapter we report the first example of highly active Co_{core}-Pt_{shell} electrocatalyts synthesized through a novel and potentially general wet chemistry approach that utilizes the redox transmetalation (electroless deposition) method.[118, 193, 226, 227] Our approach here is beneficial for the fuel cell applications. Firstly, the Pt usage can be reduced as almost all the Pt atoms reside on the surface. Secondly, the Co metal on the core can enhance the activity of the Pt surface layer. Thirdly, the formation of solid Co_{core}-Pt_{shell} can prevent the extensive dissolution of the Co metal during the fuel cell operation, which is usually observed for PtCo/C alloy. The electrocatalytic activity, morphology, composition and crystal phase structure were

characterized using linear polarization technique, cyclic voltammetry, X-ray diffraction, thermogravimetric analysis, UV-vis, energy-dispersive X-ray spectrometry and transmission electron microscopy.

6.2. Experimental and characterization methods

6.2.1. Preparation techniques

Firstly, the Co nanoparticles loaded on carbon black were prepared by the reduction of $CoCl_2$ by $NaBH_4$ with tetraoctylammonium bromide as the stabilizer in ethanol solution. Stabilization of nanoparticles by surfactant tetraoctylammonium bromide (TOAB) is advantageous because firstly its long chain favors the formation of small nanoparticles and secondly it could be easily removed from the particle surface.[118, 228] Briefly, 0.2 mmol of $CoCl_2.6H_2O$ and 0.2 mmol of TOAB were dissolved in 25 mL ethanol and then mixed with homogeneous carbon black slurry (82 mg in 25 mL ethanol). Prior to the experiment, all the solvents used were degassed using an ultrasonicator and purged with N_2 for at least 1 hour to make sure that the solvents were free from dissolved O_2. Upon mixing, freshly prepared $NaBH_4$ solution in ethanol (18 mg in 25 ml ethanol) was added directly under vigorous stirring. Within seconds, the evolution of H_2 gas was observed according to the following reactions.

$$CoCl_2 + 2NaBH_4 \rightarrow Co + H_2 + B_2H_6 + 2NaCl$$

$$B_2H_6 + 6CH_3CH_2OH \rightarrow 2B(OCH_2CH_3)_3 + 6H_2$$

To avoid the oxidation of Co nanoparticles, high purity N_2 was kept flowing during the whole procedure. The pH of the solution after the Co^{2+} reduction process was 11. Thirty minutes later, 100 ml of deaerated de-ionized (DI) water was added to

decompose any remaining $NaBH_4$. The electroless deposition was performed by simply mixing the resulted Co nanoparticles with Pt precursor, but the pH of the Pt precursor solution was varied. Briefly, three hours after adding the DI water, 25 ml of 0.067 mmol K_2PtCl_4 in DI water was added dropwise to the above solution. The pH of the aged K_2PtCl_4 aqueous solution was varied by adding 0.2 M aqueous HCl solution, the variations were pH=4 (without adding HCl), pH=2.5 and pH=1.5. After overnight stirring, the resulted product was centrifuged and washed several times using ethanol and DI water and finally isolated in powder form using filtration and then dried under vacuum. For the annealed Co/C, the as-prepared Co/C was subjected to a thermal treatment at 600^{o}C under Ar flow for 4 hours.

6.2.2. Characterizations

The X-ray diffraction patterns were collected using D8 Bruker AXS X-ray diffractometer using Cu Kα radiation at a potential of 40 mV and current of 40 mA. The 2θ diffraction angles ranged from 30^{o} to 90^{o}, using a step scan of 0.02^{o} and holding time of 10 seconds. Peak profiles and crystallographic data were analyzed using TOPAS by Bruker AXS. For the as-prepared Co/C, the XRD experiment was conducted as soon as the sample was isolated in powder form after washing with deaerated ethanol and dried in vacuum for 30 minutes to prevent further oxidation of the Co/C. TEM measurements were performed using JEM-1400 (JEOL) operated at 100 kV. The particle suspension in ethanol was sonicated and then dropped cast onto carbon-coated copper grid followed by solvent evaporation in air at room temperature. TGA was carried out by heating the dry powder samples at a rate of 10^{o}C/min with a flow of air at 100 mL/min in the range of 25-700^{o}C using TA Instrument SDT Q600.

Typical samples weighed ~5 mg and were heated in a platinum pan. The UV-vis spectrum of the solution was collected using UV-vis spectroscopy (Shimadzu 2450) equipped with quartz cell. The compositional analysis using EDX was performed using a scanning electron microscopy JEOL JSM-6390LA operating at 20 kV and working distance of 10 mm. The samples were deposited on copper tabs which were cut to fit the sample holder. About 5-10 large areas were probed and the average was used to determine the composition.

"All the electrochemical performance tests were carried out at room temperature condition (25^{o}C) and were performed in a rotating disk electrode system using Autolab PGSTAT302 potentiostat. Prior to every experiment, the glassy carbon electrode (GCE) with a diameter of 5 mm was polished using 0.05 μm alumina paste. Pt wire was used as the counter electrode and the electrode potentials were measured using saturated calomel electrode (SCE) when using $HClO_4$ or H_2SO_4 as the electrolyte, and Hg/HgO when using KOH as the electrolyte but all the potentials throughout this paper are reported versus the reversible hydrogen electrode (RHE) under the same conditions. The preparation of the working electrode was based on the thin film method. Briefly 5 mg of the sample was mixed with 5 ml of DI water and sonicated to form a homogeneous ink, then 20μL of the ink was deposited using microsyringe onto the GCE and then left dry in open air. After that, 10μL of 0.05% Nafion solution (diluted from 5% solution using isopropanol) was dropped on top of the disk to fix the catalyst powder. All the solutions were deaerated using pure N_2 or pure Ar for at least 30 minutes prior to any measurement. The ORR activity measurements were conducted by recording the potentiodynamic voltammograms in

0.1 M $HClO_4$ saturated with O_2. Prior to this experiment the PtCo/C or Pt/C electrodes were electrochemically cleaned by cycling in 0.1 M $HClO_4$ at 100 $mV.s^{-1}$ until reproducible voltammograms were obtained and the hydrogen adsorption-desorption area obtained after double layer correction was used to determine the active surface area of Pt."[157]

6.3. Results and discussion

The procedure and conditions described in the experimental section were found to be optimal for the preparation of solid Co_{core}-Pt_{shell} nanoparticles. In particular when $NaBH_4$ used is less than 2 times of the $CoCl_2$ mole, then not all the Co^{2+} ions will be reduced. But when the amount of $NaBH_4$ is much higher than 2, then the excess $NaBH_4$ might reduce the Pt precursor once it is added into the as-prepared Co/C solution. This will prevent the replacement reaction between Pt precursor and Co to start because sodium borohydride reduction potential is much lower than the reduction potential of Co^{2+}/Co.[229] That is why in this experiment the molar ratio between $NaBH_4$ and $CoCl_2$ was just slightly higher than 2. Moreover, it was already proposed by Glavee et al,[230] that a 2:1 molar ratio of $NaBH_4$ over $CoCl_2$ is enough to reduce all the Co^{2+}. To make sure that the small excess of $NaBH_2$ would not affect the replacement reaction, prior to adding the K_2PtCl_4 solution, DI water was added to accelerate the hydrolysis rate of $NaBH_4$.

The formation of Co_{core}-Pt_{shell} can be explained as follows. Since the standard reduction potential of $PtCl_4^{2-}$/Pt (0.67 V vs SHE) is much higher than Co^{2+}/Co (-0.277 vs SHE). The spontaneous replacement reaction will take place as soon as the K_2PtCl_4 solution was added into the Co/C solution according to the following reaction

$$Co + PtCl_4^{2-} + \rightarrow Co^{2+} + Pt + 4Cl^-$$

From the replacement reaction, it can be seen that one Co atom must be oxidized in order to reduce one $PtCl_4^{2-}$ ion. The Co atoms on the surface of the Co nanoparticles will be oxidized first, forming Pt atoms on the outer layer of the Co nanoparticles. By using fewer amounts of $PtCl^{4-}$ ions compared to Co, a complete Co replacement can be prevented thus forming solid Co_{core}-Pt_{shell} nanoparticles. By using Pt to Co molar nominal ratio of 1:3, it is expected that the final Pt to Co molar ratio is 1:2. The use of K_2PtCl_4 as the Pt precursor in this experiment is beneficial to keep the original morphology of the Co nanoparticles, unlike when Pt^{4+} precursor like H_2PtCl_6 or K_2PtCl_6 is used. In this case, the final product will be as of a porous structure due to two Co atoms will be replaced by one Pt^{4+} ion.

6.3.1. UV-vis analysis

Fig. 6.1 shows the UV-visible spectra of the supernatant collected after the centrifugation step of the PtCo/C catalysts prepared at different pHs. The results are compared with the spectra of K_2PtCl_4 aqueous solution and $CoCl_2 \cdot 6H_2O$ aqueous solution with the same initial concentrations as in the preparation step which are 0.38 mM and 1.14 mM respectively. It is worth noting that even though the initial color of the $CoCl_2 \cdot 6H_2O$ dissolved in ethanol is blue, but after adding a small amount of water the color changes to pink and the UV-vis spectrum of $CoCl_2 \cdot 6H_2O$ dissolved in pure water and the spectrum of $CoCl_2 \cdot 6H_2O$ dissolved in a mixture of ethanol and water show the same intensity and the same absorption peak which is located at ~510 nm.[194] For K_2PtCl_4 solution, the color and absorption peaks are the same when it is dissolved in pure water and in a mixture of ethanol and water, which are light brown and two

strong peaks at ~310 nm and ~385 nm respectively. These two peaks can be ascribed to the characteristic of platinum complex of $PtCl_4^{2-}$.[231]

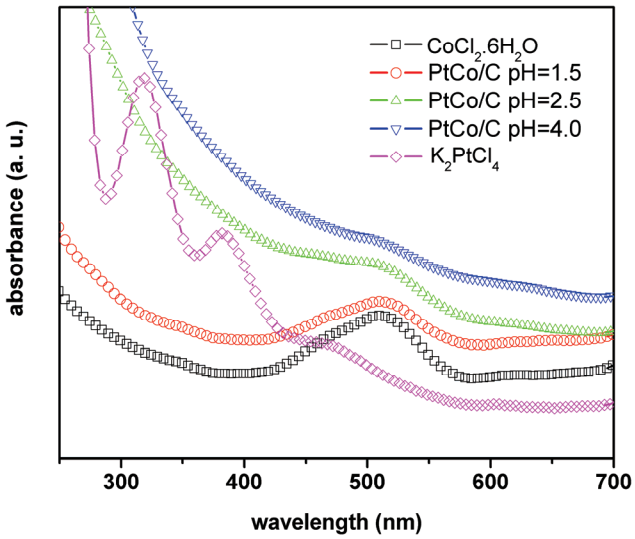

Fig. 6.1. UV-vis spectra of solutions of $CoCl_2.6H_2O$, K_2PtCl_4 and the supernatant collected after the centrifugation step of PtCo/C prepared at different pHs.

At the end of the replacement reaction, after the centrifugation, the supernatant was collected and the UV-vis spectrum was recorded for the PtCo/C prepared at different pHs. For the PtCo/C pH 4, there is a small shoulder located at ~510 nm which is very close to the absorbance peak of $CoCl_2•6H_2O$. For the PtCo/C prepared at lower pHs (2.5 and 1.5), the shoulder develops into strong peak especially for the PtCo/C prepared at pH 1.5. This confirms the existence of Co^{2+} ions in the supernatant. Moreover the absorbance peaks at 310 nm and 385 nm, which are the characteristic of K_2PtCl_4, are no longer visible in the supernatant, suggesting all the Pt ions were reduced by Co that confirm the replacement reaction. Interestingly, the supernatant color of the PtCo/C prepared at pH 1.5 is very similar to the initial color of $CoCl_2•6H_2O$ aqueous solution which is light pink suggesting that the supernatant contains more Co^{2+} ions than the PtCo/C prepared at pH

2.5 and 4. This color observation corroborates well with the UV-vis spectrum where the peak is almost as strong as the peak of $CoCl_2 \cdot 6H_2O$ solution.

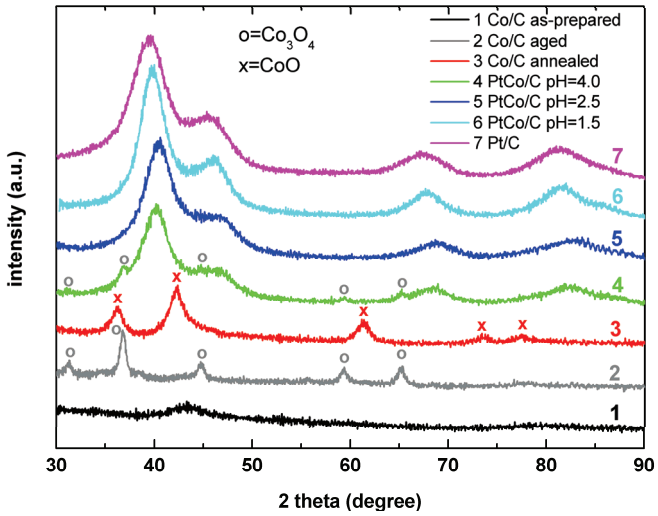

Fig. 6.2. XRD patterns of as prepared Co/C, Co/C after annealing, PtCo/C prepared at different pHs and Pt/C.

6.3.2. XRD analysis

The comparison of the XRD patterns for the as-prepared Co/C, Co/C after aging in air environment, Co/C after annealing in Ar flow at 600°C for 4 hours, PtCo/C prepared at different pH and Pt/C are shown in Fig. 6.2. For the as-prepared Co/C, there is only one broad peak around 44° that corresponds to (111) face centered cubic (fcc) cobalt (space group Fm-3m (225); PDF-# (15-0806); a=3.545). The appearance of this broad peak suggests that either the as-prepared Co is poorly crystalline or the grain size is very small. But after aging the as-prepared Co/C in open air at room temperature for around 10 days, the broad peak disappeared, and there are new peaks that located at 2-theta values of 31.4°, 36.9°, 44.9°, 59.5° and 65.4°. These peaks are in good agreement with the characteristic of fcc Co_3O_4 (space group Fd-3m (227); PDF-# (65-3103); a=8.056) and can be assigned to (220), (311),

(400), (511) and (440) planes respectively. While after annealing the as-prepared Co/C under Ar flow for 4 hours at 600°C, the Co changed to CoO as revealed by the XRD pattern. The peak at 36.5°, 42.4°, 61.5°, 73.7°, and 77.56° can be assigned to (111), (200), (220), (311), and (222) of fcc CoO (space group Fm-3m (225); PDF-# (43-1004); a=4.260 Å). The as-prepared Co/C, aged Co/C and annealed Co/C only show the diffraction lines of Co fcc, Co_3O_4 fcc and CoO fcc without any appearance of Co-B alloy diffraction patterns. This Co-B pattern can be found usually when the reduction of $CoCl_2$ by $NaBH_4$ is carried out in aqueous solution even after the sample was annealed in O_2 free environment.[230, 232-235] To verify this explanation, we conducted EDX analysis for the Co/C and the result is shown in Fig. 6.4.A. The result reveals that there is no existence of B; only Co and O are present in the sample. Therefore, using this simple preparation technique, we can fabricate pure Co nanoparticles. The formation of CoO after the annealing might be induced by the trace amount of O_2 remaining in the Ar gas source (~2 ppm). High temperature accelerates the oxide formation because fcc Co is very susceptible to oxidation, especially for a very small particle size, as can be observed from the XRD patterns of the aged Co/C.[236]

As for the Pt/C all the peaks resemble the characteristic of fcc crystalline Pt (space group Fm-3m (225); PDF-# (65-2868); a=3.924) corresponding to (111), (200), (220), (311) and planes at 2-theta values of 39.6°, 46.2°, 67.5°, and 81.3° respectively; while for the PtCo/C electrocatalyts, these five diffraction peaks are shifted to higher 2-theta values, indicating the contraction of the lattice due to the incorporation of Co atoms in the fcc structure of Pt. For the PtCo/C prepared at pH 1.5 and 2.5, no

characteristic of peaks for Co or Co oxides were detected, that indicates the formation of principally single-phase solid solution. But for the PtCo/C prepared at pH 4, there are other small peaks that do not belong to Pt fcc. These peaks are in good correspondence with the characteristic of fcc Co_3O_4 like the aged Co/C XRD pattern. The presence of Co_3O_4 indicates that at preparation condition of pH 4, the surface of the PtCo solid solution does not entirely consist of Pt atoms. These surface Co species are in the form Co_3O_4. This observation stresses the significance of pH during the replacement reaction.

The diffraction peaks of PtCo/C electrocatalyts are broader compared to Pt/C suggesting that their particle sizes are smaller than Pt/C. By using Scherrer's equation, the average size of the electrocatalyts was estimated from full peak width at half maximum of the (220) plane reflection. The mean particle size and the lattice parameter for all the PtCo/C electrocatalyts determined from XRD analysis can be seen in Table 6.1.

Table 6.1. Comparison of nominal and real compositions, particle size and analysis by XRD and specific ORR activity at 0.9 V for various PtCo/C and Pt/C.

Catalyst	Pt:Co (nominal atomic ratio)	pH	Particle size[a] (nm)	2 theta [111] (degree)	Lattice parameter (Å)	Pt-Pt interatomic distance (Å)	Metal loading[b] (%)	Pt:Co (real atomic ratio)[c]	Specific activity, j_k (mA/cm^2_{Pt})
PtCo/C	1:3	4.0	2.5	40.174	3.881	2.744	17.4	1:2.8	0.555
PtCo/C	1:3	2.5	2.6	40.521	3.849	2.722	16.3	1:2.2	0.894
PtCo/C	1:3	1.5	3.1	39.834	3.920	2.770	11.2	9:1	0.497
Pt/C	-		2.5	39.575	3.931	2.780	22.1	-	0.230

[a] Estimated from XRD data using Scherrer formula.

[b] Determined by TGA analysis without any correction.

[c] Based on EDX analysis.

It is evident that the synthesis procedure in this work can produce small bimetallic nanoparticles with PtCo/C prepared at pH 4 has the smallest size and PtCo/C prepared at pH 1.5 has the biggest size. When comparing the lattice parameters, all the PtCo/C electrocatalyts have lower lattice parameter than Pt/C. This indicates that the Pt-Pt interatomic distance for all the PtCo/C electrocatalyts are lower compared to Pt/C, with PtCo/C prepared at pH 2.5 being the lowest as shown in Table 6.1. The Pt-Pt interatomic distance will be discussed in the context of their ORR activity in the later section.

6.3.3. TGA analysis

The loading of the particles on carbon black and the interfacial reactivities with oxygen as a function of temperature were studied further using TGA. Fig. 6.3 shows the typical TGA data for the as-synthesized PtCo/C at different pHs, Pt/C, as prepared Co/C and carbon black. It can be seen that carbon black starts to oxidize at ~550^{o}C, but when Co or Pt or a CoPt mixture are deposited on carbon black, the oxidization temperatures become lower indicating a catalyzing mechanism where the metals promote the oxidation of carbon black at low temperature.[166] The slight decrease in temperature at ~430^{o}C and ~450^{o}C for Pt/C and PtCo/C pH 1.5 were due to the exothermic oxidation of the carbon support, respectively.[167, 209] While for the PtCo/C pH 2.5 and PtCo/C pH 4, the exothermic oxidation of carbon black happens at ~500^{o}C.

From the mass change in Fig. 6.3 for the PtCo/C prepared at different pHs and Co/C, the metal loading was observed to be lower than the nominal loading. The nominal loading for the PtCo/C prepared at different pHs was 20%, while for the Co/C was 30%. Considering that the as-prepared Co will transform into Co-oxide when it is in

contact with oxygen, the final loading of the Co/C should be higher than the nominal loading. This difference compared to expected nominal weight is likely due to contribution of the surfactant (TOAB) because once the nanoparticles are formed; TOAB will attach and bind onto the nanoparticle surface and thereby adding the total weight. Unfortunately, the weight contribution of TOAB can not be determined using TGA analysis because it has been suggested that TOAB can be removed from the nanoparticle surface at low temperature due to its low melting point that overlaps with the weight loss due to water evaporation.[118]

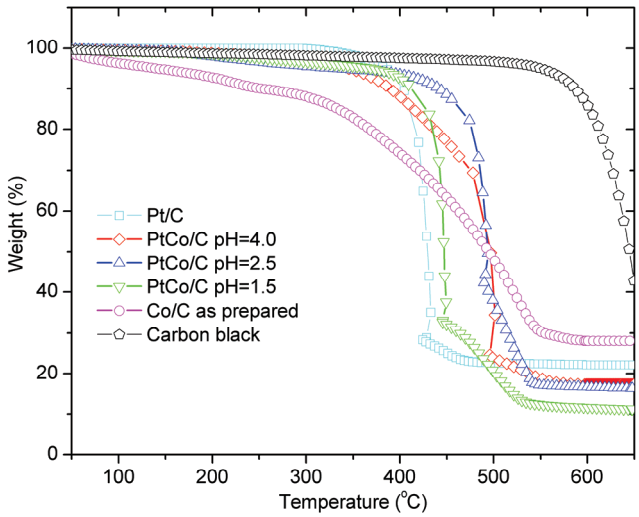

Fig. 6.3. TGA curves for Pt/C, Co/C as prepared, carbon black and PtCo/C prepared at different pHs.

Interestingly, the PtCo/C catalysts behave differently compared to Pt/C during TGA experiment where the oxidation temperatures shift to higher temperature. But the shifts are different for different pHs. The oxidation temperature for PtCo/C pH 1.5 is closer to that of Pt/C compared to other PtCo/C, implying that it contains more Pt; while the PtCo/C pH 2.5 and PtCo/C pH 4.0 have the same sharp weight loss at 500°C but with different starting temperature. The decay in weight loss for PtCo/C pH 4 started before

that of PtCo/C pH 2.5 and the early rate of weight loss seems the same as that of Co/C. We presumed that this is due to the existence of Co-containing species on the surface of PtCo/C pH 4, while the same sharp weight loss at 500^{o}C and roughly the same total metal loading for PtCo/C pH 4 and PtCo/C pH 2.5 indicate that the Pt/Co atomic ratio for these two catalysts are almost the same. To verify these, we analyze the composition of the remaining residue after the TGA analysis using EDX and the results can be seen in Fig. 6.4 and tabulated in Table 1. It can be seen that for PtCo/C pH 4 and PtCo/C pH 2.5, the Pt/Co atomic ratio are quite close to each other but lower than the expected ratio (for a full replacement reaction, the final Pt:Co ratio should be 1:2); while for the PtCo/C pH 1.5, the Pt:Co ratio is much higher. This observation corroborates with the UV-vis analysis where the PtCo/C pH 1.5 supernatant contains higher amount of Co^{2+} compared to PtCo/C pH 2.5 and PtCo/C pH 4. This phenomenon will be discussed in the mechanism part.

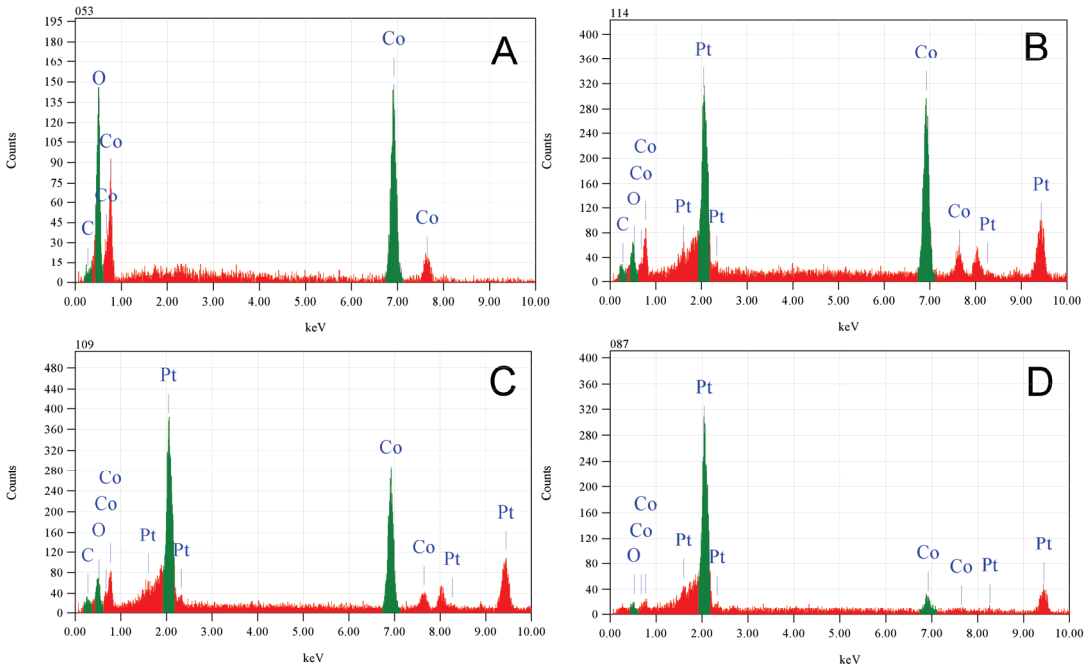

Fig. 6.4. The EDX analysis of A) Co/C; B) PtCo/C pH 4; C) PtCo/C pH 2.5; D) PtCo/C pH 1.5.

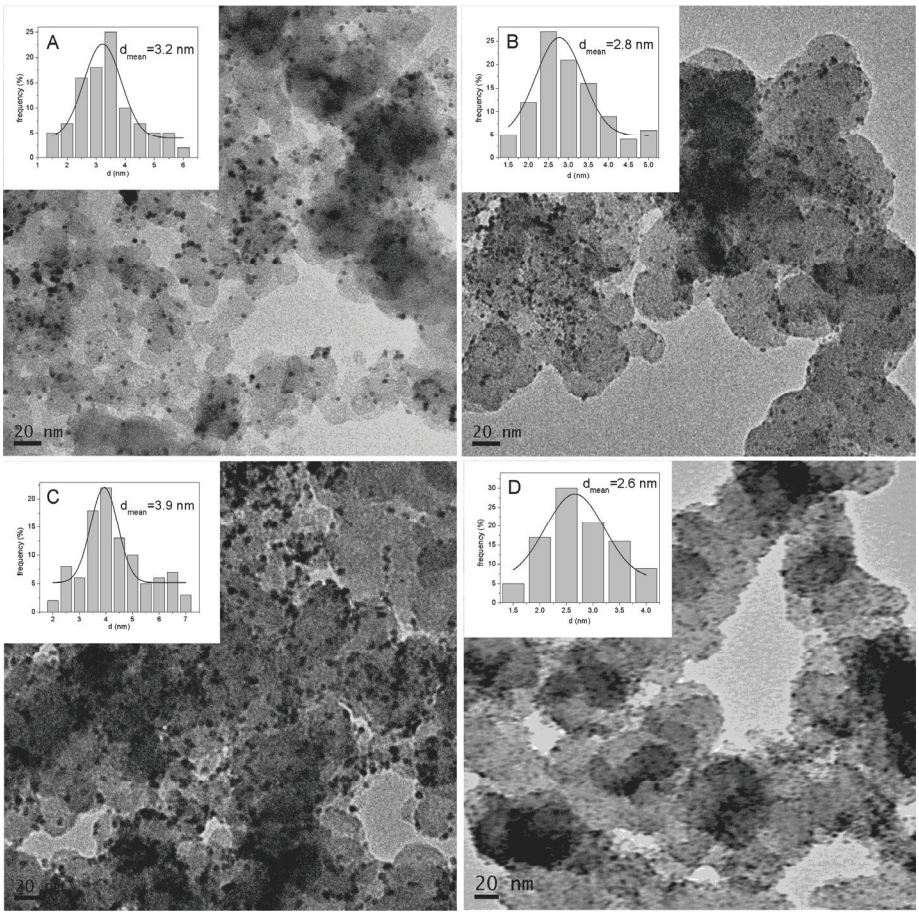

Fig. 6.5. TEM images of A) PtCo/C pH 4.0; B) PtCo/C pH 2.5; C) PtCo/C pH 1.5 and D) Pt/C. All the scale bar is equal to 20 nm

6.3.4. TEM analysis

Fig. 6.5 shows the TEM graphs and the size distribution of PtCo/C prepared at different pHs. It is evident that the mean particle sizes are quite close to the values obtained using Scherrer correlation from XRD data. The histograms of the particle size distribution, which are based on the analyses of several different regions and counting of over 300 particles, reflect quantitatively the uniformity of the size distribution. As can be seen in Fig. 6.5, the dispersion of the catalysts on carbon black is quite uniform, but unfortunately there are some aggregations observed in the image especially for the PtCo/C pH 4 despite TOAB was used to prevent the aggregations.

This is due to the magnetic characteristic of Co that favors the aggregation of the nanoparticles.

6.3.5. CV in alkaline electrolyte

CV is a surface sensitive electrochemical approach that detects only the electrochemical properties of the surface atoms instead of the bulk atoms. To characterize the surface properties of the PtCo/C electrodes, the CV response of all the PtCo/C and Pt/C was analyzed in the potential range between hydrogen and oxygen evolution in 0.1 M KOH solution. It is well known that Pt-based non-noble metal catalysts show corrosion behavior when they are immersed in acidic electrolyte, so it is impossible to probe the existence of Co on the surface of the electrocatalysts in acidic electrolyte. To study whether the Co dissolution occurs and changes the surface structure of the catalyst upon potential cycling in acidic electrolyte, the CV response of all the electrocatalyts before and after potential cycling in 0.1 M $HClO_4$ was also recorded.

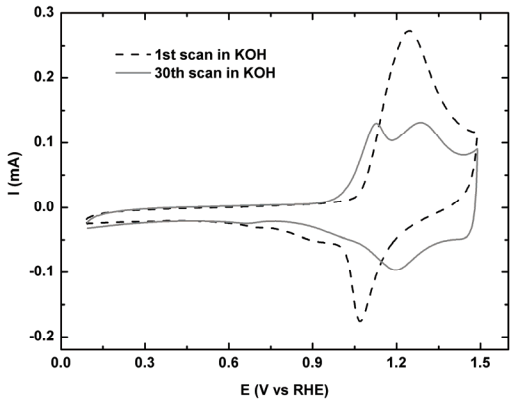

Fig. 6.6. CV of aged Co/C (30 wt%) in deaerated 0.1 M KOH at 100 mVs^{-1}.

To probe the characteristic of Co/C, we conducted the CV analysis for the aged Co/C and the result is shown in Fig. 6.6. It can be seen for the 1st scan that there

is only one peak in the anodic scan; one peak and a broad shoulder in the cathodic scan. In the repeated sweeps up to 30 scans, the peak in the anodic scan develops into two continuous peaks at ~1.1 V and ~1.3 V and for the cathodic scan there are one broad peak at 1.2 V and a small discernible peak at 0.65 V. From the analysis of the Pourbaix diagram for cobalt species,[237] it is shown that at pH 12.8 and in the range of 0.05 to 1.5 V in which our experiment was conducted, Co can exist as either $Co(OH)_2$, Co_3O_4, $Co(OH)_3$ or CoO_2, depending on the potential. This suggests that the redox transitions corresponding to the $Co^{II} \rightarrow Co^{III} \rightarrow Co^{IV}$ electrochemical processes happen during the potential cycling in 0.1 M KOH.[238-241] Thus the predominant species formed at 1.1 V in the anodic scan might be $Co(OH)_3$ through the oxidation of $Co(OH)_2$ with Co_3O_4 as the intermediate product (from the Pourbaix diagram, the stability region of Co_3O_4 is very narrow). While the oxidation process at 1.3 V might involves the formation of CoO_2. For the cathodic scan, the broad peak at 1.2 V and the small discernible peak at 0.65 V can be assigned to the reduction process from Co^{IV} to Co^{II}.

Fig. 6.7 part A shows the CV profiles for Pt/C in 0.1 M KOH before and after potential cycling in 0.1 M $HClO_4$. As in the case of polycrystalline Pt, hydrogen monolayer adsorption and desorption are very pronounced. Besides, there is no constant current in the double-layer region and a broad oxide formation starts just after hydrogen desorption. A pair of sharp peaks can be observed at ~0.3 V that correspond to Pt (110) facets and the pair of quite discernible shoulders at ~0.4 V can be attributed to Pt (100) step sites,[242-244] while a broad cathodic current peak appearing around ~0.75 V in the negative-going potential sweep can be assigned to

the reduction of the Pt oxide layer. The potential cycling in 0.1 M $HClO_4$ did not change the electrode surfaces because there is no significant difference on the CVs before and after the potential cycling in acid electrolyte.

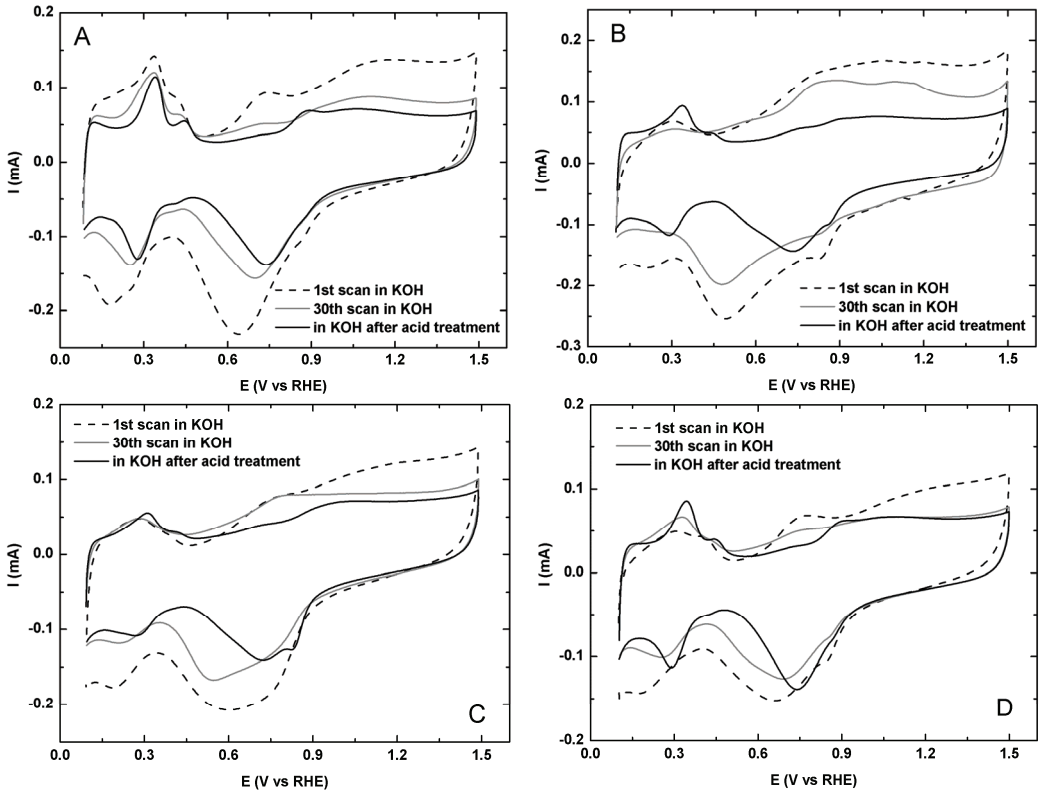

Fig. 6.7. CVs in 0.1M KOH before and after electrochemical treatment of A) Pt/C; B) PtCo/C pH=4.0; C) PtCo/C pH=2.5; D) PtCo/C pH=1.5. Scan rate is 100mV s^{-1}.

The CV responses of PtCo/C electrodes prepared at pH 4, pH 2.5 and pH 1.5 in 0.1 M KOH before and after potential cycling in 0.1 M $HClO_4$ can be seen in Fig. 6.7. For the PtCo/C pH 4.0, the H_{upd} region is not so obvious before cycling in acid electrolyte, instead a very broad oxidation layer above 0.6 V that developed into two broad continuous shoulders at ~0.8 V and ~1.1 V on the anodic sweep can be observed after 30 scans. The appearance of these new responses for the PtCo/C pH 4.0, different from Pt/C, can be assigned to Co redox current. But the formation of Pt-oxide in the potential region of 0.8-0.9 V can not be neglected, especially the

formation of shoulder at ~0.9 V indicates the formation of Pt-OH overlaps with the peak in the anodic scan at 0.8 V. Thus only the peak at 1.1 V can be used to probe the existence of Co on the surface of the PtCo/C catalysts. For the cathodic scan, the observed broad peak around 0.45 V is still far different from that of Pt/C where the reduction of Pt-oxide for Pt/C can be observed at 0.75 V; and it is somewhat different from the reduction peaks of Co/C (1.2 V and 0.65 V). Accordingly we suggest that the broad peak at 0.45 V is attributed to the reduction of Pt-Oxide and also the reduction of Co-(hydr)oxide species. The difference in the peak potentials corresponding to Co redox current observed from the PtCo/C especially for the anodic scan, at least partially, are due to the effects of platinum on the electronic structure of the electrode and their effects in the redox potential. Due to the existence of the small peak at 1.1 V for the PtCo/C pH 4.0 we conclude that the surface of PtCo/C prepared at pH 4 still consists of Co-oxygen containing species which corroborates with the XRD and TGA analysis.

After cycling in 0.1 M $HClO_4$, the CV for the PtCo/C prepared at pH 4 does not show the characteristics of Co-(hydr)oxide containing species anymore. Instead the common Pt/C responses such as the H_{upd} region and Pt oxide reduction peak can be observed. This confirms the dissolution of Co-(hydr)oxide in acidic media and the surface become enriched with Pt upon the electrochemical treatment in acidic solution, as observed in other studies.[224, 245]

For the PtCo/C electrode prepared at pH 2.5, the CV responses before cycling in acid media are quite similar to the PtCo/C prepared at pH 4, but the two oxidation peaks in the anodic scan at high potential can not be observed anymore and the oxide

reduction peak in the cathodic scan shift positively. This suggests that the surface of the electrode is composed almost entirely of Pt. Interestingly for the PtCo/C prepared at pH 1.5, the characteristic of Co-oxygen containing species can not be observed anymore. The absence of the Co-(hydr)oxide redox current peaks for the PtCo/C prepared at pH 1.5 confirms that the surface consists of pure Pt. These observations once more stress the importance of pH on the final product.

Moreover, a closer look at the H_{upd} region of the CVs for the PtCo/C electrodes shows that after potential cycling in 0.1 M $HClO_4$, all the PtCo/C electrodes except for the PtCo/C prepared at pH 2.5 have a pair of sharp peaks at 0.3 V that correspond to Pt (110) facets, contrary to that before cycling in acid electrolyte. This suggests that during the potential cycling in acid media, the Pt atoms undergo a surface reconstruction where many steps and/or defects ascribed to Pt (110) formed. But it is not the case for PtCo/C prepared at pH 2.5 where the voltammetry responses in the H_{upd} region do not show any appreciable difference in terms of the sharpness of the peak around 0.3 V, which suggest that PtCo/C prepared at pH 2.5 has fewer steps and defects compared to PtCo/C prepared at pH 4 and pH 1.5.

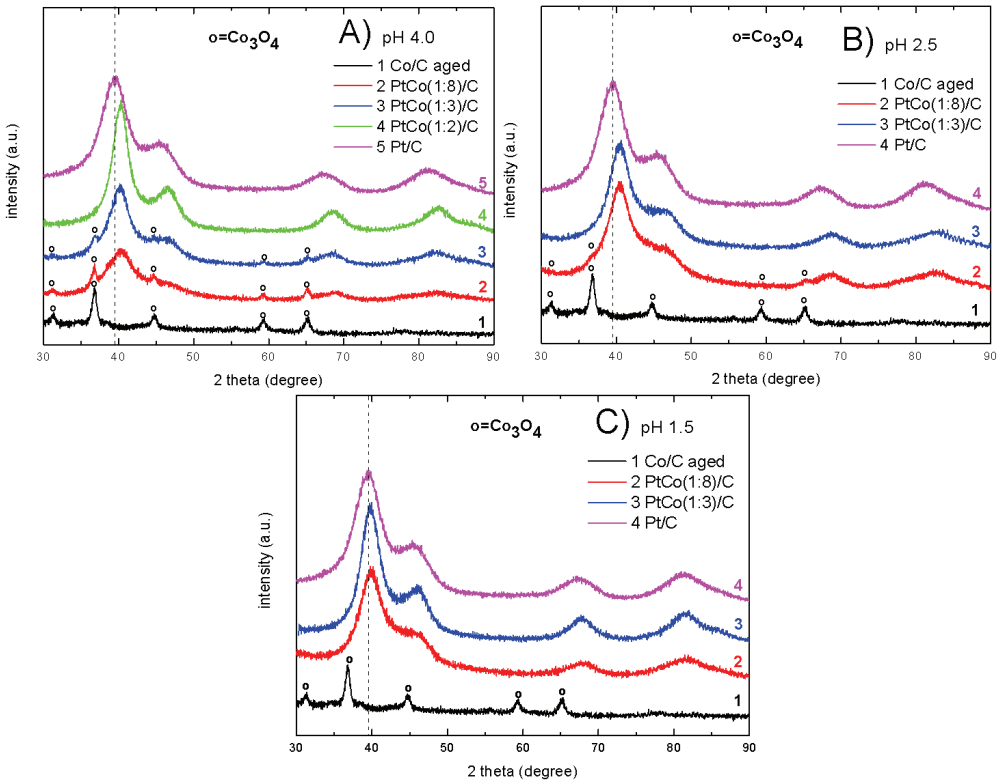

Fig. 6.8. XRD patterns of aged Co/C, Pt/C and PtCo/C with different nominal Pt:Co mole ratios prepared at A) pH 4.0; B) pH 2.5 and C) pH 1.5.

6.3.6. Mechanism

To study the replacement mechanism, which is influenced by pH, we prepared PtCo nanoparticles with different ratios at different pHs and we monitored the pH after the replacement reaction. The XRD patterns for the PtCo prepared at pH 4.0 with different Pt/Co mole ratio, PtCo prepared at pH 2.5 with different Pt/Co mole ratio and PtCo prepared at pH 1.5 with different Pt/Co mole ratio can be seen in Fig. 6.8. It can be seen that at pH 2.5, when the Pt:Co ratio is lower than 1:3, Co_3O_4 pattern can be observed. While at pH 4, when the PtCo ratio is higher than 1:3, Co_3O_4 did not form. This shows that at Pt:Co mole ratio of 1:3, different preparation pH will lead to different surface composition. To further study the surface composition, the voltammetry responses in alkaline electrolyte were recorded before and after cycling

in acidic media and the results are shown in Fig. 6.9. It can be seen that for PtCo (1:8) prepared at pH 4.0, Co atoms still exist on the surface where the oxidation peak at ~1.1 V belonging to the Co oxidation still can be observed on the CV scan before acid treatment, but for PtCo(1:2) prepared at pH 4.0, the Co oxidation peak can not be seen anymore suggesting the complete covering of Co-core by Pt-shell. It is the same case for pH 2.5, where the Co oxidation peak at 1.1 V still can be observed when the Pt:Co ratio was lowered to 1:8. But for the pH 1.5, when the Pt:Co ratio was lowered to 1:8, the Co_3O_4 pattern can not be observed from the XRD data and the Co oxidation peak can not be observed from the CV analysis either.

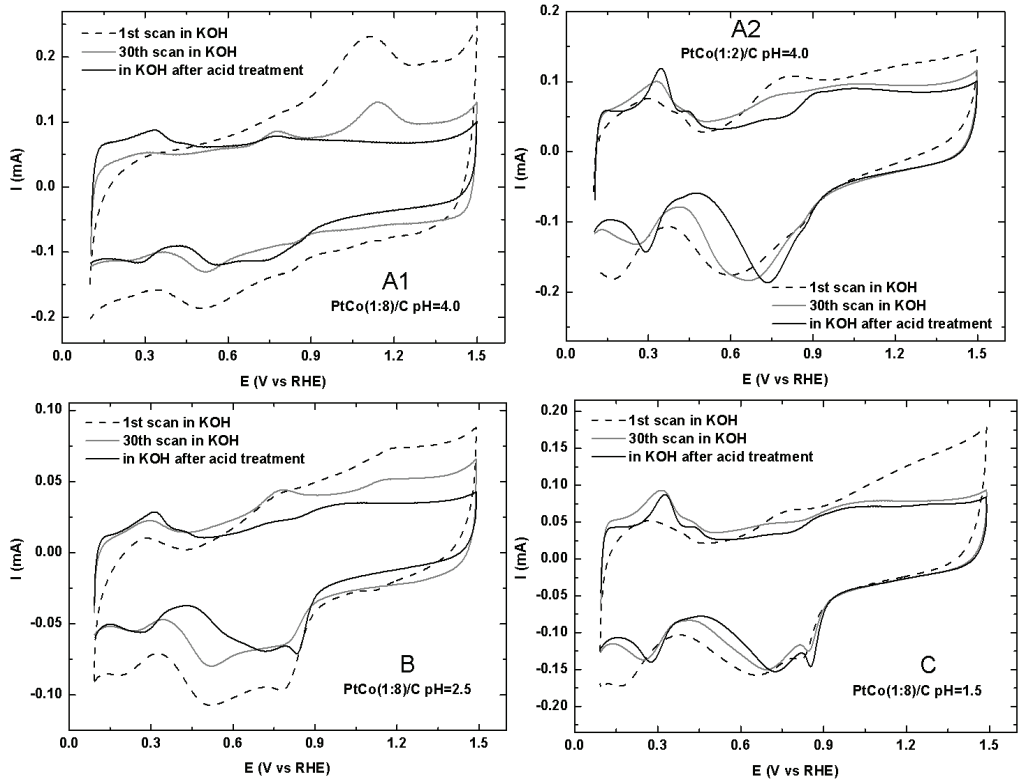

Fig. 6.9. CVs in 0.1M KOH before and after electrochemical treatment of A1) PtCo/C pH=4.0 with Pt:Co nominal loading of 1:8; A2) PtCo/C pH=4.0 with Pt:Co nominal loading of 1:2; B) PtCo/C pH=2.5 with Pt:Co nominal loading of 1:8; C) PtCo/C pH=1.5 with Pt:Co nominal loading of 1:8. Scan rate is 100mV s^{-1}.

Table 6.2. pH effect of K_2PtCl_4 solution for different nominal Pt:Co ratio on the final product.

initial pH of $K_2PtCl_{4(aq)}$	Pt:Co (nominal atomic ratio)	final pH	Co_3O_4 pattern can be observed from XRD data?	Co oxidation peak at ~1.1V can be observed from the CV analysis?	Pt:Co (real atomic ratio)[a]
4	1:8	9.0	Yes	Yes	-
4	1:3	8.5	Yes	Yes	1:2.8
4	1:2	7.8	No	No	1:0.98
2.5	1:8	7.9	Yes	Yes	-
2.5	1:3	7.4	No	No	1:2.2
1.5	1:8	3.2	No	No	2:1
1.5	1:3	2.8	No	No	9:1

[a]: Based on EDX analysis

The pH after the replacement reaction was also measured and the results are tabulated in Table 6.2 together with the observation of Co_3O_4 pattern from the XRD data and Co oxidation peak at 1.1 V from the CV in 0.1 M KOH and the real Pt:Co atomic ratio based on the EDX analysis. It should be kept in mind that at the end of the Co^{2+} reduction process, the pH of the solution was 11. As can be seen the pH of the K_2PtCl_4 solution and the Pt:Co ratio are the main factors in achieving the desired final product (Co_{core}-Pt_{shell}). Based on these observations we proposed a formation mechanism as shown in Scheme 6.1.

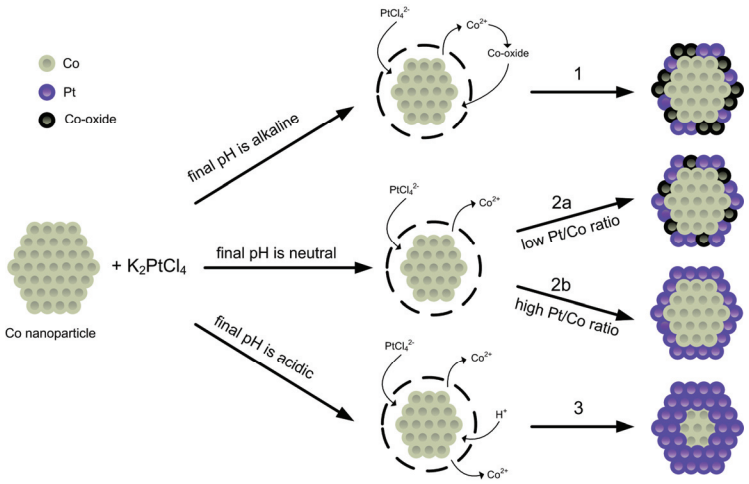

Scheme 6.1. The proposed mechanism for the replacement reaction observed at different final pHs

From the Pourbaix diagram,[237] it can be understood that Co^{2+} is not a stable species when the pH of the solution is slightly alkaline; the more stable forms are $Co(OH)_2$, $Co(OH)_3$, Co_3O_4 and CoO_2 . In the present study, the fact that the Co-(hydr)oxide species can be observed from the XRD and CV analysis for the PtCo/C samples that have slightly alkaline pH in the final solution may be attributed to this reason. So, as the replacement reaction between $PtCl_4^{2-}$ and Co proceeds, the slightly alkaline environment will favor the formation of Co-(hydr)oxide instead of Co^{2+} that subsequently deposit on the surface as shown in step 1. However, the pH of the final solution should not be acidic, or a hydrogen evolution side reaction will compete with the $PtCl_4^{2-}$ and Co displacement reaction, resulting in over-dissolution of the Co nanoparticles as shown in step 3. The acidic pH will not just cause the over-dissolution of the Co but will also weaken the surfactant stabilizing effect that lead to bigger particle size as revealed by XRD and TEM analysis due to the removal of the surfactant and subsequent aggregation. The removal of the surfactant can be seen in the large H_{UPD} area that PtCo/C prepared at pH 1.5 possesses compared to the other PtCo/C despite it has lower total metal loading and bigger particle size. Thus the preferred pH in the final solution to form a complete Pt shell without extensive Co dissolution and formation of any Co-oxide is neutral. When the initial pH of K_2PtCl_4 was not modified, i.e. pH 4.0, at Pt/Co nominal ratio of 1:3, the formation of a complete Pt shell should be favored, but due to the slightly alkaline environment, Co-oxide formed and deposited on the surface. This observation corroborates with the XRD analysis and compositional analysis using EDX for PtCo prepared at pH 4 where the final Pt/Co mole ratio is 1:2.8 indicating the formation of Co-oxide. But

when the Pt/Co ratio was increased to 1:2, the final pH of the solution become neutral and no Co-oxide characteristic can be seen in either XRD data or CV analysis and the final Pt:Co ratio is close with the theoritical Pt:Co ratio based on complete replacement reaction .

For the K_2PtCl_4 with an initial pH of 1.5, adding less K_2PtCl_4 does not result in the formation of Co_3O_4. This can be understood that low pH in the final solution (3.2 for Pt/Co ratio of 1:8 and 2.8 for Pt/Co ratio of 1:3) will favor the dissolution of Co-oxide impurities and the exposed Co core, resulting in a very low Co content as revealed by EDX analysis for PtCo/C prepared at pH 1.5.

For the K_2PtCl_4 with an initial pH of 2.5, there are two possible final structures that can be obtained when the Pt/Co ratio was varied. Even though the final pH was neutral for both cases (7.9 for Pt/Co ratio of 1:8 and 7.4 for Pt/Co ratio of 1:3), at low Pt/Co ratio, i.e. 1:8, the Co-oxide characteristic still can be seen from the XRD data and CV analysis. This can be explained that at this ratio, the amount of Pt is not sufficient enough to form a complete shell thus leaving some Co atoms on the surface that subsequently transform to Co_3O_4 when the Co is in contact with oxygen. But Pt/Co ratio of 1:3 is sufficient enough to form a complete shell as revealed by CV analysis and EDX analysis where the Pt/Co ratio is very close to the expected ratio.

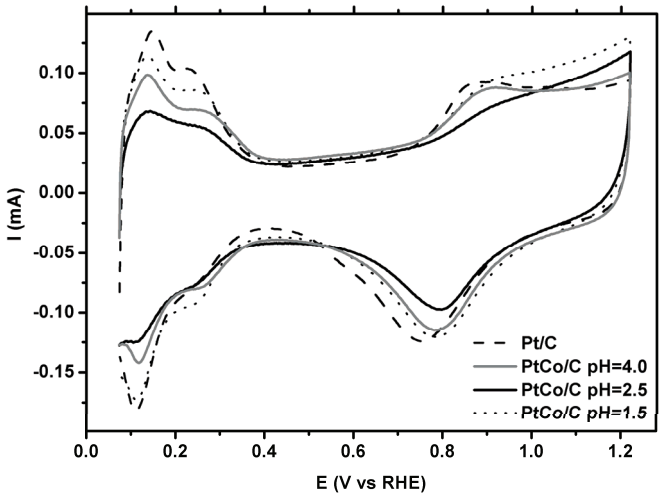

Fig. 6.10. CVs of PtCo/C prepared at different pH and Pt/C in deaerated 0.1 M $HClO_4$ at 100mV s^{-1}.

6.3.7. CV in acidic electrolyte

The CVs of Pt/C and the PtCo/C prepared at different pHs shown in Fig. 6.10 exhibit three characteristic potential regions of Pt: the hydrogen adsorption-desorption potential region between 0.07 and 0.35 V, the double layer potential region, and finally above ~0.7 V, OH adsorption region that leads to oxide formation on the anodic scan and a sharp peak at ~0.8 V on the cathodic scan that related to the reduction of the oxygenated species. In the hydrogen underpotential deposition region, a pair of quite discernible peaks between ~0.1 and ~0.2 V is associated with Pt (110) facets while one pair of broad peaks at ~0.26 V is the characteristic of Pt (100) step sites. It is interesting to note that the peaks in the H_{upd} region for PtCo/C prepared at pH 4 and 1.5 show almost similar behavior compared with Pt/C, but it is not the case for the PtCo/C prepared at pH 2.5 where the peak at ~0.12 V becomes less pronounced and the peak at ~0.28 V becomes not as distinct as for the Pt/C and the other PtCo/C. Note that the CVs were recorded when the reproducible cyclic voltammograms were obtained, i.e. the 50^{th} scan at 0.1 $V.s^{-1}$.

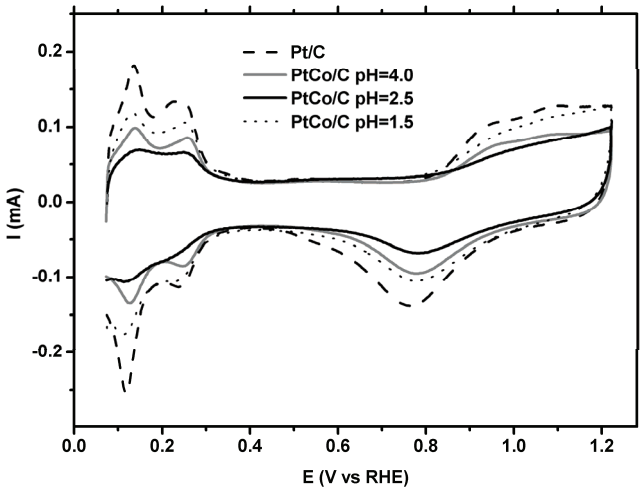

Fig. 6.11. CVs of PtCo(1:3)/C prepared at different pH and Pt/C in deaerated 0.5 M H_2SO_4 at 100 mVs^{-1}.

Since the difference in H_{upd} region is not clearly resolved in perchloric acid electrolyte, we conducted the CV characterization in sulfuric acid as the supporting electrolyte in order to obtain better-resolved structural features. Fig. 6.11 displays the CVs in 0.5 M H_2SO_4. As expected, the difference becomes clearer in H_{upd} region. The two distinct symmetrical peaks at ~0.14 V and ~0.28 V is the typical features of polycrystalline Pt. The first peak corresponds to Pt (110) sites and the last peak indicates the presence of Pt (100) step sites. For the PtCo/C prepared at pH 2.5, the corresponding CV is, once again, very different from that of Pt/C and the other PtCo/C. where the two pair peaks are not sharp. This indicates that the PtCo/C prepared at pH 2.5 contains fewer Pt (110) and Pt (100) sites compared with Pt/C and the other PtCo/C, or in other words, fewer steps and defects. This corroborates with the analysis of the CV in 0.1 M KOH and in 0.1 M $HClO_4$. The smaller low-coordination numbers that the PtCo/C pH 2.5 possesses will be discussed in terms of the oxygen reduction reactivity in the next part.

As shown in Fig. 6.10, the onset of the Pt-OH formation shifts toward more

positive potentials on the PtCo/C electrocatalysts compared to Pt/C, implying the delayed formation of Pt-OH, while the oxide-reduction peak shift positively suggesting weaker Pt-oxygenated species bond. These show that the oxophilicity of the PtCo/C catalysts are lower compared to Pt/C with PtCo/C prepared at pH 2.5 being the least oxophilic. The CVs in Fig. 6.11 also show the same trend even though the difference is not as distinct as in Fig. 6.10 due to the strong anion adsorption effect in H_2SO_4 electrolyte.

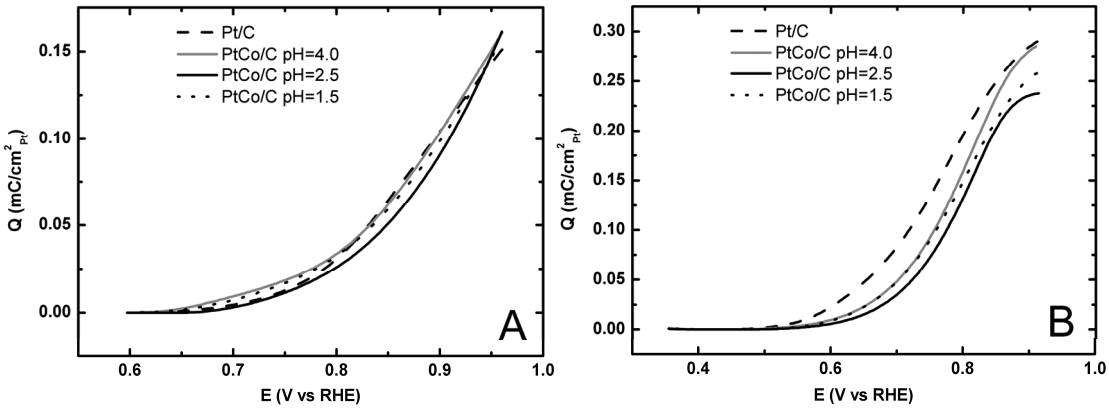

Fig. 6.12. Charge density associated with Pt-OH formation on the A) anodic scan and B) cathodic scan after background correction at $10mVs^{-1}$ in N_2-purged 0.1 M $HClO_4$. The integrated charge was normalized to the real Pt active surface area based on H_{upd}-area assuming a charge of $210\mu C/cm^2$.

Since the comparison of the cyclic voltammograms can not be made directly due to the difference in real active surface area and the contributions of the capacitance of the support, the charge density related with the water activation-adsorption of oxygen containing species on Pt on the anodic scan and reduction of the oxygenated species on Pt on the cathodic scan as a function of potential were normalized in terms of the specific surface area (cm^2_{Pt}) using the charge under the H_{upd}-area (assuming a charge constant of $210\mu C/cm^2_{Pt}$) and a background correction for the varying 'double layer' capacitance. To get rid of the scan rate effect that can

lead to false representation, a slower scan rate was used (10 mVs^{-1}) and the results are presented in Fig. 6.12. Although obviously explicit from the CVs in Fig. 6, interestingly the positive shift of the Pt-OH formation for the PtCo/C catalysts compared to Pt/C is not so clear on the anodic scan (Fig. 7A). The charge density of all the four samples up to 1.0 V was comparable, implying the same degree of surface oxidation for PtCo/C prepared at different pH and Pt/C.[6, 246, 247] On the other hand, a considerable difference in the amount of charge per Pt area in the cathodic scan can be observed in Fig. 7B where the charge density of Pt/C being the highest and Pt/Co prepared at pH 2.5 being the lowest. This is also clearly reflected in Fig. 6.10 where the oxide reduction peak in the cathodic scan is shifted around 30 mV toward positive potential for the PtCo/C prepared at pH 2.5 compared to Pt/C, with that of the PtCo/C prepared at pH 4 an pH 1.5 in-between. This confirms that the oxophilicity of PtCo/C decreases compared to Pt/C. This fact may faciliate the adsorption of oxygen at low overpotential and subsequently enhance the ORR rate.

6.3.8. ORR activity

Fig. 6.13 shows the linear sweep voltamograms of the oxygen reduction reaction on the Pt/C and PtCo/C electrodes prepared at different pH in 0.1 M $HClO_4$ with various rotation rates. The current is represented as the current over the glassy carbon electrode area (0.196 cm^2). As shown in Fig. 6.13, for all the electrodes, after sweeping the potential from about 0.17 V, the diffusion limiting currents can be observed up to ~0.7 V. At the potential range from 0.7 V to 0.95 V, the ORR is under diffusion-kinetic control (0.7 V< E < 0.95 V) and under pure kinetic control at potentials higher than 0.95 V. To remove the hysteresis in the kinetic region due to

the irreversible adsorption of oxides at the electrode surface and the deviation in the diffusion limiting currents due to the capacitance of the carbon support, the ORR currents were corrected for the background current which were obtained in deaerated 0.1 M $HClO_4$ at identical potential scan settings but without rotation. This non-faradaic current can contribute up to 20% of the overall current, which reflects the importance of the background subtraction to avoid misrepresentation of the real ORR current.

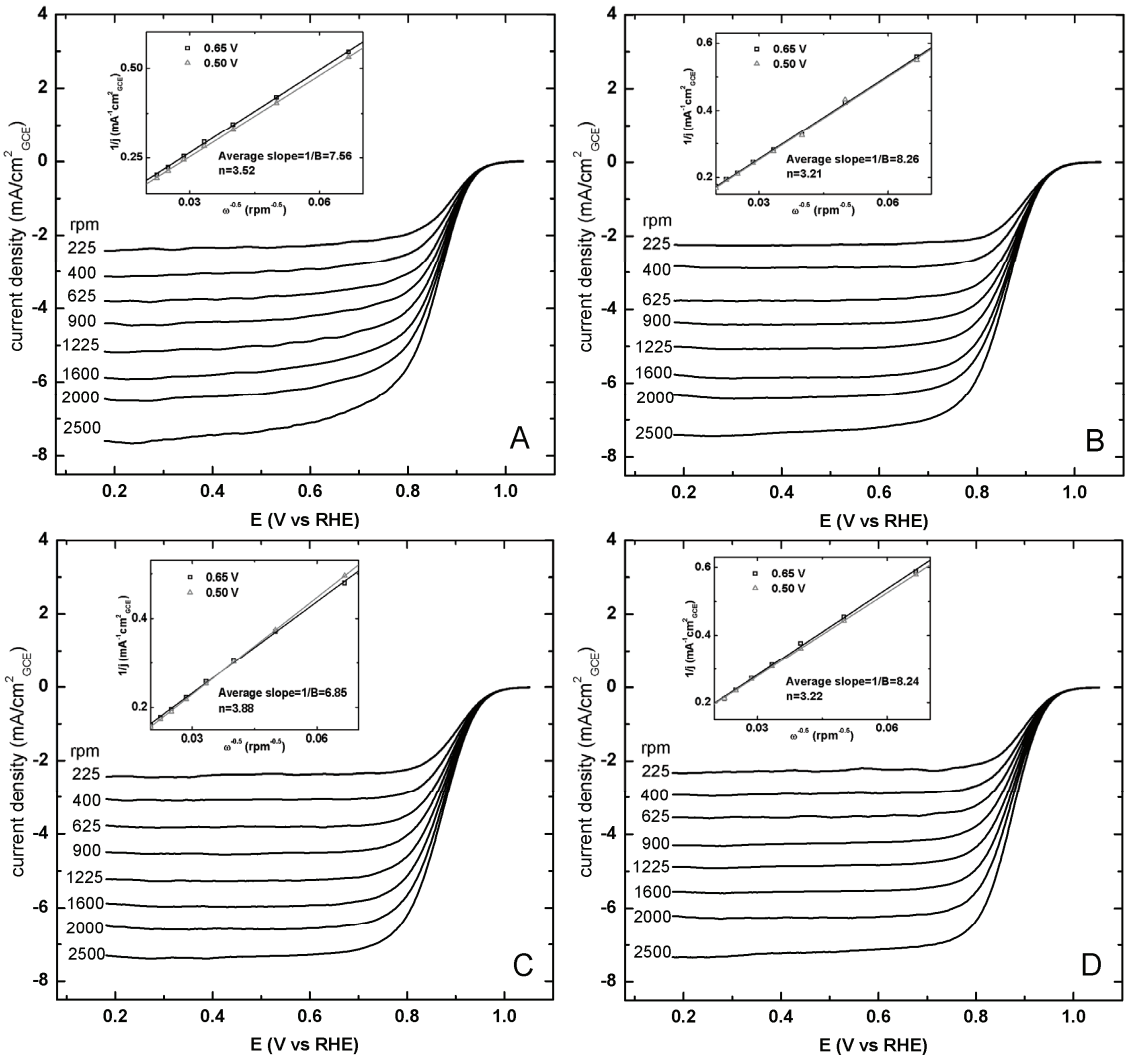

Fig. 6.13. Linear sweep voltamograms in O_2 saturated 0.1M $HClO_4$ at 20 mV/s after background correction of A) Pt/C; B) PtCo/C pH=4.0; C) PtCo/C pH=2.5; D) PtCo/C pH=1.5. Inset shows Koutecky-Levich plot at 0.65 V and 0.5 V.

The insets in Fig. 6.13 show the Koutecky-Levich plot assessed from the data at 0.65 V and 0.5 V. It can be seen that straight lines with almost the same slope were obtained in all the plots, which is very close to the theoretically predicted slope for a four-electron reaction of ORR, indicating that ORR on all the PtCo/C electrodes and Pt/C electrode is a four-electron process with water as final product. One thing needs to be mentioned is that the open circuit potential of all the PtCo/C catalysts in the electrolyte is about 10 to 20 mV higher than that of Pt/C, suggesting a more favored adsorption of oxygen on the PtCo/C surface than on Pt surface.

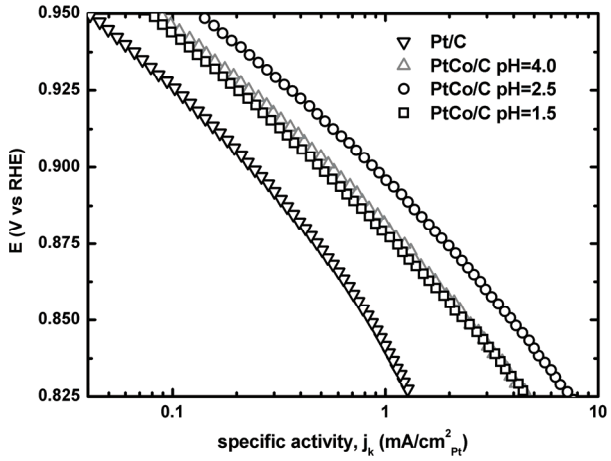

Fig. 6.14. Tafel plots of PtCo/C prepared at different pHs and Pt/C in O_2-saturated 0.1 M $HClO_4$ at 20 mV/s after background subtraction and mass transport correction at 1600 rpm. Current is represented as kinetic current normalized by Pt active surface area.

For the purpose of comparing the real activity of all the PtCo/C electrodes with Pt/C, the ORR currents after background subtraction were corrected with the mass-transport currents and presented in the form of Tafel plot. The real kinetic currents were then normalized by the Pt-active surface area from the H_{upd} charge and are shown in Fig. 6.14. From the Fig. 6.14, the common Tafel slopes can be obtained. At high potential (above 0.9 V) the obtained Tafel slopes for the Pt/C, PtCo/C prepared at pH 4, PtCo/C prepared at pH 2.5 and PtCo/C prepared at pH 1.5 are 56, 55, 57 and

58 mV decade^{-1}, respectively. We can conclude that ORR on all the electrocatalysts studied here follows same pathway and has same rate determining step.

Furthermore, at 0.9 V, the specific activity of all the PtCo/C electrodes are higher than Pt/C. The specific activity of Pt/C is 0.230 mA/cm$^2_{Pt}$ which coincides very well with the activity of the common Pt/C observed in other study.[248] While the activity of PtCo/C prepared at pH 4, pH 2.5 and pH 1.5 are 0.555 mA/cm$^2_{Pt}$, 0.894 mA/cm$^2_{Pt}$, and 0.497 mA/cm$^2_{Pt}$, respectively. These enhancements are about 2-4 times higher than Pt/C. This activity enhancement is in agreement with previously reported specific activity enhancement for PtCo catalysts.

Generally, most of the studies done on PtCo alloy catalysts reported an ORR activity enhancement by factor of 1.5 to 3 compared to pure Pt. The activity improvement towards ORR on Pt-based alloys can be explained by a few reasons. Mukerjee et al, explained the enhanced ORR activities of Pt-based alloys in terms of combination of surface geometric (favorable Pt-Pt mean interatomic distance) and surface electronic (increase in Pt d-band vacancy) properties.[100, 101] Paulus et al explained that the activtiy improvement on Pt-Co alloy was due to the inhibition of OH adsorption on Pt atomic sites surrounded by 'oxide' covered Co atoms analogous to the 'common-ion' effect where the presence of OH species on the surface repels like species from forming nearby.[102, 103] The latter mechanism can be ruled out in this study because from the CV analysis it can be concluded that if there is any Co-(hydr)oxides on the surface then most of this species will dissolve out from the surface during the potential cycling in acid media. The particle size effect also can be excluded from this study since the crystallite size of the various PtCo/C are

comparable to that of Pt/C based on XRD analysis.

Among all the proposed enhanced mechanism, the formation of pure Pt atomic monolayer (Pt-skin) on PtCo surface is the most accepted one.[130, 249, 250] The activity improvement comes from the electronic modification of the Pt surface skin layer by the Co-rich second subsurface layer, which results in a modification of the Pt-(Oxgen containing species) bonding energy due to the downshift in the d-band centre of the Pt.[113, 115, 124, 127-130] We attributed the enhancement on the ORR activity for the PtCo/C catalysts to the formation of Pt-shell layer as revealed by the CV analysis, where the PtCo/C electrodes show a delayed formation of Pt-OH and faster reduction of the Pt-oxygenated containing species compared to Pt/C with minimum existence of Co or Co-(hydr)oxides on the surface.

While the specific activity of PtCo/C prepared at pH 1.5 and PtCo/C prepared at pH 4 are about 2-2.5 times higher than Pt/C. The specific activity of the PtCo/C prepared at pH 2.5 outweighs the other catalysts, with an enhancement of 4 times higher than Pt/C. We suspect that, besides the formation of Pt-skin surface on top of the Co-rich core, such a dramatic improvement compared to the other PtCo/C electrodes is likely to be accounted for by the existence of less steps and defects on the surface of PtCo/C prepared at pH 2.5, as revealed by the CVs analysis in deaerated 0.1 M $HClO_4$ and 0.5 M H_2SO_4. Because the specific activity for the ORR on Pt surface is highly structure-sensitive, we should note that atomically smooth Pt surface with less number of low coordination atoms is more active than Pt surfaces that contains high concentrations of defects, because of the reduced interaction with hydroxyl species at high potentials that could block the Pt active surface area for the ORR. But the effect of the favorable Pt-Pt

interatomic distance can not be neglected, since from the XRD analysis the PtCo/C prepared at pH 2.5 has a Pt-Pt interatomic distance of 2.722 Å which lies in the optimum Pt-Pt interatomic distance of 2.71 to 2.73 Å based on the study by Mukerjee and McBreen group. Thus our synthesis technique here has stressed the importance of pH on the preparation of Co_{core}-Pt_{shell} via the redox transmetallation reaction that could favor the formation of highly active electrocatalysts for ORR.

6.3.9. Durability test

The long term stability of the PtCo/c pH 2.5 was evaluated by monitoring the degradation of the ECSA by repeated cyclic voltammetry with the appropriate lower and upper limit potentials in an acidic electrolyte and compared with that of Pt/C.[190, 202] The durability tests were conducted by cycling the working electrode potential 700 times between 0.05 V and 1.35 V at a scan rate of 50 mVs^{-1} in a deaerated 0.1 M $HClO_4$ electrolyte and the results are shown in Fig. 6.15.

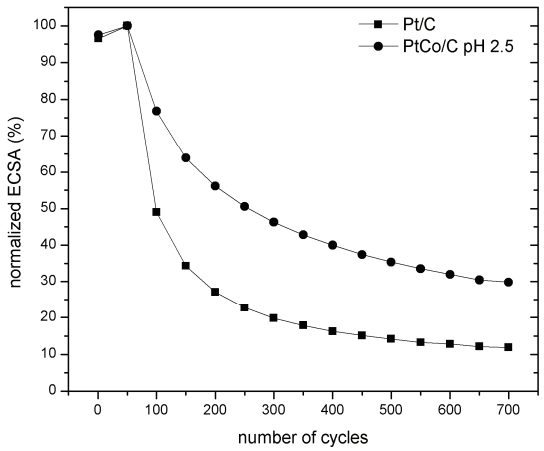

Fig. 6.15. Loss of ECSA of Pt/C and PtCo/C pH 2.5 as a function of CV cycles in the potential range of 0.05 V to 1.35 V in 0.1 M $HClO_4$ at 50 mVs^{-1}.

It can be seen that by using such a high upper limit potential, the Pt/C shows a significant decrease in the Pt ECSA, where it losses almost 90% of its initial maximum

ECSA after 700 cycles.[190, 202] PtCo/C pH 2.5 also shows a significant decrease in ECSA, but not as severe as that of Pt/C, where after 700 cycles it losses 70% of its ECSA. The possible modes for the ECSA loss for these two catalysts are roughly the same because they used carbon black as the support and their particle sizes are roughly the same (2-3 nm) which are the platinum nanoparticles dissolution and aggregation due to the carbon support corrosion.[203, 204] The only possible reason that the PtCo/C pH 2.5 shows less significant decrease in the ECSA is due to the stabilizing effect of Co,[128, 129, 246] where the incorporation of Co underneath the Pt shell will increase the Pt stability from dissolution[202] while the formation of complete Pt shell also prevent the dissolution of Co during the potential cycling.

6.4. Conclusions

The preparation of PtCo/C electrocatalysts using redox transmetalation reaction at different pH values has been studied. The final pH that favors the formation of Co-core Pt-shell structure without the formation of Co-oxide impurities and excessive Co-core dissolution is neutral (pH 7-8); such a pH condition can be achieved by modifying the initial pH of the K_2PtCl_4 solution or increasing the K_2PtCl_4 to Co mole ratio. The presence of Co helped increase the specific activity of the PtCo/C with an enhancement factor of 2-4 times of that of Pt/C. The higher activity of PtCo/C pH 2.5 compared to the other PtCo/C is attributed to the less defect that this catalyst possesses as revealed by the cyclic voltammetry analysis and also to the favorable Pt-Pt intermetallic distance as revealed by XRD analysis.

Chapter 7

Conclusions and future outlook

7.1. Conclusions

The present research work deals with the syntheses of Pt_{shell}-Au_{core}, Pt-decorated Au and Pt_{shell}-Co_{core} electrocatalysts and their electrocatalytic properties for fuel cell reactions. The Pt_{shell}-Au_{core} and Pt-decorated Au electrocatalysts have been synthesized using the successive reduction method, while the Pt_{shell}-Co_{core} electrocatalyst was prepared by the replacement reaction between Pt precursor and Co nanoparticles. The significant findings of this work are:

1) Improved Pt utilization is obtained on Pt_{shell}-Au_{core} electrocatalyts which exhibit more than 3 times higher mass activity towards methanol oxidation compared to that of Pt/C, when the Pt shell formed is thin and complete.. Instead, the formation of incomplete Pt shell shows a significantly lower activity for methanol oxidation due to the stronger Pt-CO bonding on the PtAu surfaces and presence of less ensemble sites.
2) A new type of electrocatalysts, Pt-decorated Au nanoparticles have been successfully developed with extremely low Pt loading. Such a novel structure shows a high electro-activity towards formic acid oxidation especially for low Pt/Au mole ratio, presumably due to the unique Pt atoms configuration on the Au surface that could oxidize formic acid oxidation via the direct oxidation pathway. The origin of the enhancement as studied by electrochemical

techniques has been attributed to the ensemble and electronic effect. Based on the EIS analysis, a new formic acid oxidation mechanism is proposed.

3) Pt-decorated Au electrocatalysts with different Au sizes have been successfully prepared and the effect of particle size on the activity and durability for formic acid oxidation has been evaluated. It was found that the smallest Pt-decorated Au (2nm) in this study possesses the highest activity toward formic oxidation albeit with low durability. With respect to this, the structure of the 2 nm Pt-decorated Au was optimized by subsequently reducing Au precursor onto the as-prepared Pt-decorated Au and it was found that the addition of Au increases the activity and durability of the Pt-decorated Au of the size 2 nm towards formic acid oxidation. It is presumed that the subsequent reduction of Au precursor will create less continuous Pt ensemble sites that are beneficial for the direct oxidation of formic acid.

4) The preparation of PtCo/C electrocatalysts using replacement reaction at different pH values has been studied. The final pH that favors the formation of Co_{core} Pt_{shell} structure without the formation of Co-oxide impurities and excessive Co-core dissolution is neutral (pH 7-8). The presence of Co underneath the Pt shell increases the specific activity of the PtCo/C with an enhancement factor of 2-4 times of that of Pt/C. The higher activity of PtCo/C prepared at pH 2.5 compared to the other PtCo/C is attributed to the less defects that this catalyst possesses as revealed by the cyclic voltammetry analysis and also to the favorable Pt-Pt intermetallic distance as revealed by XRD analysis.

7.2. Recommendations for future work

While this work has successfully prepared several electrocatalysts with low Pt loading and address the origin of the enhanced activity these catalysts possess, it has also brought up new questions. Below is the list of some issues that should be looked into further

1. Use of advanced electroanalytical techiques such as in situ infrared spectroscopy and differential electrochemical mass spectrometry (DEMS) to study in detail the mechanistic aspect of formic acid oxidation on the Pt-decorated Au surfaces. Moreover, the use of XPS to give direct experimental evidence on the electronic effect and theoretical calculation should also be explored to fully understand and prove which of these effects (ensemble vs electronic) plays the dominant role for HCOOH electrooxidation on the Pt-decorated surfaces.
2. Use of smooth Au polycrystalline or Au single crystal to study the extent of Pt ordering on these two different surfaces and their implications for formic acid oxidation. The ordering could be probe using advanced nanoscale techniques such as atomic force microscopy (AFM).
3. Further optimizations of the Pt-decorated structure. The aggregations issues relating to the carbon corrosion may have room for improvement such as the use of more corrosion resistant support or the synthesis of large hollow Au nanotubes as the support could be explored.
4. Pt decorated structure with other metals such as Ag could also be studied given that the base metal could survive in the harsh acidic environment.
5. Exploring the surface replacement reaction to prepare other types of core-shell metals such as Pd_{shell}-Co_{core}, Pt_{shell}-Cu_{core} and Pd_{shell}-Cu_{core} electrocatalyts.

The recommendation number 5 has been explored and in short we describe our initial findings for the Pt_{shell}-Cu_{core} system here.

Borrowing the simple preparation techiques described in chapter 6, we have synthesized Pt_{shell}-Cu_{core} electrocatalyts without the use of any surfactant or molecular stabilizer.

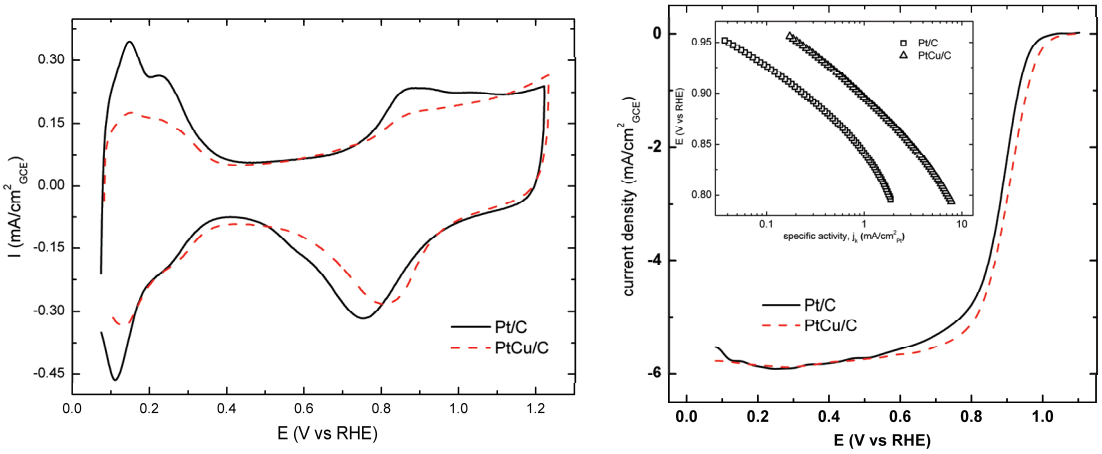

Fig.7.1. Left image shows the CVs of Pt_{shell}-Cu_{core} and Pt/C in 0.1 M $HClO_4$ at $20mVs^{-1}$. Right image shows the ORR activity of Pt_{shell}-Cu_{core} and Pt/C in 0.1 M $HClO_4$ at 20mVs-1 with the inset showing the Tafel plot.

It can be seen that Pt_{shell}-Cu_{core} has significantly higher ORR activity of up to 4 times higher compared to that of Pt/C as the result of lower oxophilicity this electrocatalyts possesses. Further systematic approach should be taken to completely understand the behavior of this catalyst in fuel cell reactions.

References

1. http://www.iea.org/
2. Ramani, V., Fuel cells. *The Electrochemical Society Interface* **2006**, 41-44.
3. He, C.; Desai, S.; Brown, G.; Bollepalli, S., PEM Fuel Cell Catalysts: Cost, Performance and Durability. *The Electrochemical Society Interface* **2005**, 41-44.
4. Ramani, V.; Kunz, H. R.; Fenton, J. M., The Polymer Electrolyte Fuel Cell. *The Electrochemical Society Interface* **2004**, 17-19.
5. Arenz, M.; Mayrhofer, K. J. J.; Stamenkovic, V.; Blizanac, B. B.; Tomoyuki, T.; Ross, P. N.; Markovic, N. M., The effect of the particle size on the kinetics of CO electrooxidation on high surface area Pt catalysts. *Journal of the American Chemical Society* **2005,** 127, (18), 6819-6829.
6. Mayrhofer, K. J. J.; Blizanac, B. B.; Arenz, M.; Stamenkovic, V. R.; Ross, P. N.; Markovic, N. M., The impact of geometric and surface electronic properties of Pt-catalysts on the particle size effect in electrocatalysis. *Journal of Physical Chemistry B* **2005,** 109, (30), 14433-14440.
7. Vielstich, W., *Handbook of Fuel Cells-Fundamentals, Technology and Applications*. Wiley: Chichester, UK, 2003.
8. Larminie, J.; Dicks, A., *Fuel Cell Systems Explained* **2000**.
9. Winter, M.; Brodd, R. J., What are batteries, fuel cells, and supercapacitors? *Chemical Reviews* **2004,** 104, (10), 4245-4269.
10. Heinzel, A.; Hebling, C.; Muller, M.; Zedda, M.; Muller, C., Fuel cells for low power applications. *Journal of Power Sources* **2002,** 105, (2), 250-255.
11. Cohen, J. L.; Volpe, D. J.; Abruna, H. D., Electrochemical determination of activation energies for methanol oxidation on polycrystalline platinum in acidic and alkaline electrolytes. *Physical Chemistry Chemical Physics* **2007,** 9, (1), 49-77.
12. Hamnett, A., Mechanism and electrocatalysis in the direct methanol fuel cell. *Catalysis Today* **1997,** 38, (4), 445-457.
13. Iwasita, T., Electrocatalysis of methanol oxidation. *Electrochimica Acta* **2002,** 47, (22-23), 3663-3674.
14. Leger, J. M., Mechanistic aspects of methanol oxidation on platinum-based electrocatalysts. *Journal of Applied Electrochemistry* **2001,** 31, (7), 767-771.
15. Lu, G. Q.; Chrzanowski, W.; Wieckowski, A., Catalytic methanol decomposition pathways on a platinum electrode. *Journal of Physical Chemistry B* **2000,** 104, (23), 5566-5572.
16. Vielstich, W., Electrochemical energy conversion - Methanol fuel cell as example. *Journal of the Brazilian Chemical Society* **2003,** 14, (4), 503-509.
17. Wasmus, S.; Kover, A., Methanol oxidation and direct methanol fuel cells: A selective review. *Journal of Electroanalytical Chemistry* **1999,** 461, (1-2), 14-31.
18. Janik, M. J.; Taylor, C. D.; Neurock, M., First principles analysis of the electrocatalytic oxidation of methanol and carbon monoxide. *Topics in Catalysis* **2007,** 46, (3-4), 306-319.
19. Rhee, Y. W.; Ha, S. Y.; Masel, R. I., Crossover of formic acid through Nafion® membranes. *Journal of Power Sources* **2003,** 117, (1-2), 35-38.
20. Rice, C.; Ha, S.; Masel, R. I.; Waszczuk, P.; Wieckowski, A.; Barnard, T., Direct formic acid fuel cells. *Journal of Power Sources* **2002,** 111, (1), 83-89.
21. Wang, X.; Hu, J. M.; Hsing, I. M., Electrochemical investigation of formic acid electro-oxidation and its crossover through a Nafion® membrane. *Journal of Electroanalytical Chemistry* **2004,** 562, (1), 73-80.
22. Yu, X.; Pickup, P. G., Recent advances in direct formic acid fuel cells (DFAFC). *Journal of Power Sources* **2008,** 182, (1), 124-132.
23. Ha, S.; Larsen, R.; Masel, R. I., Performance characterization of Pd/C nanocatalyst for direct formic acid fuel cells. *Journal of Power Sources* **2005,** 144, (1), 28-34.

24. Larsen, R.; Ha, S.; Zakzeski, J.; Masel, R. I., Unusually active palladium-based catalysts for the electrooxidation of formic acid. *Journal of Power Sources* **2006,** 157, (1), 78-84.
25. Larsen, R.; Zakzeski, J.; Masel, R. I., Unexpected activity of palladium on vanadia catalysts for formic acid electro-oxidation. *Electrochemical and Solid-State Letters* **2005,** 8, (6).
26. Liu, Z.; Hong, L.; Tham, M. P.; Lim, T. H.; Jiang, H., Nanostructured Pt/C and Pd/C catalysts for direct formic acid fuel cells. *Journal of Power Sources* **2006,** 161, (2), 831-835.
27. Rice, C.; Ha, S.; Masel, R. I.; Wieckowski, A., Catalysts for direct formic acid fuel cells. *Journal of Power Sources* **2003,** 115, (2), 229-235.
28. Weber, M.; Wang, J. T.; Wasmus, S.; Savinell, R. F., Formic acid oxidation in a polymer electrolyte fuel cell: A real-time mass-spectrometry study. *Journal of the Electrochemical Society* **1996,** 143, (7).
29. Zhu, Y.; Ha, S. Y.; Masel, R. I., High power density direct formic acid fuel cells. *Journal of Power Sources* **2004,** 130, (1-2), 8-14.
30. Zhu, Y.; Khan, Z.; Masel, R. I., The behavior of palladium catalysts in direct formic acid fuel cells. *Journal of Power Sources* **2005,** 139, (1-2), 15-20.
31. Capon, A.; Parsons, R., The oxidation of formic acid at noble metal electrodes. Part III. Intermediates and mechanism on platinum electrodes. *Journal of Electroanalytical Chemistry* **1973,** 45, (2), 205-231.
32. Parsons, R.; VanderNoot, T., The oxidation of small organic molecules. A survey of recent fuel cell related research. *Journal of Electroanalytical Chemistry* **1988,** 257, (1-2), 9-45.
33. Miki, A.; Ye, S.; Osawa, M., Surface-enhanced IR absorption on platinum nanoparticles: An application to real-time monitoring of electrocatalytic reactions. *Chemical Communications* **2002**, (14), 1500-1501.
34. Samjeske, G.; Miki, A.; Ye, S.; Osawa, M., Mechanistic study of electrocatalytic oxidation of formic acid at platinum in acidic solution by time-resolved surface-enhanced infrared absorption spectroscopy. *Journal of Physical Chemistry B* **2006,** 110, (33), 16559-16566.
35. Samjeske, G.; Miki, A.; Ye, S.; Yamakata, A.; Mukouyama, Y.; Okamoto, H.; Osawa, M., Potential oscillations in galvanostatic electrooxidation of formic acid on platinum: A time-resolved surface-enhanced infrared study. *Journal of Physical Chemistry B* **2005,** 109, (49), 23509-23516.
36. Samjeske, G.; Osawa, M., Current oscillations during formic acid oxidation on a Pt electrode-Insight into the mechanism by time-resolved IR spectroscopy. *Angewandte Chemie, International Edition* **2005,** 44, 5694-5698.
37. Lamy, C.; Lima, A.; LeRhun, V.; Delime, F.; Coutanceau, C.; Leger, J. M., Recent advances in the development of direct alcohol fuel cells (DAFC). *Journal of Power Sources* **2002,** 105, (2), 283-296.
38. Petry, O. A.; Podlovchenko, B. I.; Frumkin, A. N.; Lal, H., The behaviour of platinized-platinum and platinum-ruthenium electrodes in methanol solutions. *Journal of Electroanalytical Chemistry* **1965,** 10, (4), 253-269.
39. Tripkovic, A. V.; Popovic, K. D.; Grgur, B. N.; Blizanac, B.; Ross, P. N.; Markovic, N. M., Methanol electrooxidation on supported Pt and PtRu catalysts in acid and alkaline solutions. *Electrochimica Acta* **2002,** 47, (22-23), 3707-3714.
40. Antolini, E., Platinum-based ternary catalysts for low temperature fuel cells. Part II. Electrochemical properties. *Applied Catalysis B: Environmental* **2007,** 74, (3-4), 337-350.
41. Antolini, E., Platinum-based ternary catalysts for low temperature fuel cells. Part I. Preparation methods and structural characteristics. *Applied Catalysis B: Environmental* **2007,** 74, (3-4), 324-336.
42. Coutanceau, C.; Brimaud, S.; Lamy, C.; Leger, J. M.; Dubau, L.; Rousseau, S.; Vigier, F., Review of different methods for developing nanoelectrocatalysts for the oxidation of organic compounds. *Electrochimica Acta* **2008,** 53, (23), 6865-6880.

43. Coutanceau, C.; Rakotondrainiba, A. F.; Lima, A.; Garnier, E.; Pronier, S.; Leger, J. M.; Lamy, C., Preparation of Pt-Ru bimetallic anodes by galvanostatic pulse electrodeposition: Characterization and application to the direct methanol fuel cell. *Journal of Applied Electrochemistry* **2004,** 34, (1), 61-66.
44. Dubau, L.; Coutanceau, C.; Garnier, E.; Leger, J. M.; Lamy, C., Electrooxidation of methanol at platinum-ruthenium catalysts prepared from colloidal precursors: Atomic composition and temperature effects. *Journal of Applied Electrochemistry* **2003,** 33, (5), 419-429.
45. Dubau, L.; Hahn, F.; Coutanceau, C.; Leger, J. M.; Lamy, C., On the structure effects of bimetallic PtRu electrocatalysts towards methanol oxidation. *Journal of Electroanalytical Chemistry* **2003,** 554-555, (1), 407-415.
46. Janssen, M. M. P.; Moolhuysen, J., Platinum-tin catalysts for methanol fuel cells prepared by a novel immersion technique, by electrocodeposition and by alloying. *Electrochimica Acta* **1976,** 21, (11), 861-868.
47. Rojas, S.; Garcia-Garcia, F. J.; Jaras, S.; Martinez-Huerta, M. V.; Fierro, J. L. G.; Boutonnet, M., Preparation of carbon supported Pt and PtRu nanoparticles from microemulsion: Electrocatalysts for fuel cell applications. *Applied Catalysis A: General* **2005,** 285, (1-2), 24-35.
48. Schmidt, T. J.; Gasteiger, H. A.; Behm, R. J., Methanol electrooxidation on a colloidal PtRu-alloy fuel-cell catalyst. *Electrochemistry Communications* **1999,** 1, (1), 1-4.
49. Schmidt, T. J.; Noeske, M.; Gasteiger, H. A.; Behm, R. J.; Britz, P.; Bonnemann, H., PtRu alloy colloids as precursors for fuel cell catalysts: A combined XPS, AFM, HRTEM, and RDE study. *Journal of the Electrochemical Society* **1998,** 145, (3), 925-931.
50. Iwasita, T.; Hoster, H.; John-Anacker, A.; Lin, W. F.; Vielstich, W., Methanol oxidation on PtRu electrodes. Influence of surface structure and Pt-Ru atom distribution. *Langmuir* **2000,** 16, (2), 522-529.
51. Delime, F.; Leger, J. M.; Lamy, C., Enhancement of the electrooxidation of ethanol on a Pt-PEM electrode modified by tin. Part I: Half cell study. *Journal of Applied Electrochemistry* **1999,** 29, (11), 1249-1254.
52. Waszczuk, P.; Lu, G. Q.; Wieckowski, A.; Lu, C.; Rice, C.; Masel, R. I., UHV and electrochemical studies of CO and methanol adsorbed at platinum/ruthenium surfaces, and reference to fuel cell catalysis. *Electrochimica Acta* **2002,** 47, (22-23), 3637-3652.
53. Waszczuk, P.; Solla-Gullen, J.; Kim, H. S.; Tong, Y. Y.; Montiel, V.; Aldaz, A.; Wieckowski, A., Methanol electrooxidation on platinum/ruthenium nanoparticle catalysts. *Journal of Catalysis* **2001,** 203, (1), 1-6.
54. Waszczuk, P.; Wieckowski, A.; Zelenay, P.; Gottesfeld, S.; Coutanceau, C.; Leger, J. M.; Lamy, C., Adsorption of CO poison on fuel cell nanoparticle electrodes from methanol solutions: A radioactive labeling study. *Journal of Electroanalytical Chemistry* **2001,** 511, (1-2), 55-64.
55. Lu, C.; Rice, C.; Masel, R. I.; Babu, P. K.; Waszczuk, P.; Kim, H. S.; Oldfield, E.; Wieckowski, A., UHV, electrochemical NMR, and electrochemical studies of platinum/ruthenium fuel cell catalysts. *Journal of Physical Chemistry B* **2002,** 106, (37), 9581-9589.
56. Kim, T.; Kobayashi, K.; Takahashi, M.; Nagai, M., Effect of Sn in Pt-Ru-Sn ternary catalysts for CO/H_2 and methanol electrooxidation. *Chemistry Letters* **2005,** 34, (6), 798-799.
57. Liang, Y.; Zhang, H.; Tian, Z.; Zhu, X.; Wang, X.; Yi, B., Synthesis and structure-activity relationship exploration of carbon-supported PtRuNi nanocomposite as a CO-tolerant electrocatalyst for proton exchange membrane fuel cells. *Journal of Physical Chemistry B* **2006,** 110, (15), 7828-7834.
58. Liang, Y.; Zhang, H.; Zhong, H.; Zhu, X.; Tian, Z.; Xu, D.; Yi, B., Preparation and characterization of carbon-supported PtRuIr catalyst with excellent CO-tolerant performance for proton-exchange membrane fuel cells. *Journal of Catalysis* **2006,** 238, (2), 468-476.
59. Lima, A.; Coutanceau, C.; Leger, J. M.; Lamy, C., Investigation of ternary catalysts for methanol electrooxidation. *Journal of Applied Electrochemistry* **2001,** 31, (4), 379-386.

60. Lima, A.; Hahn, F.; Leger, J. M., Oxidation of methanol on Pt, Pt-Ru, and Pt-Ru-Mo electrocatalysts dispersed in polyaniline: An in situ infrared reflectance spectroscopy study. *Russian Journal of Electrochemistry* **2004,** 40, (3), 326-336.
61. Lu, G.; Cooper, J. S.; McGinn, P. J., SECM characterization of Pt-Ru-WC and Pt-Ru-Co ternary thin film combinatorial libraries as anode electrocatalysts for PEMFC. *Journal of Power Sources* **2006,** 161, (1), 106-114.
62. Papageorgopoulos, D. C.; Keijzer, M.; De Bruijn, F. A., The inclusion of Mo, Nb and Ta in Pt and PtRu carbon supported electrocatalysts in the quest for improved CO tolerant PEMFC anodes. *Electrochimica Acta* **2002,** 48, (2), 197-204.
63. Roth, C.; Goetz, M.; Fuess, H., Synthesis and characterization of carbon-supported Pt-Ru-WO_x catalysts by spectroscopic and diffraction methods. *Journal of Applied Electrochemistry* **2001,** 31, (7), 793-798.
64. Venkataraman, R.; Kunz, H. R.; Fenton, J. M., Development of new CO tolerant ternary anode catalysts for proton exchange membrane fuel cells. *Journal of the Electrochemical Society* **2003,** 150, (3).
65. Zhang, X.; Zhang, F.; Chan, K. Y., Preparation of Pt-Ru-Co trimetallic nanoparticles and their electrocatalytic properties. *Catalysis Communications* **2004,** 5, (12), 749-753.
66. Zhou, W. J.; Li, W. Z.; Song, S. Q.; Zhou, Z. H.; Jiang, L. H.; Sun, G. Q.; Xin, Q.; Poulianitis, K.; Kontou, S.; Tsiakaras, P., Bi- and tri-metallic Pt-based anode catalysts for direct ethanol fuel cells. *Journal of Power Sources* **2004,** 131, (1-2), 217-223.
67. Dinh, H. N.; Ren, X.; Garzon, F. H.; Piotr, Z.; Gottesfeld, S., Electrocatalysis in direct methanol fuel cells: In-situ probing of PtRu anode catalyst surfaces. *Journal of Electroanalytical Chemistry* **2000,** 491, (1-2), 222-233.
68. Watanabe, M.; Uchida, M.; Motoo, S., Preparation of highly dispersed Pt + Ru alloy clusters and the activity for the electrooxidation of methanol. *Journal of Electroanalytical Chemistry* **1987,** 229, (1-2), 395-406.
69. Gasteiger, H. A.; Markovic, N.; Ross Jr, P. N.; Cairns, E. J., Methanol electrooxidation on well-characterized Pt-Ru alloys. *Journal of Physical Chemistry* **1993,** 97, (46), 12020-12029.
70. Gasteiger, H. A.; Markovic, N.; Ross Jr, P. N.; Cairns, E. J., Electro-oxidation of small organic molecules on well-characterized PtRu alloys. *Electrochimica Acta* **1994,** 39, (11-12), 1825-1832.
71. Tong, Y. Y.; Hee, S. K.; Babu, P. K.; Waszczuk, P.; Wieckowski, A.; Oldfield, E., An NMR investigation of CO tolerance in a Pt/Ru fuel cell catalyst. *Journal of the American Chemical Society* **2002,** 124, (3), 468-473.
72. Capon, A.; Parsons, R., The oxidation of formic acid at noble metal electrodes. I. Review of previous work. *Journal of Electroanalytical Chemistry* **1973,** 44, (1), 1-7.
73. Capon, A.; Parsons, R., The oxidation of formic acid on noble metal electrodes II. A comparison of the behaviour of pure electrodes. *Journal of Electroanalytical Chemistry* **1973,** 44, (2), 239-254.
74. Alden, L. R.; Han, D. K.; Matsumoto, F.; Abruna, H. D.; DiSalvo, F. J., Intermetallic PtPb nanoparticles prepared by sodium naphthalide reduction of metal-organic precursors: Electrocatalytic oxidation of formic acid. *Chemistry of Materials* **2006,** 18, (23), 5591-5596.
75. Alden, L. R.; Roychowdhury, C.; Matsumoto, F.; Han, D. K.; Zeldovich, V. B.; Abruna, H. D.; DiSalvo, F. J., Synthesis, characterization, and electrocatalytic activity of PtPb nanoparticles prepared by two synthetic approaches. *Langmuir* **2006,** 22, (25), 10465-10471.
76. Arenz, M.; Stamenkovic, V.; Ross, P. N.; Markovic, N. M., Surface (electro-)chemistry on Pt(111) modified by a Pseudomorphic Pd monolayer. *Surface Science* **2004,** 573, (1), 57-66.
77. Casado-Rivera, E.; Volpe, D. J.; Alden, L.; Lind, C.; Downie, C.; Vazquez-Alvarez, T.; Angelo, A. C. D.; DiSalvo, F. J.; Abruna, H. D., Electrocatalytic Activity of Ordered Intermetallic Phases for Fuel Cell Applications. *Journal of the American Chemical Society* **2004,** 126, (12), 4043-4049.

78. Choi, J. H.; Jeong, K. J.; Dong, Y.; Han, J.; Lim, T. H.; Lee, J. S.; Sung, Y. E., Electro-oxidation of methanol and formic acid on PtRu and PtAu for direct liquid fuel cells. *Journal of Power Sources* **2006,** 163, (1 SPEC. ISS.), 71-75.
79. Gojkovic, S. L.; Tripkovic, A. V.; Stevanovic, R. M.; Krstajic, N. V., High activity of Pt_4Mo alloy for the electrochemical oxidation of formic acid. *Langmuir* **2007,** 23, (25), 12760-12764.
80. Herrero, E.; Fernandez-Vega, A.; Feliu, J. M.; Aldaz, A., Poison formation reaction from formic acid and methanol on Pt(111) electrodes modified by irreversibly adsorbed Bi and As. *Journal of Electroanalytical Chemistry* **1993,** 350, (1-2), 73-88.
81. Jayashree, R. S.; Spendelow, J. S.; Yeom, J.; Rastogi, C.; Shannon, M. A.; Kenis, P. J. A., Characterization and application of electrodeposited Pt, Pt/Pd, and Pd catalyst structures for direct formic acid micro fuel cells. *Electrochimica Acta* **2005,** 50, (24), 4674-4682.
82. Macia, M. D.; Herrero, E.; Feliu, J. M., Formic acid oxidation on Bi-Pt(1 1 1) electrode in perchloric acid media. A kinetic study. *Journal of Electroanalytical Chemistry* **2003,** 554-555, (1), 25-34.
83. Markovic, N. M.; Gasteiger, H. A.; Ross Jr, P. N.; Jiang, X.; Villegas, I.; Weaver, M. J., Electro-oxidation mechanisms of methanol and formic acid on Pt-Ru alloy surfaces. *Electrochimica Acta* **1995,** 40, (1), 91-98.
84. Matsumoto, F.; Roychowdhury, C.; DiSalvo, F. J.; Abruna, H. D., Electrocatalytic activity of ordered intermetallic PtPb nanoparticles prepared by borohydride reduction toward formic acid oxidation. *Journal of the Electrochemical Society* **2008,** 155, (2).
85. Park, I. S.; Lee, K. S.; Choi, J. H.; Park, H. Y.; Sung, Y. E., Surface structure of Pt-modified Au nanoparticles and electrocatalytic activity in formic acid electro-oxidation. *Journal Of Physical Chemistry C* **2007,** 111, (51), 19126-19133.
86. Song, C.; Khanfar, M.; Pickup, P. G., Mo oxide modified catalysts for direct methanol, formaldehyde and formic acid fuel cells. *Journal of Applied Electrochemistry* **2006,** 36, (3), 339-345.
87. Thomas, F. S.; Masel, R. I., Formic acid decomposition on palladium-coated Pt(110). *Surface Science* **2004,** 573, (2), 169-175.
88. Tripkovic, A. V.; Gojkovic, S. L.; Popovic, K. D.; Lovic, J. D.; Kowal, A., Study of the kinetics and the influence of Bi_{irr} on formic acid oxidation at Pt_2Ru_3/C. *Electrochimica Acta* **2007,** 53, (2), 887-893.
89. Uhm, S.; Chung, S. T.; Lee, J., Activity of Pt anode catalyst modified by underpotential deposited Pb in a direct formic acid fuel cell. *Electrochemistry Communications* **2007,** 9, (8), 2027-2031.
90. Volpe, D.; Casado-Rivera, E.; Alden, L.; Lind, C.; Hagerdon, K.; Downie, C.; Korzeniewski, C.; DiSalvo, F. J.; Abruna, H. D., Surface treatment effects on the electrocatalytic activity and characterization of intermetallic phases. *Journal of the Electrochemical Society* **2004,** 151, (7).
91. Xia, X. H.; Iwasita, T., Influence of underpotential deposited lead upon the oxidation of HCOOH in $HClO_4$ at platinum electrodes. *Journal of the Electrochemical Society* **1993,** 140, (9), 2559-2565.
92. Zhang, L.; Tang, Y.; Bao, J.; Lu, T.; Li, C., A carbon-supported Pd-P catalyst as the anodic catalyst in a direct formic acid fuel cell. *Journal of Power Sources* **2006,** 162, (1), 177-179.
93. Zhou, X.; Xing, W.; Liu, C.; Lu, T., Platinum-macrocycle co-catalyst for electro-oxidation of formic acid. *Electrochemistry Communications* **2007,** 9, (7), 1469-1473.
94. Baldauf, M.; Kolb, D. M., Formic acid oxidation on ultrathin Pd films on Au(hkl) and Pt(hkl) electrodes. *Journal of Physical Chemistry* **1996,** 100, (27), 11375-11381.
95. Borup, R.; Meyers, J.; Pivovar, B.; Kim, Y. S.; Mukundan, R.; Garland, N.; Myers, D.; Wilson, M.; Garzon, F.; Wood, D.; Zelenay, P.; More, K.; Stroh, K.; Zawodzinski, T.; Boncella,

J.; McGrath, J. E.; Inaba, M.; Miyatake, K.; Hori, M.; Ota, K.; Ogumi, Z.; Miyata, S.; Nishikata, A.; Siroma, Z.; Uchimoto, Y.; Yasuda, K.; Kimijima, K. I.; Iwashita, N., Scientific aspects of polymer electrolyte fuel cell durability and degradation. *Chemical Reviews* **2007,** 107, (10), 3904-3951.

96. Neergat, M.; Shukla, A. K.; Gandhi, K. S., Platinum-based alloys as oxygen-reduction catalysts for solid-polymer-electrolyte direct methanol fuel cells. *Journal of Applied Electrochemistry* **2001,** 31, (4), 373-378.

97. Stamenkovic, V. R.; Mun, B. S.; Arenz, M.; Mayrhofer, K. J. J.; Lucas, C. A.; Wang, G.; Ross, P. N.; Markovic, N. M., Trends in electrocatalysis on extended and nanoscale Pt-bimetallic alloy surfaces. *Nature Materials* **2007,** 6, (3), 241-247.

98. Costamagna, P.; Srinivasan, S., Quantum jumps in the PEMFC science and technology from the 1960s to the year 2000: Part I. Fundamental scientific aspects. *Journal of Power Sources* **2001,** 102, (1-2), 242-252.

99. Mukerjee, S.; McBreen, J., Effect of particle size on the electrocatalysis by carbon-supported Pt electrocatalysts: An in situ XAS investigation. *Journal of Electroanalytical Chemistry* **1998,** 448, (2), 163-171.

100. Mukerjee, S.; Srinivasan, S.; Soriaga, M. P.; McBreen, J., Role of structural and electronic properties of Pt and Pt alloys on electrocatalysis of oxygen reduction. *Journal of the Electrochemical Society* **1995,** 142, 1409-1422.

101. Mukerjee, S.; Srinivasan, S.; Soriaga, M. P.; McBreen, J., Effect of Preparation Conditions of Pt Alloys on Their Electronic, Structural, and Electrocatalytic Activities for Oxygen Reduction - XRD, XAS, and Electrochemical Studies. *Journal of Physical Chemistry* **1995,** 99, (13), 4577-4589.

102. Paulus, U. A.; Wokaun, A.; Scherer, G. G.; Schmidt, T. J.; Stamenkovic, V. R.; Markovic, N. M.; Ross, P. N., Oxygen reduction on high surface area Pt-based alloy catalysts in comparison to well defined smooth bulk alloy electrodes. *Electrochimica Acta* **2002,** 47, 3787-3798.

103. Paulus, U. A.; Wokaun, A.; Scherer, G. G.; Schmidt, T. J.; Stamenkovic, V. R.; Radmilovic, V.; Markovic, N. M.; Ross, P. N., Oxygen reduction on carbon supported Pt-Ni and Pt-Co alloy catalysts. *Journal of Physical Chemistry B* **2002,** 106, 4181-4191.

104. Shukla, A. K.; Raman, R. K.; Choudhury, N. A.; Priolkar, K. R.; Sarode, P. R.; Emura, S.; Kumashiro, R., Carbon-supported Pt-Fe alloy as a methanol-resistant oxygen-reduction catalyst for direct methanol fuel cells. *Journal of Electroanalytical Chemistry* **2004,** 563, (2), 181-190.

105. Srivastava, R.; Mani, P.; Hahn, N.; Strasser, P., Efficient oxygen reduction fuel cell electrocatalysis on voltammetrically dealloyed Pt-Cu-Co nanoparticles. *Angewandte Chemie - International Edition* **2007,** 46, (47), 8988-8991.

106. Stamenkovic, V. R.; Fowler, B.; Mun, B. S.; Wang, G.; Ross, P. N.; Lucas, C. A.; Markovic, N. M., Improved oxygen reduction activity on $Pt_3Ni(111)$ via increased surface site availability. *Science* **2007,** 315, (5811), 493-497.

107. Stamenkovic, V. R.; Mun, B. S.; Mayrhofer, K. J. J.; Ross, P. N.; Markovic, N. M., Effect of surface composition on electronic structure, stability, and electrocatalytic properties of Pt-transition metal alloys: Pt-skin versus Pt-skeleton surfaces. *Journal of the American Chemical Society* **2006,** 128, (27), 8813-8819.

108. Toda, T.; Igarashi, H.; Uchida, H.; Watanabe, M., Enhancement of the electroreduction of oxygen on Pt alloys with Fe, Ni, and Co. *Journal of the Electrochemical Society* **1999,** 146, (10), 3750-3756.

109. Yang, H.; Alonso-Vante, N.; Leger, J. M.; Lamy, C., Tailoring, Structure, and Activity of Carbon-Supported Nanosized Pt-Cr Alloy Electrocatalysts for Oxygen Reduction in Pure and Methanol-Containing Electrolytes. *Journal of Physical Chemistry B* **2004,** 108, (6), 1938-1947.

110. Turkevich, J.; Stevenson, P. C.; Hillier, J., A study of the nucleation and growth processes in the synthesis of colloidal gold. *Discussions of the Faraday Society* **1951,** 11, 55-75.
111. Schmid, G.; Lehnert, A.; Malm, J. O.; Bovin, J. O., Ligand-stabilized bimetallic colloids identified by HRTEM and EDX. *Angewandte Chemie (International Edition in English)* **1991,** 30, (7), 874-876.
112. Schmid, G.; West, H.; Mehles, H.; Lehnert, A., Hydrosilation Reactions Catalyzed by Supported Bimetallic Colloids. *Inorganic Chemistry* **1997,** 36, (5), 891-895.
113. Adzic, R. R.; Zhang, J.; Sasaki, K.; Vukmirovic, M. B.; Shao, M.; Wang, J. X.; Nilekar, A. U.; Mavrikakis, M.; Valerio, J. A.; Uribe, F., Platinum monolayer fuel cell electrocatalysts. *Topics in Catalysis* **2007,** 46, 249-262.
114. Inoue, H.; Brankovic, S. R.; Wang, J. X.; Adzic, R. R., Oxygen reduction on bare and Pt monolayer-modified Ru(0001), Ru(100) and Ru nanostructured surfaces. *Electrochimica Acta* **2002,** 47, 3777-3785.
115. Lima, F. H. B.; Zhang, J.; Shao, M. H.; Sasaki, K.; Vukmirovic, M. B.; Ticianelli, E. A.; Adzic, R. R., Catalytic Activity-d-Band Center Correlation for the O_2 Reduction Reaction on Platinum in Alkaline Solutions. *Journal of Physical Chemistry C* **2007,** 111, 404-410.
116. Sasaki, K.; Mo, Y.; Wang, J. X.; Balasubramanian, M.; Uribe, F.; McBreen, J.; Adzic, R. R., Pt submonolayers on metal nanoparticles - Novel electrocatalysts for H_2 oxidation and O_2 reduction. *Electrochimica Acta* **2003,** 48, (25-26), 3841-3849.
117. Sasaki, K.; Zhang, J.; Wang, J.; Uribe, F.; Adzic, R., Platinum submonolayer-monolayer electrocatalysts: An electrochemical and X-ray absorption spectroscopy study. *Research on Chemical Intermediates* **2006,** 32, (5-6), 543-559.
118. Shao, M.; Sasaki, K.; Marinkovic, N. S.; Zhang, L.; Adzic, R. R., Synthesis and characterization of platinum monolayer oxygen-reduction electrocatalysts with Co-Pd core-shell nanoparticle supports. *Electrochemistry Communications* **2007,** 9, 2848-2853.
119. Vukmirovic, M. B.; Zhang, J.; Sasaki, K.; Nilekar, A. U.; Uribe, F.; Mavrikakis, M.; Adzic, R. R., Platinum monolayer electrocatalysts for oxygen reduction. *Electrochimica Acta* **2007,** 52, (6), 2257-2263.
120. Zhang, J.; Lima, F. H. B.; Shao, M. H.; Sasaki, K.; Wang, J. X.; Hanson, J.; Adzic, R. R., Platinum monolayer on nonnoble metal-noble metal core-shell nanoparticle electrocatalysts for O_2 reduction. *Journal of Physical Chemistry B* **2005,** 109, (48), 22701-22704.
121. Zhang, J.; Mo, Y.; Vukmirovic, M. B.; Klie, R.; Sasaki, K.; Adzic, R. R., Platinum monolayer electrocatalysts for O_2 reduction: Pt monolayer on Pd(111) and on carbon-supported Pd nanoparticles. *Journal of Physical Chemistry B* **2004,** 108, (30), 10955-10964.
122. Zhang, J.; Sasaki, K.; Sutter, E.; Adzic, R. R., Stabilization of platinum oxygen-reduction electrocatalysts using gold clusters. *Science* **2007,** 315, (5809), 220-222.
123. Zhang, J.; Shao, M. H.; Sasaki, K.; Vukmirovic, M. B.; Uribe, F.; Adzic, R. R. In *Platinum and mixed platinum-metal monolayer fuel cell electrocatalysts: Design, activity and long-term performance stability*, ECS Transactions, 2006; 2006; pp 31-36.
124. Zhang, J.; Vukmirovic, M. B.; Xu, Y.; Mavrikakis, M.; Adzic, R. R., Controlling the catalytic activity of Pt-monolayer electrocatalysts for O_2 reduction with different substrates. *Angewandte Chemie, International Edition* **2005,** 44, (2132-2135).
125. Scott, R. W. J.; Wilson, O. M.; Oh, S. K.; Kenik, E. A.; Crooks, R. M., Bimetallic Palladium - Gold dendrimer-encapsulated catalysts. *Journal of the American Chemical Society* **2004,** 126, (47), 15583-15591.
126. Toshima, N.; Yonezawa, T., Bimetallic nanoparticles - Novel materials for chemical and physical applications. *New Journal of Chemistry* **1998,** 22, (11), 1179-1201.
127. Demirci, U. B., Theoretical means for searching bimetallic alloys as anode electrocatalysts for direct liquid-feed fuel cells. *Journal of Power Sources* **2007,** 173, (1), 11-18.
128. Hammer, B.; Norskov, J. K., Electronic factors determining the reactivity of metal surfaces. *Surface Science* **1995,** 343, (3), 211-220.

129. Hammer, B.; Norskov, J. K., Theoretical surface science and catalysis-calculations and concepts. *Advances in Catalysis* **2000,** 45, 71-129.
130. Stamenkovic, V. R.; Mun, B. S.; Mayrhofer, K. J. J.; Ross, P. N.; Markovic, N. M.; Rossmeisl, J.; Greeley, J.; Norskov, J. K., Changing the activity of electrocatalytsts for oxygen reduction by tuning the surface eletronic structure. *Angewandte Chemie, International Edition* **2006,** 45, 2897-2901.
131. Papadimitriou, S.; Tegou, A.; Pavlidou, E.; Armyanov, S.; Valova, E.; Kokkinidis, G.; Sotiropoulos, S., Preparation and characterisation of platinum- and gold-coated copper, iron, cobalt and nickel deposits on glassy carbon substrates. *Electrochimica Acta* **2008,** 53, (22), 6559-6567.
132. Papadimitriou, S.; Tegou, A.; Pavlidou, E.; Kokkinidis, G.; Sotiropoulos, S., Methanol oxidation at platinized lead coatings prepared by a two-step electrodeposition-electroless deposition process on glassy carbon and platinum substrates. *Electrochimica Acta* **2007,** 52, (21), 6254-6260.
133. Tegou, A.; Papadimitriou, S.; Pavlidou, E.; Kokkinidis, G.; Sotiropoulos, S., Oxygen reduction at platinum- and gold-coated copper deposits on glassy carbon substrates. *Journal of Electroanalytical Chemistry* **2007,** 608, (1), 67-77.
134. Grabar, K. C.; Allison, K. J.; Baker, B. E.; Bright, R. M.; Brown, K. R.; Freeman, R. G.; Fox, A. P.; Keating, C. D.; Musick, M. D.; Natan, M. J., Two-dimensional arrays of colloidal gold particles: A flexible approach to macroscopic metal surfaces. *Langmuir* **1996,** 12, (10), 2353-2361.
135. Schmidt, T. J.; Gasteiger, H. A.; Stab, G. D.; Urban, P. M.; Kolb, D. M.; Behm, R. J., Characterization of high-surface-area electrocatalysts using a rotating disk electrode configuration. *Journal of the Electrochemical Society* **1998,** 145, (7), 2354-2358.
136. Li, W.; Liang, C.; Zhou, W.; Qiu, J.; Zhou, Z.; Sun, G.; Xin, Q., Preparation and characterization of multiwalled carbon nanotube-supported platinum for cathode catalysts of direct methanol fuel cells. *Journal of Physical Chemistry B* **2003,** 107, (26), 6292-6299.
137. Nath, S.; Praharaj, S.; Panigrahi, S.; Ghosh, S. K.; Kundu, S.; Basu, S.; Pal, T., Synthesis and characterization of N,N-Dimethyldodecylamine-capped Au_{core}-Pd_{shell} nanoparticles in toluene. *Langmuir* **2005,** 21, (23), 10405-10408.
138. Yonezawa, T.; Toshima, N., Mechanistic consideration of formation of polymer-protected nanoscopic bimetallic clusters. *Journal of the Chemical Society, Faraday Transactions* **1995,** 91, (22), 4111-4119.
139. Henglein, A., Preparation and Optical Aborption Spectra of $Au_{core}Pt_{shell}$ and $Pt_{core}Au_{shell}$ Colloidal Nanoparticles in Aqueous Solution. *Journal of Physical Chemistry B* **2000,** 104, (10), 2201-2203.
140. Wu, M. L.; Chen, D. H.; Huang, T. C., Preparation of Au/Pt bimetallic nanoparticles in water-in-oil microemulsions. *Chemistry of Materials* **2001,** 13, (2), 599-606.
141. Hamelin, A., Cyclic voltammetry at gold single-crystal surfaces. Part 1. Behaviour at low-index faces. *Journal of Electroanalytical Chemistry* **1996,** 407, (1-2), 1-11.
142. Park, S.; Yang, P.; Corredor, P.; Weaver, M. J., Transition metal-coated nanoparticle films: Vibrational characterization with surface-enhanced Raman scattering. *Journal of the American Chemical Society* **2002,** 124, (11), 2428-2429.
143. Yoo, S. H.; Park, S., Platinum-coated, nanoporous gold nanorod arrays: Synthesis and characterization. *Advanced Materials* **2007,** 19, (12), 1612-1615.
144. Dean, J. A., *Lange's Handbook of Chemistry* **1985**.
145. Du, B.; Tong, Y., A coverage-dependent study of Pt spontaneously deposited onto Au and Ru surfaces: Direct experimental evidence of the ensemble effect for methanol electro-oxidation on Pt. *Journal of Physical Chemistry B* **2005,** 109, (38), 17775-17780.

146. Song, C.; Ge, Q.; Wang, L., DFT studies of Pt/Au bimetallic clusters and their interactions with the CO molecule. *Journal of Physical Chemistry B* **2005,** 109, (47), 22341-22350.
147. Clavilier, J.; Sun, S. G., Electrochemical study of the chemisorbed species formed from formic acid dissociation at platinum single crystal electrodes. *Journal of Electroanalytical Chemistry* **1986,** 199, (2), 471-480.
148. Kita, H.; Lei, H. W., Oxidation of formic acid in acid solution on Pt single-crystal electrodes. *Journal of Electroanalytical Chemistry* **1995,** 388, (1-2), 167-177.
149. Sun, S. G.; Clavilier, J., Electrochemical study on the poisoning intermediate formed from methanol dissociation at low index and stepped platinum surfaces. *Journal of Electroanalytical Chemistry* **1987,** 236, (1-2), 95-112.
150. Arenz, M.; Stamenkovic, V.; Schmidt, T. J.; Wandelt, K.; Ross, P. N.; Markovic, N. M., The electro-oxidation of formic acid on Pt-Pd single crystal bimetallic surfaces. *Physical Chemistry Chemical Physics* **2003,** 5, (19), 4242-4251.
151. Casado-Rivera, E.; Gal, Z.; Angelo, A. C. D.; Lind, C.; DiSalvo, F. J.; Abruna, H. D., Electrocatalytic oxidation of formic acid at an ordered intermetallic PtBi surface. *ChemPhysChem* **2003,** 4, (2), 193-199.
152. Chen, W.; Kim, J.; Sun, S.; Chen, S., Electro-oxidation of formic acid catalyzed by FePt nanoparticles. *Physical Chemistry Chemical Physics* **2006,** 8, (23), 2779-2786.
153. Chen, W.; Kim, J.; Sun, S.; Chen, S., Composition effects of FePt alloy nanoparticles on the electro-oxidation of formic acid. *Langmuir* **2007,** 23, (22), 11303-11310.
154. Gasteiger, H. A.; Markovic, N.; Ross Jr, P. N.; Cairns, E. J., CO electrooxidation on well-characterized Pt-Ru alloys. *Journal of Physical Chemistry* **1994,** 98, (2), 617-625.
155. Tripkovic, A. V.; Popovic, K. D.; Stevanovic, R. M.; Socha, R.; Kowal, A., Activity of a PtBi alloy in the electrochemical oxidation of formic acid. *Electrochemistry Communications* **2006,** 8, (9), 1492-1498.
156. Waszczuk, P.; Barnard, T. M.; Rice, C.; Masel, R. I.; Wieckowski, A., A nanoparticle catalyst with superior activity for electrooxidation of formic acid. *Electrochemistry Communications* **2002,** 4, (7), 599-603.
157. Kristian, N.; Wang, X., Pt_{shell}-Au_{core}/C electrocatalyst with a controlled shell thickness and improved Pt utilization for fuel cell reactions. *Electrochemistry Communications* **2008,** 10, (1), 12-15.
158. Kristian, N.; Wang, X. In *Pt-decorated Au nanoparticles: Highly active catalyst for formic acid oxidation*, ECS Transactions, 2008; 2008; pp 639-645.
159. Kristian, N.; Yan, Y.; Wang, X., Highly efficient submonolayer Pt-decorated Au nano-catalysts for formic acid oxidation. *Chemical Communications* **2008**, (3), 353-355.
160. Kristian, N.; Yu, Y.; Gunawan, P.; Xu, R.; Deng, W.; Liu, X.; Wang, X., Controlled synthesis of Pt-decorated Au nanostructure and its promoted activity toward formic acid electro-oxidation. *Electrochimica Acta* **2009,** 54, (21), 4916-4924.
161. Llorca, M. J.; Feliu, J. M.; Aldaz, A.; Clavilier, J., Formic acid oxidation on Pd_{ad} + Pt(100) and Pd_{ad} + Pt(111) electrodes. *Journal of Electroanalytical Chemistry* **1994,** 376, (1-2), 151-160.
162. Grzelczak, M.; Perez-Juste, J.; Rodriguez-Gonzalez, B.; Liz-Marzan, L. M., Influence of silver ions on the growth mode of platinum on gold nanorods. *Journal of Materials Chemistry* **2006,** 16, (40), 3946-3951.
163. Zhao, D.; Xu, B. Q., Platinum covering of gold nanoparticles for utilization enhancement of Pt in electrocatalysts. *Physical Chemistry Chemical Physics* **2006,** 8, (43), 5106-5114.
164. Liz-Marzan, L. M.; Philipse, A. P., Stable hydrosols of metallic and bimetallic nanoparticles immobilized on imogolite fibers. *Journal of Physical Chemistry* **1995,** 99, (41), 15120-15128.

165. Kan, C.; Cai, W.; Li, C.; Zhang, L.; Hofmeister, H., Ultrasonic synthesis and optical properties of Au/Pd bimetallic nanoparticles in ethylene glycol. *Journal of Physics D: Applied Physics* **2003,** 36, (13), 1609-1614.
166. Stevens, D. A.; Dahn, J. R., Thermal degradation of the support in carbon-supported platinum electrocatalysts for PEM fuel cells. *Carbon* **2005,** 43, 179-188.
167. Luo, J.; Kariuki, N.; Han, L.; Wang, L.; Zhong, C. J.; He, T., Preparation and characterization of carbon-supported PtVFe electrocatalysts. *Electrochimica Acta* **2006,** 51, (23), 4821-4827.
168. Hamelin, A., Cyclic voltammetry at gold single crystal surfaces. Part 1. Behavious at low-index faces. *Journal of Electroanalytical Chemistry* **1996,** 407, 1-11.
169. Lovic, J. D.; Tripkovic, A. V.; Gojkovic, S. L.; Popovic, K. D.; Tripkovic, D. V.; Olszewski, P.; Kowal, A., Kinetic study of formic acid oxidation on carbon-supported platinum electrocatalyst. *Journal of Electroanalytical Chemistry* **2005,** 581, (2), 294-302.
170. Neurock, M.; Janik, M.; Wieckowski, A., A first principles comparison of the mechanism and site requirements for the electrocatalytic oxidation of methanol and formic acid over Pt. *Faraday Discussions* **2008,** 140, 363-378.
171. Kim, J.; Jung, C.; Rhee, C. K.; Lim, T. H., Electrocatalytic oxidation of formic acid and methanol on Pt deposits on Au(111). *Langmuir* **2007,** 23, (21), 10831-10836.
172. Leiva, E.; Iwasita, T.; Herrero, E.; Feliu, J. M., Effect of adatoms in the electrocatalysis of HCOOH oxidation. A theoretical model. *Langmuir* **1997,** 13, (23), 6287-6293.
173. Park, S.; Xie, Y.; Weaver, M. J., Electrocatalytic pathways on carbon-supported platinum nanoparticles: Comparison of particle-size-dependent rates of methanol, formic acid, and formaldehyde electrooxidation. *Langmuir* **2002,** 18, (15), 5792-5798.
174. Pedersen, M. O.; Helveg, S.; Ruban, A.; Stensgaard, I.; Laegsgaard, E.; Norskov, J. K.; Besenbacher, F., How a gold substrate can increase the reactivity of a Pt overlayer. *Surface Science* **1999,** 426, (3), 395-409.
175. Casado-Rivera, E.; Gal, Z.; Angelo, A. C. D.; Lind, C.; DiSalvo, F. J.; Abruna, H. D., Electrocatalytic oxidation of formic acid at an ordered intermetallic PtBi surface. *Chem. Phys. Chem.* **2003,** 4, 193-199.
176. Kim, J.; Jung, C.; Rhee, C. K.; Lim, T., Electrocatalytic oxidation of formic acid and methanol on Pt deposits on Au(111). *Langmuir* **2007,** 23, 10831-10836.
177. Pedersen, M. Ø.; Helveg, S.; Ruban, A.; Stensgaard, I.; Lægsgaard, E.; Nørskov, J. K., How a gold substrate can increase the reactivity of a Pt overlayer. *Surface Science* **1999,** 426, 395-409.
178. Schmidt, T. J.; Stamenkovic, V. R.; Lucas, C. A.; Markovic, N. M.; Ross, P. N., Surface processes and electrocatalysis on the Pt*(hkl)*/Bi-solution interface. *Physical Chemistry Chemical Physics* **2001,** 3, 3879-3890.
179. Smith, S. P. E.; Ben-Dor, K. F.; Abruna, H. D., Structural effects on the oxidation of HCOOH by Bismuth-modified Pt(111) electrodes with (100) monoatomic steps. *Langmuir* **1999,** 15, 7325-7332.
180. Tripkovic, A. V.; Popovic, K. D.; Stevanovic, R. M.; Socha, R.; Kowal, A., Activity of a PtBi alloy in the electrochemical oxidation of formic acid. *Electrochemistry Communications* **2006,** 8, 1492-1498.
181. Waibel, H. F.; Kleinert, M.; Kibler, L. A.; Kolb, D. M., Initial stages of Pt deposition on Au(111) and Au(100). *Electrochimica Acta* **2002,** 47, (9), 1461-1467.
182. Sun, S. G.; Yang, Y. Y., Studies of kinetics of HCOOH oxidation on Pt(100), Pt(110), Pt(111), Pt(510) and Pt(911) single crystal electrodes. *Journal of Electroanalytical Chemistry* **1999,** 467, (1), 121-131.
183. Yu, Y.; Hu, Y.; Liu, X.; Deng, W.; Wang, X., The study of Pt@Au electrocatalyst based on Cu underpotential deposition and Pt redox replacement. *Electrochimica Acta* **2009,** 54, (11), 3092-3097.

184. Melnick, R. E.; Palmore, G. T. R., Impedance spectroscopy of the electro-oxidation of methanol on polished polycrystalline platinum. *Journal of Physical Chemistry B* **2001,** 105, (5), 1012-1025.
185. Iwasita, T.; Xia, X., Adsorption of water at Pt(111) electrode in $HClO_4$ solutions. the potential of zero charge. *Journal of Electroanalytical Chemistry* **1996,** 411, (1-2), 95-102.
186. Schmidt, T. J.; Grgur, B. N.; Markovic, N. M.; Ross P.N, Jr., Oscillatory behavior in the electrochemical oxidation of formic acid on Pt(100): Rotation and temperature effects. *Journal of Electroanalytical Chemistry* **2001,** 500, (1-2), 36-43.
187. Tian, M.; Conway, B. E., Electrocatalysis in oscillatory kinetics of anodic oxidation of formic acid: At Pt; nanogravimetry and voltammetry studies on the role of reactive surface oxide. *Journal of Electroanalytical Chemistry* **2008,** 616, (1-2), 45-56.
188. Iwasita, T.; Xia, X. H.; Liess, H. D.; Vielstich, W., Electrocatalysis of organic oxidations: influence of water adsorption on the rate of reaction. *Journal of Physical Chemistry B* **1997,** 101, (38), 7542-7547.
189. Shiroishi, H.; Ayato, Y.; Kunimatsu, K.; Okada, T., Study of adsorbed water on Pt during methanol oxidation by ATR-SEIRAS (surface-enhanced infrared absorption spectroscopy). *Journal of Electroanalytical Chemistry* **2005,** 581, (1), 132-138.
190. Chen, Z.; Waje, M.; Li, W.; Yan, Y., Supportless Pt and PtPd nanotubes as electrocatalysts for oxygen-reduction reactions. *Angewandte Chemie - International Edition* **2007,** 46, (22), 4060-4063.
191. Huang, Q.; Yang, H.; Tang, Y.; Lu, T.; Akins, D. L., Carbon-supported Pt-Co alloy nanoparticles for oxygen reduction reaction. *Electrochemistry Communications* **2006,** 8, 1220-1224.
192. Li, X.; Hsing, I. M., Electrooxidation of formic acid on carbon supported Pt_xPd_{1-x} (x=0-1) nanocatalysts. *Electrochimica Acta* **2006,** 51, (17), 3477-3483.
193. Liang, H.-P.; Guo, Y.-G.; Zhang, H.-M.; Hu, J.-S.; Wang, L.-J.; Bai, C.-L., Controllable AuPt bimetallic hollow nanostructures. *Chemical Communications* **2004**, 1496-1497.
194. Mandal, S.; Krishnan, K. M., $Co_{core}Au_{shell}$ nanoparticles: evolution of magnetic properties in the displacement reaction. *Journal of Materials Chemistry* **2007,** 17, 372-376.
195. Duff, D. G.; Baiker, A.; Edwards, P. P., A new hydrosol of gold clusters. 1. Formation and particle size variation. *Langmuir* **1993,** 9, (9), 2301-2309.
196. Duff, D. G.; Baiker, A.; Edwards, P. P., A new hydrosol of gold clusters. *Journal of the Chemical Society, Chemical Communications* **1993**, (1), 96-98.
197. Duff, D. G.; Baiker, A.; Gameson, I.; Edwards, P. P., A new hydrosol of gold clusters. 2. A comparison of some different measurement techniques. *Langmuir* **1993,** 9, (9), 2310-2317.
198. Frens, G., Controlled nucletion for the regulation of the particle size in monodiperse gold suspensions. *Nature* **1973,** 241, 20-22.
199. Chen, S.; Wang, Z. L.; Ballato, J.; Foulger, S. H.; Carroll, D. L., Monopod, Bipod, Tripod, and Tetrapod Gold Nanocrystals. *Journal of the American Chemical Society* **2003,** 125, (52), 16186-16187.
200. Metraux, G. S.; Cao, Y. C.; Jin, R.; Mirkin, C. A., Triangular nanoframes made of gold and silver. *Nano Letters* **2003,** 3, (4), 519-522.
201. Zhou, Y.; Wang, C. Y.; Zhu, Y. R.; Chen, Z. Y., A novel ultraviolet irradiation technique for shape-controlled synthesis of gold nanoparticles at room temperature. *Chemistry of Materials* **1999,** 11, (9), 2310-2312.
202. Waje, M. M.; Li, W.; Chen, Z.; Larsen, P.; Yan, Y. In *Effect of scan range on Pt surface area loss in potential cycling experiments*, ECS Transactions, 2007; 2007; pp 1227-1233.
203. Ferreira, P. J.; La O, G. J.; Shao-Horn, Y.; Morgan, D.; Makharia, R.; Kocha, S.; Gasteiger, H. A., Instability of Pt/C electrocatalysts in proton exchange membrane fuel cells: A mechanistic investigation. *Journal of the Electrochemical Society* **2005,** 152, (11), A2256-A2271.

204. Shao-Horn, Y.; Sheng, W. C.; Chen, S.; Ferreira, P. J.; Holby, E. F.; Morgan, D., Instability of supported platinum nanoparticles in low-temperature fuel cells. *Topics in Catalysis* **2007,** 46, (3-4), 285-305.
205. Liu, Z.; Yu, C.; Rusakova, I. A.; Huang, D.; Strasser, P., Synthesis of Pt_3Co alloy nanocatalyst via reverse micelle for oxygen reduction reaction in PEMFCs. *Topics in Catalysis* **2008,** 49, 241-250.
206. Xiong, L.; Manthiram, A., Nanostructured Pt-M/C (M=Fe and Co) catalysts prepared by a microemulsion method for oxygen reduction in proton exchange membrane fuel cells. *Electrochimica Acta* **2005,** 50, 2323-2329.
207. Zhang, X.; Tsang, K. Y.; Chan, K. Y., Electrocatalytic properties of supported platinum-cobalt nanoparticles with uniform and cotrolled composition. *Journal of Electroanalytical Chemistry* **2004,** 573, 1-9.
208. Zhang, Y.; Chan, K. Y., Microemulsion synthesis and electrocatalytic properties of platinum cobalt nanoparticles. *Journal of Materials Chemistry* **2002,** 12, 1203-1206.
209. Luo, J.; Wang, L.; Mott, D.; Njoki, P. N.; Kariuki, N.; Zhong, C. J.; He, T., Ternary alloy nanoparticles with controllable sizes and composition and electrocatalytic activity. *Journal of Materials Chemistry* **2006,** 16, 1665-1673.
210. Santiago, E. I.; Varanda, L. C.; Villullas, H. M., Carbon-supported Pt-Co catalysts prepared by modified polyol process as cathodes for PEM Fuel cells. *Journal of Physical Chemistry C* **2007,** 111, 3146-3151.
211. Chen, G.; Xia, D.; Nie, Z.; Wang, Z.; Wang, L.; Zhang, L.; Zhang, J., Facile synthesis of Co-Pt hollow sphere electrocatalysts. *Chemistry of Materials* **2007,** 19, 1840-1844.
212. Do, J. S.; Chen, Y. T.; Lee, M. H., Effect of thermal annealing on the properties of $Co_{richcore}$-$Pt_{richshell}$/C oxygen reduction electrocatalysts. *Journal of Power Sources* **2007,** 172, 623-632.
213. Yamada, M.; Maesaka, M.; Kurihara, M.; Sakamoto, M.; Miyake, M., Novel synthetic approach to creating PtCo alloy nanoparticles by reduction of metal coordination nano-polymers. *Chemical Communications* **2005**, 4851-4853.
214. Salgado, J. R. C.; Antolini, E.; Gonzalez, E. R., Structure and activity of carbon-supported Pt-Co electrocatalysts for oxygen reduction. *Journal of Physical Chemistry B* **2004,** 108, 17767-17774.
215. Salgado, J. R. C.; Antolini, E.; Gonzalez, E. R., Carbon supported Pt-Co alloys as methanol-resistant oxygen-reduction electrocatalysts for direct methanol fuel cells. *Applied Catalysis B: Environmental* **2005,** 57, 283-290.
216. Xiong, L.; Manthiram, A., Influence of atomic ordering on the electrocatalytic activity of Pt-Co alloys in alkaline electrolyte and proton exchange membrane fuel cells. *Journal of Materials Chemistry* **2004,** 14, 1454-1460.
217. Koh, S.; Hahn, N.; Yu, C.; Strasser, P., Effects of composition and annealing conditions on catalytic activities of dealloyed Pt-Cu nanoparticle electrocatalysts for PEMFC. *Journal of the Electrochemical Society* **2008,** 12, B1281-B1288.
218. Koh, S.; Strasser, P., Electrocatalysis on bimetallic surfaces: Modifying catalytic reactivity for oxygen reduction by voltammetric surface dealloying. *Journal of the American Chemical Society* **2007,** 129, 12624-12625.
219. Mani, P.; Srivastava, R.; Strasser, P., Dealloyed Pt-Cu core-shell nanoparticle electrocatalysts for use in PEM fuel cell cathodes. *Journal Of Physical Chemistry C* **2008,** 112, 2770-2778.
220. Strasser, P.; Koh, S.; Greeley, J., Voltammetric surface dealloying of Pt bimetallic nanoparticles: an experimental and DFT computational analysis. *Physical Chemistry Chemical Physics* **2008,** 10, 3670-3683.

221. Liu, H.; Manthiram, A., Controlled synthesis and characterization of carbon-supported Pd_4Co nanoalloy electrocatalysts for oxygen reduction reaction in fuel cells. *Energy & Environmental Science* **2009,** 2, 124-132.
222. Sarkar, A.; Vadivel Murugan, A.; Manthiram, A., Low cost Pd-W nanoalloy electrocatalytsts for oxygen reduction reaction in fuel cells. *Journal of Materials Chemistry* **2009,** 19, 159-165.
223. Wells, P. P.; Crabb, E. M.; King, C. R.; Wiltshire, R.; Billsborrow, B.; Thompsett, D.; Russell, A. E., Preparation, structure and stability of Pt and Pd monolayer modified Pd and Pt electrocatalysts. *Physical Chemistry Chemical Physics* **2009,** 11, 5773-5781.
224. Hwang, B. J.; Kumar, S. M. S.; Chen, C. H.; Monalisa; Cheng, M. Y.; Liu, D. G.; Lee, J. F., An investigation of structure-catalytic activity relationship for Pt-Co/C bimetallic nanoparticles toward the oxygen reduction reaction. *Journal of Physical Chemistry C* **2007,** 111, (42), 15267-15276.
225. Lee, M. H.; Wang, P. S.; Do, J. S., Effect of acid treatment of $Co_{richcore}$-$Pt_{richshell}$/C electrocatalyst on oxygen reduction reaction. *Journal of Solid State Electrochemistry* **2008,** 12, 879-884.
226. Lee, W. R.; Kim, M. G.; Choi, J. R.; Park, J. I.; Ko, S. J.; Oh, S. J.; Cheon, J., Redox-transmetalation process as a generalized synthetic strategy for core-shell magnetic nanoparticles. *Journal of the American Chemical Society* **2005,** 127, 16090-16097.
227. Park, J. I.; Kim, M. G.; Jun, Y. W.; Lee, J. S.; Lee, W. R.; Cheon, J., Characterization of superparamagnetic core-shell nanoparticles and monitoring their anisotropic phase transition to ferromagnetic solid solution nanoalloys. *Journal of the American Chemical Society* **2004,** 126, 9072-9078.
228. Prabhuram, J.; Wang, X.; Hui, C. L.; Hsing, I.-M., Synthesis and characterization of surfactant-stabilized Pt/C nanocatalysts for fuel cell applications. *Journal of Physical Chemistry B* **2003,** 107, 11057-11064.
229. Lu, J.; Dreisinger, D. B.; Cooper, W. C., Cobalt precipitation by reduction with sodium borohydride. *Hydrometallurgy* **1997,** 45, 305-322.
230. Jackelen, A. M. L.; Jungbaer, M.; Glavee, G. N., Nanoscale materials synthesis. 1. Solvent effects on Hydridoborate reduction of copper ions. *Langmuir* **1999,** 15, 2322-2326.
231. Henglein, A.; Ershov, B. G.; Malow, M., Absorption spectrum and some chemical reactions of colloidal platinum in aqueous solution. *Journal of Physical Chemistry* **1995,** 99, (38), 14129-14136.
232. Glavee, G. N.; Klabunde, K. J.; Sorensen, C. M.; Hadjipanayis, G. C., Borohydride reductions of metal ions. A new understanding of the chemistry leading to nanoscale particles of metals, borides and metal borates. *Langmuir* **1992,** 8, 771-773.
233. Glavee, G. N.; Klabunde, K. J.; Sorensen, C. M.; Hadjipanayis, G. C., Sodium Borohydride reduction of cobalt ions in nonaqueous media. Formation of ultrafine particles (nanoscale) of cobalt metal. *Inorganic Chemistry* **1993,** 32, 474-477.
234. Glavee, G. N.; Klabunde, K. J.; Sorensen, C. M.; Hadjipanayis, G. C., Borohyride reduction of cobalt ions in water. Chemistry leading to nanoscale metal, boride or borate particles. *Langmuir* **1993,** 9, 162-169.
235. Srivastava, A. K.; Madhavi, S.; White, T. J.; Ramanujan, R. V., Template assisted assembly of cobalt nanobowl arrays. *Journal of Materials Chemistry* **2005,** 15, 4424-4428.
236. Li, T.; Yang, S.; Huang, L.; Gu, B.; Du, Y., A novel process from cobalt nanowire to Co_3O_4 nanotube. *Nanotechnology* **2004,** 15, 1479-1482.
237. Pourbaix, M., *Atlas of Electrochemical Equilibrium in Aqueous Solution*. National Association of Corrosion Engineers: Houston, TX, 1974; p 322-329.
238. Behl, W. K.; Toni, J. E., Anodic oxidation of cobalt in potassium hydrooxide electrolytes. *Journal of Electroanalytical Chemistry* **1971,** 31, (1), 63-75.

239. Casella, I. G.; Guascito, M. R., Electrochemical preparation of a composite gold-cobalt electrode and its electrocatalytic activity in alkaline medium. *Electrochimica Acta* **1999,** 45, 1113-1120.
240. Cataldi, T. R. I.; Casella, I. G.; Desimoni, E.; Rotunno, T., Cobalt-based glassy carbon chemically modified electrode for constant-potential amperometric detection of carbohydrates in flow-injection analysis and liquid chromatography. *Analytica Chimica Acta* **1992,** 270, (1), 161-171.
241. Herrero, E.; Li, J.; Abruna, H. D., Electrochemical, in-situ surface EXAFS and CTR studies of Co monolayers irreversibly adsorbed onto Pt(111). *Electrochimica Acta* **1999,** 44, 2385-2396.
242. Markovic, N. M.; Gasteiger, H. A.; Ross, P. N., Oxygen reduction on platinum low-index single-crystal surfaces in alkaline solution. *Journal of Physical Chemistry* **1996,** 100, 6715-6721.
243. Schmidt, T. J.; Ross, P. N.; Markovic, N. M., Temperature-dependent surface electrochemistry on Pt single crystal in alkaline electrolyte: Part 1: CO Oxidation. *Journal of Physical Chemistry B* **2001,** 105, 12082-12086.
244. Schmidt, T. J.; Stamenkovic, V. R.; Ross, P. N.; Markovic, N. M., Temperature dependent surface electrochemistry on Pt single crystals in alkaline electrolyte. *Physical Chemistry Chemical Physics* **2003,** 2003, (5), 400-406.
245. Duong, H. T.; Rigsby, M. A.; Zhou, W.-P.; Wieckowski, A., Oxygen reduction catalysis of the Pt_3Co alloy in alkaline and acidic media studied by x-ray photoelectron spectroscopy and electrochemical methods. *Journal of Physical Chemistry C* **2007,** 111, 13460-13465.
246. Chen, S.; Sheng, W.; Yabuuchi, N.; Ferreira, P. J.; Allard, L. F.; Shao-Horn, Y., Origin of oxygen reduction reaction activity on "PtCo" nanoparticles: Atomically resolved chemical compositions and structures. *Journal Of Physical Chemistry C* **2009,** 113, (3), 1109-1125.
247. Wakisaka, M. S., H.; Mitsui, S.; Uchida, H.; Watanabe, M., Increased oxygen coverage at Pt-Fe alloy cathode for the enhanced oxygen reduction reaction studied by EC-XPS. *Journal of Physical Chemistry C* **2008,** 112, (7), 2750-2755.
248. Gasteiger, H. A.; Kocha, S. S.; Sompalli, B.; Wagner, F. T., Activity benchmarks and requirements for Pt, Pt-alloy, and non-Pt oxygen reduction catalysts for PEMFCs. *Applied Catalysis B: Environmental* **2005,** 56, 9-35.
249. Stamenkovic, V. R.; Schmidt, T. J.; Ross, P. N.; Markovic, N. M., Surface composition effects in electrocatalysis: kinetics of oxygen reduction on well-defined Pt_3Ni and Pt_3Co alloy surfaces. *Journal of Physical Chemistry B* **2002,** 106, 11970-11979.
250. Stamenkovic, V. R.; Schmidt, T. J.; Ross, P. N.; Markovic, N. M., Surface segregation effects in electrocatalysis: kinetics of oxygen reduction reaction on polycrystalline Pt_3Ni alloy surfaces. *Journal of Electroanalytical Chemistry* **2003,** 554, 191-199.